Evaluation of Gas Insulated Lines (GIL) for Long Distance HVAC Power Transfer

A thesis submitted to Cardiff University
in candidature for the degree of
Doctor of Philosophy

By

Khalifa Elnaddab

School of Engineering
Cardiff University
December 2014

DECLARATION

This work has not previously been accepted in substance for any degree and is not concurrently submitted in candidature for any degree.

Signed……..…… (Candidate) Date…….

STATEMENT 1

This thesis is being submitted in partial fulfilment of the requirements for the degree of PhD.

Signed……..…… (Candidate) Date…….

STATEMENT 2

This thesis is the result of my own independent work/investigation, except where otherwise stated. Other sources are acknowledged by explicit references.

Signed……..…… (Candidate) Date…….

STATEMENT 3

I hereby give consent for my thesis, if accepted, to be available for photocopying and for inter-library loan, and for the title and summary to be made available to outside organisations.

Signed……..…… (Candidate) Date…….

STATEMENT 4

I hereby give consent for my thesis, if accepted, to be available for photocopying and for inter-library loans after expiry of a bar on access previously approved by the Graduate Development Committee.

Signed……..…… (Candidate) Date…….

In the name of Allah, the Most Gracious, the Most Merciful
Peace and blessings be upon our Prophet Muhammad
and upon his family and companions

ACKNOWLEDGEMENTS

First and foremost, I would like to thank the Almighty Allah for enabling me to complete this work; peace and blessings be upon our Prophet Muhammad and upon his family and companions.

I would like to express my extreme appreciation and sincere gratitude to my supervisor, Professor Manu Haddad. His guidance, encouragement and advice were essential in helping me to finish this work.

My sincere appreciation also goes to my second supervisor, Dr Huw Griffiths, for his valuable advice and constructive criticism during our weekly meetings and annual progress assessment.

I would also like to thank the following for their contributions:

Professor Abdelhafid BAYADI from Ferhat ABBAS University of Setif, Algeria for his extensive knowledge and help in the EMTP simulation program

All the members of the academic and administrative staff of School of Engineering, Cardiff University

Dr Alex Bogias, Dr Maurizio Albano, Dr David Clark, Fabian Moore, Dr Muhammad Saufi Kamarudin, Philip Widger, Tony Chen, for valuable discussions and for their friendship

And my special thanks to my wife, my daughter, and my parents for the selfless patience and endless support which they have shown throughout the period of my studies.

Lastly, I would like to thank my older brother Abu Baker for his financial support during my PhD studies.

PUBLICATIONS

i. K. H. Elnaddab, A. Haddad, H. Griffiths, "The transmission characteristics of gas insulated lines (GIL) over long distance," Universities Power Engineering Conference (UPEC), 2012 47th International, vol., no., p.1,5, 4-7 Sept. 2012 doi: 10.1109/UPEC.2012.6398633

ii. K. H. Elnaddab, A. Haddad, H. Griffiths, 'Future Gas Insulation Lines for Transmission Networks', Fifth Universities High Voltage Network (UHVNet), 18-19 January 2012, Leicester, UK

iii. K. H. Elnaddab, L. Chen, M.S. Kamarudin, A. Haddad, and H. Griffiths, 'Gas Insulated Transmission Lines Using CF3I', Sixth Universities High Voltage Network (UHVNet), 16-17 January 2013, Glasgow, UK

iv. M. S. Kamarudin, P. Widger, L. Chen, K. H. Elnaddab, A. Haddad, H. Griffiths, 'CF3I and Its Mixtures: Potential for Electrical Insulation', International Council on Large Electric Systems (CIGRE) Session 45, D1-309_2014, Paris, France

SUMMARY

Offshore wind power is a key element in EU policies to reduce the greenhouse effect and secure energy sources. In order to accomplish the EU's target of a 20% share of energy from renewable sources by 2020, some of the planned projects have to be placed far away from the shoreline to benefit from the high wind speeds in the open sea area.

However, a traditional transmission system for offshore wind farms based on a High Voltage Alternating Current (HVAC) utilizing conventional cables is not appropriate for long distances. In contrast, a High Voltage Direct Current (HVDC) can transmit electrical power over such distances, but the complicated concept of converting the HVAC offshore generated power into DC and then converting the DC power at the onshore grid back to AC requires sophisticated and expensive converter stations at both ends.

Therefore, developing a new infrastructure solution based on HVAC transmission technology, which has been in operation for more than a century and which runs almost entire electrical systems, to support and advance the development of offshore wind energy is a highly desirable outcome.

This research work was conducted to examine and determine the suitability of using an HVAC gas-insulated transmission line (GIL) as a long-distance transmission system for offshore wind farms in terms of technical and economic costs.

A computer model of GIL has been built using the Electromagnetic Transient Program (EMTP) to assess the suitability of GIL and quantify the voltage, current and power transfer characteristics of the GIL under different steady state conditions. Furthermore, a suitable model has been developed for the simulation of the switching transient during energisation of the GIL transmission system and various wind farm components.

The development concept of GIL as a submarine Power Transmission Pipeline (PTP) is described, and the practical side of installing the PTP technology and the special design requirements of the offshore wind farms were illustrated. The PTP components, the maximum transmission capacity of the PTP system and the layout options were addressed. In addition, the challenges facing this technology were discussed.

An economic comparison of the total cost for both HVAC-GIL and HVDC-VSC transmission systems is made, including annual costs (operation, maintenance, and losses) during the lifetime of the projects. The initial investment costs are added to the annual costs in order to obtain the total cost for the assumed project. Furthermore, the Power Transmission Cost (PTC) is calculated for each MVA-km being delivered to the receiving end of the GIL transmission line.

Table of Contents

LIST OF FIGURES

LIST OF TABLES

CHAPTER 1: INTRODUCTION

1.1 Introduction

Due to its commitment to the Kyoto Protocol about reducing greenhouse gases and regarding the security of energy supplies, the European Union parliament has set a target of a 20% share of energy from renewable sources in the gross of final consumption of electrical power by 2020 [1], [2]. Wind power is one of the richest renewable energy sources in the EU and has the ability to fulfil a significant part of the EU target. In the past decade, wind power has experienced rapid growth compared to other renewable energy sources, and it is expected to increase significantly in the near future. Therefore, wind power is expected to play an important role in the energy market to accomplish the EU target.

Even though onshore wind power is much easier as regards installation and maintenance, and there are still large areas with huge potential as locations for wind turbines, there are several reasons why offshore wind power development is being given serious consideration.

First, the wind power is proportional to the cube of the wind speed; therefore, the high wind speed at the open sea area will improve the capacity factor of the wind farm and increase its energy output. Second, the wind speed is more constant offshore and does not increase with height as it does onshore, which allows the use of turbines with shorter towers. Third, the large open sea area allows the implementation of large scale wind farms, which is not possible in countries with densely populated areas [3].

The number of wind power plants under construction or planned for offshore installations is increasing rapidly. Since the first offshore wind farm was installed in 1991 at 1.5 km from the Danish coast [4], experience has made it possible to improve the design, structure and technical performance of offshore wind farms. By the end of 2012, there were just under than 5 GW of installed offshore wind energy in Europe [5]. An additional 4.5 GW were under construction and consent had been given for around 18 GW of offshore projects. EWEA estimates that by 2020, about 40 GW could be generated from offshore wind power plants. This is enough to power the equivalent of 39 million households. By 2020, offshore wind will represent 30% of the new installations of the annual wind market [6].

By 2030, EWEA expects 150 GW of cumulative offshore wind capacity in European waters, enough to power 145 million households [3]. Offshore wind will represent 60% of the new annual installations, exceeding the onshore market. EWEA has identified 141 GW of projects in European waters, which are either online, under construction, or have obtained or applied for planning permission [7].

Most of these developments are taking place in the North Sea and Baltic Sea, with 62% of total approved capacity in the North Sea. The Mediterranean could begin exploiting its offshore potential with 8% of approved capacity in that time frame, along with the Baltic Sea with 21% of approved capacity, and 9% will be in the Atlantic Ocean. Finally, by 2050, offshore wind power generation could reach 460 GW, producing 1,813 TWh, with 50% of the European power supply coming from wind power generation [7], [8].

The numbers look very promising, but on the other hand, there are huge challenges slowing down the development of this industry. Wind farms are growing ever bigger in size. In addition, they are moving farther from the shoreline. Some of the approved projects in the North Sea are more than 200 km from the shoreline [9]. Therefore, there is a clear need to find new power transmission options or possible electrical structures to connect high power and long-distance offshore wind farms to a nearby on-land transmission system.

1.2 Transmission System for Offshore Wind Frames

There are two technologies for electricity transmission, namely, HVAC and HVDC. HVAC has been in practical use for decades transmitting and distributing electrical power. For offshore transmission, HVAC technology utilizes HV/EHV AC submarine cables, which are using cross-linked polyethylene (XLPE) insulation. High voltage cables are limited by their high capacitance, which generates large amounts of reactive power along the cable length. This reduces the ability of the cable to transmit active power, especially over longer distances.

At certain distance, reactive compensation needs to be installed at both ends of the cable to increase the amount of active power that can be transmitted and to help reduce losses. Increasing the line length beyond this distance requires additional shunt compensation to be installed at the middle of the line length. In offshore applications, this is very expensive, as it requires additional offshore platforms; therefore, in economic and technical terms, transmission distances are limited for XLPE cables.

Moreover, conventional cables are also limited by the transmission capacity. For high transmission capacity, more cables are required, but to find routes and landing points for all of them is especially complex. Therefore, this type of cables are not able to fulfil the requirement of future offshore power generated transmission [10].

On the other hand, in the HVDC transmission technology, the frequency is not an issue as it is direct current, which means no reactive power is generated along the cables. This advantage allows HVDC technology to transmit high amounts of power over long distances, while reducing the power losses and solving the stability problems caused by compensation equipment [11]. There are two types of HVDC transmission technologies. The first is Line-Commutated Current Source Converters (LCC); this is known also as classical HVDC and is used for extremely long line distances. The second is Self-Commutated Voltage Source Converters (VSC).

HVDC-LCC technology is based on electronic semiconductor valves (thyristors) that are switched on by a pulse and switched off when the current flowing through them decreases to zero. The converters need to be connected to a reliable AC system, since the AC voltage forces the current to commutate from one phase to another. The thyristor can withstand a high current and a high power rating. The LCC connection also has high efficiency of up to 98%, including the converter at both ends [12].

The power connection in the HVDC-LCC technology is grid controlled. It is dependent upon the existence of a relatively powerful three-phase grid. However, there is a delay between the current and the voltage and, because of this delay,

reactive power compensation is required, which consists of a harmonic filter and usually other capacitors in the magnitude of about 50% of the converter rated power. This requires a considerable amount of space and so represents a major cost factor, especially on an offshore platform. The HVDC-LCC also generates a harmonic current, with the amplitude depending on the amount of power being transmitted. For this reason, harmonic filters are normally used at both end; again, these require a considerable amount of room [13].

Additionally, a diesel generator is required for black-start the link in the case of failure; this requires a large diesel storage compartment that might cause environmental concerns when implemented in offshore substations. Consequently, HVDC-LCC has not been implemented as a transmission system for offshore applications.

The HVDC-VSC technology is based on insulation gate bipolar transistors (IGBT) which can be switched on and off extremely quickly. This means that not only the active power can be controlled, but also the reactive power can be controlled as well independently from each other, which gives the advantage that no additional reactive power compensation is required [14]. The fast control over the reactive power improves the voltage stability and transfer capacity of the AC grids at both ends of the link.

An HVDC-VSC transmission system can control the amplitude of the output voltage, which reduces losses. Moreover, the current can flow in both directions and is independent of the power level, which is ideal for multi-terminal systems [12]. The VSC shows the capability for black-starting the link since the voltage

restoration can be done by the transmission link itself without additional equipment providing when one of the terminals is working properly.

Compared to the LCC technology, only a small-sized harmonic filter is needed due to the rapid IGBT actuation. The DC voltage in the VSC is kept constant, and the polarity is not changed when the power is reversed, allowing the use of XLPE cables [12]. However, no matter how attractive the HVDC transmission technology might appear, one important issue has to be considered: the complicated concept of converting the HVAC offshore-generated power to HVDC and then converting the HVDC power at the onshore grid back to HVAC requires complicated and expensive converter stations at both ends.

Because of this disadvantage, developing a new HVAC transmission system that operates under less complicated principles, has high transmission capacity, and is capable of transmitting bulk power over long distances with high efficiency is an urgent task. Gas insulated transmission lines (GILs) have higher transmission capacities than other transmission technology, with up to 4000 MW per three-phase system [15]. In addition, GILs offer low losses and high overload capacities, which is useful for transferring the power generated by wind farms. Moreover, GILs have a proven reliability, having been used for more than 40 years inside substations without any major failures [15].

So far, GILs have only been laid over relatively short distances. A total of 300 km of GIL systems are in operation worldwide, with the longest system measuring 3,300 m [15]. Although GILs have the potential to fulfil the offshore power generated transmission requirements, using GIL as a transmission system in a submarine environment over such long distances is a completely new application

for this technology, which may be adopted to solve the special requirements of offshore wind power.

This can be done by introducing the new transmission technology called 'power transmission pipelines' or (PTP). The PTP technology is a total system for transporting electrical power generated far away from the load centre based on approaches taken from offshore oil and gas pipeline technology. The GILs form a core in the PTP transmission technology. The system includes a main collecting platform for the feed-in of electrical power from different offshore wind farm substations. At the main collecting platform, the bundled power is connected to the transmission system to transmit the power to the onshore connecting point. Moreover, the lay out technology for the transmission system is via directly buried GIL aluminium pipes coated with a thick layer of polyethylene or polypropylene for corrosion protection or via tunnel construction.

1.3 Research Objectives

The objectives of this thesis are to investigate and evaluate the technical and economical suitability of using HVAC gas-insulated transmission line (GIL) technology as a transmission system for high power capacity generated offshore over long distances ranging from 200 km to 500 km. For this purpose, an EMTP-ATP model of (GIL) has been developed based on the geometric and material properties of a typical 420 kV GIL system to study the electrical characteristics of GIL as a long transmission system under different steady state conditions. To enable comparisons to be made with the results obtained from the physical model of the GIL, an analytical method employing MATLB has been used to calculate the electrical transmission characteristics of GIL. A model of an offshore wind

farm has been developed in EMTP-ATP to analyse the switching transient during energisation of the long transmission line (GIL) and to determine the effect of such stresses on all components of the offshore wind farm. The main objectives of this study are specified as follows:

- Determine the limit of maximum transmission capacity against the line length of GIL compared to other HVAC transmission technology.
- Determine the transmission characteristics for different line lengths ranging from 200 km to 500 km.
- Determine the transmission characteristics of different load conditions for loads ranging from open end line up to a 120% load condition for 300 km and 500 km line lengths.
- Determine the transmission characteristics for various power factors at the load side for 300 km and 500 km line lengths.
- Determine the transient overvoltages that may occur during energisation along GIL and the effect of this transient on the equipment connected to the GIL at both ends.
- Analyse and determine the special requirement for installing GIL under the sea based on the transmission capacity required and the protection of GIL aluminium pipes.
- With available data, make an economic comparison between both HVAC-GIL and HVDC-VSC transmission technologies.

1.4 Contribution of Thesis

The important contributions achieved during the course of this research work are as follows:

- An extensive review is provided of the development of GIL and its potential for power transmission applications (see chapter 2).
- A model has been developed of a GIL transmission system connecting offshore wind farms to an onshore transmission network (see chapter 3).
- The maximum transmission capacity limit of the GIL was determined based on the line length (see chapter 4).
- The electrical transmission characteristics for different GIL line lengths, ranging from 200 to 500km, were determined (see chapter 4).
- The electrical transmission characteristics of different load conditions ranging from 0-120% were determined for line lengths of 300 and 500km (see chapter 4).
- The operational power factor ring for 300 and 500km GIL line length was specified (see chapter 4).
- The switching transient overvoltages arising during the energisation of a 300 km GIL transmission system have been examined (see chapter 5).
- The practical side of installing GIL based on power transmission pipeline (PTP) technology has been explained (see chapter 6).
- The total lifetime cost of a GIL transmission system has been determined per km for line lengths of 75 and 300km, in addition to the cost of each MVA delivered to the receiving end of both transmission line lengths (see chapter 7).

1.5 The Structure of the Thesis

This thesis contains eight chapters. A list of abbreviations is included in Appendix 1.

Chapter 2: **Overview of gas-insulated transmission lines (GIL)**. A definition and description of GIL is given, including a history of the development of GIL and a summary of the main features. The general technical design characteristics of GIL are detailed and the electrical parameters are compared to those of overhead lines and conventional cables. A detailed description of the GIL components is provided. The insulation and overvoltage aspects of GIL are discussed from an insulation coordination and long-term reliability aspect. In addition, both mechanical and corrosion protection for different types of installation are described. The advantages of using GIL compared to other transmission systems are explained in detail.

Chapter 3: **Modelling of GIL and the power system equipment**. This chapter describes how a 420 kV GIL transmission line was modelled based on its geometric and material properties using EMTP-ATP along with all the electrical equipment used in this study, including the equivalent of onshore network sources, 420 kV overhead lines and 2500 mm^2 420 kV XLPE cables, circuit breakers, 420/33 kV generator transformers, and the equivalent circuit of a wind power plant.

Chapter 4: **GIL behaviour under steady state conditions**, describes how a model of a 420 kV GIL was built using EMTP-ATP for the purpose of carrying out a steady state power flow study for different line lengths of GIL. The electrical characteristics of the GIL are calculated for the different factors affecting steady state conditions. The maximum transmission capacity of the GIL is studied and a brief comparison is made with other AC transmission technologies. Moreover, the electrical transmission characteristics under different line lengths are explored. In addition, the effects of different load conditions for

300 km and 500 km line lengths are studied. Finally, the effect of the variation in power factor at the receiving end for 300 km and 500 km line lengths is examined.

Chapter 5: **Transient behaviour of long GIL connecting offshore wind farms.** This chapter describes the development of a computer model using the EMTP-ATP simulation transient program for a GIL system connecting an offshore wind farm to the main grid. Moreover, this chapter investigates the voltages arising during the energisation and de-energisation of the 300 km submarine GIL, and the energisation of the submarine GIL with an offshore 420/33kV transformer.

Chapter 6: **Practical side of installation GIL based on PTP technology,** explains the practical side of installing GIL using power transmission pipeline technology "PTP" and the special design required of the offshore wind farms. The PTP component, the maximum transmission capacity of the PTP system, and the laying technology is addressed. In addition, the challenges facing this technology are illustrated.

Chapter 7: **Economic comparison between HVAC-GIL and HVDC-VSC transmission technology.** In this chapter, the estimated total build costs of a new transmission system for both transmission technologies are carried out; these are subdivided into the fixed build costs and the variable build costs. The variable operation costs are estimated as well and are divided into maintenance costs and power losses costs during the lifetime of the equipment. The overall lifetime cost of both transmission technologies are estimated as lifetime cost per km. The power transmission cost (PCT) is calculated as a lifetime cost per km for each

MVA/MW being delivered to the receiving end of the proposed transmission line length.

Chapter 8: **General Conclusions and Future Work.** Presents overall conclusions based on results and findings in this study and outlines recommendations for future investigations.

CHAPTER 2: OVERVIEW OF GAS-INSULATED TRANSMISSION LINE (GIL)

2.1. Introduction

Gas insulation technology was developed based on the excellent electrical insulation properties of Sulphur hexafluoride (SF_6). SF_6 is an artificial gas which is non-toxic, non-flammable, non-corrosive, inert and is stable over the long term [16]. It was designed in the 1920s, and its excellent electrical properties allowed high voltage and high current rating systems to be designed. The first closed chamber for an experimental set-up was built in 1960 using SF_6 under high voltage conditions for both DC and AC voltages [17], [18].

The physical nature of an aluminium pipe representing an electrical conductor held by insulators in the centre of an outer enclosure pipe made of aluminium and filled with SF_6 as an insulation gas was seen as the best solution for high electric power transmission. Both DC and AC voltages were investigated. However, the DC caused many problems to the dielectric stability of the insulation system; thus, the gas insulation technology developers have focused on an AC system [15].

Based on the excellent insulation performance of SF_6 and the high transmission capability of gas-insulated pipes, the GIL technology was introduced. In addition, the outstanding arc interruption performance of SF_6 increased the switching efficiency of circuit breakers and led to the development of a very successful high voltage switchgear with an extremely high switching capability and reliability [15].

This chapter gives an overview of GIL, including a definition and description of GIL and the history of their development. The general technical characteristics of GIL and the design factors that influenced their development are addressed. There is also a discussion of the insulation coordination and overvoltage aspects of GIL. The chapter also gives details of GIL components, illustrates the advantages of using GIL, and explains the laying method and the corrosion protection. Finally, the system control and diagnostic tools are discussed.

2.2. Definition and Description of GIL

The fundamental structure of GIL and gas insulated switchgear (GIS) are the same: the aluminium conductor pipe at high voltage is placed inside another earthed aluminium enclosure pipe and the space between the two pipes is filled with pressurised gas for insulation purposes. Solid support insulators are used to hold the conductor pipe in position inside the enclosure pipe [15], [19]. The basic structure of GIL is shown in Figure 2-1.

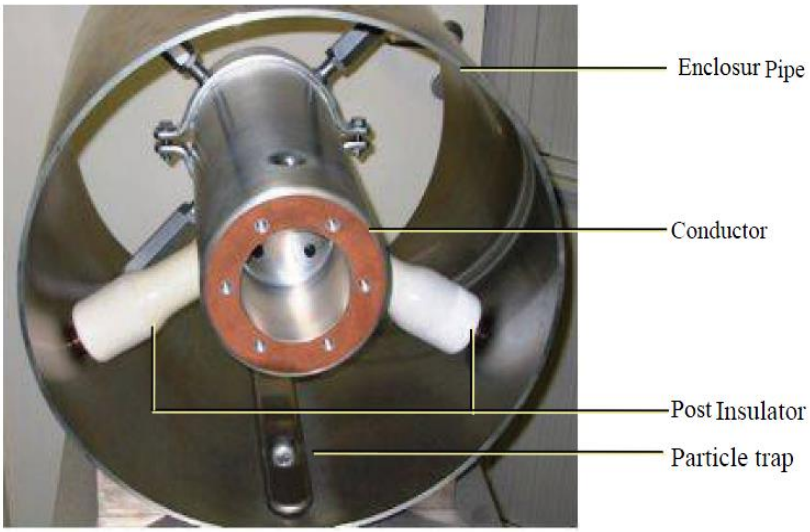

Figure 2-1: Overview of Single Phase GIL Pipeline [20]

Moreover, thermal expansion was taken into account by adding sliding contacts to the GIL design. The designer has also taken the elastic banding into account with a bending radius of up to 400 m allowed, thus making adaptation to the bends in the tunnel possible without any need for angle modules.

To change direction, an angle unit was introduced as well; it can change the direction from 4^0 up to 90^0. Disconnecting units are used to separate gas compartments and to connect high-voltage testing and monitoring equipment for the commissioning of GIL [15].

The final dimensions of GIL are determined by taking the dielectric, thermal and mechanical factors into consideration. Conductor and enclosure diameters and their thicknesses are varied according to the voltage level. The dielectric strength is the main factor in determining the dimensions and the required current rating. For more highly rated circuits, thermal considerations may be predominant and larger dimensions will be chosen to maintain temperatures within acceptable limits [15], [19], [21].

2.3. History of Development

2.3.1. First Generation of GIL

The development of the gas insulation medium is the only major difference between the GIL generations. The first generation of GIL used 100% SF_6 as the insulation medium without any flexibility for bending the aluminium pipes [15], [22]. In the 1960s, the first high voltage experimental tests were carried out using SF_6 in a closed compartment. The tests were carried out with both DC and AC voltages.

The AC voltage exhibited good results especially regarding electrical stability; therefore, the product development with AC was more successful. The first application was the section of a bus bar without any switching application [23], [24].

In 1968, the first complete SF_6 system was introduced including a switchgear circuit breaker, a ground switch, and a bus bar, which then led to the development of a very successful electrical system (GIS). The development of the GIS and GIL was in parallel with the development of other technology for jointing, monitoring, and installing GIL.

With different designs, different names were created: gas-insulated bus duct, compressed gas-insulated bus duct, bus bar, gas-insulated transmission line (GITL) or gas-insulated line (GIL). In 1998, the international standardization organization (IEC-61640) introduced the name 'Gas-Insulated Transmission Line' with the abbreviation 'GIL' as the preferred term for use world-wide [25].

In 1974, first application of first generation of GIL were built at the cavern hydropower plant of the "Schluchseewerke" in the Black Forest in Germany at a voltage level of 400 kV. A failure in the oil cable connecting the hydropower plant at the top of the mountain through the cavern led the owner to look for incombustible material for a transmission system, and GIL provided the solution [23]. The technical data for the Schluchsee project is shown in Table 2-1.

Table 2-1: Technical Data of the Schluchsee Project: First Generation of GIL [23]

Nominal Voltage	380 kV
Maximum Voltage	420 kV
Nominal Current	2000 A
Lightning impulse voltage	1640 kV
Switching impulse voltage	1200 kV
Power frequency voltage	750 kV
Rated short time current	135 kA
Insulation gas	100% SF_6

Subsequently, 700 m of a three-phase GIL system was placed in a tunnel to connect the high voltage transformers at 420 kV to the overhead line. As indicated in Table 2-1, due to the lack of experience, and to avoid any failure, high voltage test data were chosen for the first generation GIL. To date, the GIL at Schluchsee has been in a full operation for about 40 years, which proves the high reliability of GIL technology as a transmission system.

Based on the experience gained from this application, it can be concluded that, once GILs have been installed and have been put into operation, they remain reliable for a long time without any sign of aging. Moreover, this application has shown that no gas leakage is detected when the pipe joints are welded. In this case, the gas tightness of GIL did not require any gas refill during the 40 years of operation, which indicates a high reliability of the on-set welding technology of GIL.

Although the first generation of GIL showed very high reliability and high transmission capability, it was not widely used due to the following reasons:

- SF_6 is an artificial gas, which is very expensive. Therefore, in order to be used in a wide range of applications, the cost of the first generation of GIL had to be reduced as much as possible to make GIL projects economical.
- SF_6 gas has a strong molecule, which is very resistant to assault in the atmosphere. The self-cleansing property of the atmosphere is unable to deal with such super molecules. therefore, its production is now restricted under the Kyoto Protocol [26].
- Sulphur hexafluoride (SF_6) has a global-warming potential 23,900 times higher than that of CO_2. This means that one SF_6 molecule has the same effect on warming the planet as 23,900 CO_2 molecules [27].

Future transmission networks require more underground solutions with very high transmission capabilities and long transmission distances. Therefore, development second generation of GIL to replace overhead transmission lines became a crucial task.

2.3.2. Second Generation of GIL

The second generation of GIL are filled with a gas insulation mixture of 80% N_2 and 20% SF_6; they may be welded or flanged and have elastic bending to a radius of 400 m [15]. The above reasons were the basis for the development of the second generation of GIL. Since the 1970s, many research studies have been carried out to find a gas to replace SF_6. Some of the tested gases and gas mixtures showed higher insulation capabilities than SF_6, but all of them were more critical in terms of toxicity or greenhouse effect [28], [29], [30].

Research showed that there is no alternative to SF_6, especially of current interruption applications, but mixing SF_6 with other gases and reducing its percentage can give good insulation results. It was found that N_2 can form a good insulation gas in combination with SF_6; the insulation characteristics of the N_2/SF_6 gas mixtures show that with an SF_6 content of less than 20%, an insulating capability that is 70 - 80% that of pure SF_6 can be reached at the same gas pressure [31], [32].

In 1994, EDF carried out a feasibility study to develop a technical solution for a future generation of GIL. Key technical data were specified by EDF as a target for the new design of GIL [15], [33]. Table 2-2 shows key technical data for GIL from an EDF feasibility study. Three GIL design groups, namely, ABB, Alstom, and Siemens, were working on the development of the second generation of GIL. The three teams came up with two basic designs: the three-phase insulation design and the single-phase insulation design.

Table 2-2: Key Technical Data for GIL from an EDF Feasibility Study [15], [33], [34]

Power per three-phase system	3000-4000 MW
Nominal voltage	400 kV
Maximum voltage	420 kV
Current rating	4300-5700 A
System length	Up to 100 km
Isolation gas mixture	N_2> 80% and SF_6<20%
Type of laying	Directly buried

The three-phase insulation design was based on three aluminium conductors placed inside an enclosure of steel with an aluminium inlay that acted as a high-pressure vessel. The enclosure was made of steel to withstand the required 1.5-2.0 MPa gas pressure. The diameter of the three-phase design was about 1.5 m.

The single-phase design was based on one aluminium conductor in one aluminium enclosure. The gas pressure was 0.8 MPa, and the diameter was 0.5 m. The insulation gas for both designs was a mixture of (80%-98%) N_2 and (20%-2%) SF_6 depending on the gas pressure and the dimensions of the conductor and the enclosure [15], [34], [35], [36].

More research was carried out into both designs to cover all design aspects including the manufacturing possibility, laying process requirements, on-site testing, operation, and maintenance. The results showed that, from a technical point of view, both designs were possible. The single phase GIL design required more space for laying, but the jointing and laying process was simpler than that of the three-phase design. Therefore, the single-phase design was chosen for the second stage of the investigation.

In the second stage of the investigation, two prototypes of GIL were built to simulate the lifetime of the equipment of a directly buried 100 m long GIL system. One of them was built at the EDF test field in France based on the ABB design, and the other one was built at the IPH test field in Germany based on the Siemens design. The second prototype was designed and installed at the IPH test field by Siemens for tunnel layout tests [15].

The long term behaviour was investigated by simulating the GIL system in operation over a 50 years lifetime [36]. The prototypes had to prove on-site

assembly under realistic conditions covering all types of GIL elements in use, including all the stresses the GIL system may be subjected to during its operational lifetime.

The first application of second generation GIL was built in 2001 in Palexpo Geneva, Switzerland, with a gas mixture of 20% SF_6 and 80% N_2, 0.7 MPa gas pressure, and 420 m in length. It was laid in an underground tunnel [15], [37]. The technical data for the Palexpo project is shown in Table 2-3.

The GIL has been in operation since January 2001. The results demonstrate excellent power transmission behaviour and reliability, with minimal negative impact. Further details on existing GIL projects can be seen in Appendix 2.

Table 2-3: The Technical Data of the Palexpo Project [37]

Nominal Voltage	300 kV
Nominal Current	2000 A
Lightning impulse voltage	1050 kV
Switching impulse voltage	850 kV
Power frequency voltage	460 kV
Rated short time current	50 kA
Rated gas pressure	7 bar
Insulation gas	80% N_2/20%SF_6

2.3.3. Alternative Gas to SF_6

One of the main reasons for developing GIL generations is to reduce as much as possible the use of SF_6 as an insulation gas or to find a new gas that has the ability to replace SF_6 due to concerns about the greenhouse effects of using SF_6. The

global warming potential (GWP) of SF_6 is so high that its production has been restricted under the Kyoto Protocol [38].

Since the conventional gases, such as N_2, CO_2 and air, do not have enough insulation strength and lack the required interruption capability, the only solution available is to develop an insulation gas mixture with SF_6. Since 2000, many experimental works and tests have been carried out to find a replacement for SF_6 with a gas with a smaller GWP and less environmental impact [39], [32], [40], [41]. Gases and gas mixtures especially that have carbon (C) and fluorine (F) can have better dielectric strength than SF_6. Some per-fluorocarbons and related mixtures have 2.5 times greater breakdown strength than SF_6, but these are also greenhouse gases [42].

Trifluoroiodomethane (CF_3I) gas is one of the most promising candidates for substituting SF_6 gas due to its extremely low GWP, near-zero ODP, good long-term stability under ambient conditions, and relatively low toxicity; in addition, as a gas, it is colourless and non-flammable [43]. Details of the physical properties of CF_3I are given in Appendix 3.

Research into the properties of CF_3I has shown that the gas has high dielectric strength and good electronegative attachment characteristics, which would indicate its use as an insulating medium in power system applications should be extended. Table 2-4 shows the general properties of CF_3I gas compared with SF_6 gas [44]. The dielectric strength of CF_3I gas is 1.2 times greater than that of SF_6 gas under atmospheric pressure [45].

Table 2-4: General Properties Comparison of CF_3I and SF_6 [44]

Material	CF_3I	SF_6
Molecular mass	195.91	146.05
Characteristic	Colourless, Non-Flammable	Colourless, Non-Flammable
Global Warming Potential	Less than 5	23,900
Ozone Depleting Potential	0.0001	0
Lifetime in atmosphere (year)	0.005	3,200
Boiling Point (1 bar)	-22.5°C	-63.9°C

However, CF_3I has a crucial disadvantage: it cannot be used alone due to its high boiling point of -22.5° at ambient pressure [45]. In practice, the SF_6 gas in GIL is utilized at about 0.7 MPa. At this pressure level, SF_6 gas has lower a boiling point (about -30°C) while that of CF_3I gas is relatively high (about 26°C). Therefore, it is not possible to utilize CF_3I gas at this pressure level due to its high boiling point, which leads to the liquefying of the gas. However, there are several ways to avoid liquefying the gas, for example, by decreasing the partial pressure and mixing the gas with other gases such as N_2, air, or CO_2 [40], [46].

Recent studies have shown that pure CF_3I provides a better insulation performance than does SF_6. Although mixing it with other gases decreases its insulation characteristics, its performance remains at acceptable levels. According to [47], the interruption performance of CF_3I in a mixture of CO_2 is higher than in a mixture with N_2. This is due to the electron attaching properties of CO_2, which are better than those of N_2. A mixture of CF_3I-CO_2 with a ratio of 70% CO_2 and

30% CF_3I will give a dielectric strength of around 0.75 to 0.8 times that of SF_6 [40].

Thus, it can be concluded that CF_3I provides good dielectric strength properties as well as environmentally friendly characteristics, and these properties make it the most suitable gas to date to replace SF_6. Even though CF_3I cannot be used alone, and mixing it with CO_2 will reduce its dielectric strength, the dielectric strength of the gas mixture remains at a good level, which makes CF_3I-CO_2 a better gas mixture to replace SF_6.

2.4. GIL Design Criteria

A GIL system is a system for transmitting power without any switching elements or power transfer instruments. It has been defined as a coaxial configuration for power transmission with a few inhomogeneous locations [15]. Most of the cylindrical coaxial electrical field in a GIL system is quasi homogenous. The GIL design follows the IEC 62271-204 standard [48]. The main factor that affects the final dimension of the high voltage GIL system is the insulation coordination, which is related to the rated voltage of the equipment.

In some cases, the GIL is integrated with overhead lines, which are subject to lightning strikes that cause high transient overvoltages. These overvoltages depend on the type of tower structure and the geographical situation in the area where the towers are standing. This has an impact on the amplitude and probability of transient overvoltages and the related test voltages. Therefore, the lightning impulse withstand overvoltage is one of tests that is responsible for determining the insulation coordination of the GIL [49].

By connecting protection surge arresters to the GIL gas compartment at each end or at defined positions along the route, the transient overvoltage level can be limited, which leads to lower insulation levels of the GIL. The use of surge arresters reduces the diameter of the GIL and the volume of insulating gas required. This has a great impact on cost reductions.

Moreover, the rated current also has a strong impact on the final dimension design of the GIL. The current carrying capability depends on the cross section of the conductor pipe and its wall thickness. Moreover, the maximum carrying capability is limited by the maximum allowable temperature, which adds another factor that needs to be considered, namely, the thermal dimension.

The dimensions of the conductor and enclosure pipe of the GIL system depend on the heat dissipation of the temperature generated by the current into the surrounding air for tunnel layout option or into the soil for directly buried option. Another design parameter related to the current rating is the short circuit current requirement. A high short circuit rating requires GIL to have high mechanical and thermal properties. In general, GIL offers very good short circuit behaviour due to the large cross section of the outer enclosure. The following sections discuss further factors that affect the final design of GIL.

2.4.1. Dielectric Dimensioning

The dielectric dimensioning of GIL is determined by the maximum allowable electrical field strength, which is identified through voltage tests. The dielectric dimensioning is basically optimized by the best relationship between the cylindrical configuration of the inner conductor and outer enclosure pipe to give a

typical field strength of about 20 kV/mm [15]. The value 20 kV/mm can be higher if the affected area is not too large [50]. The field strength can be calculated by using Gauss's law as shown in Equation (2-1) [51]. Where V_{test} is a high frequency lightning impulse voltages test and 'a', 'b' are the outer conductor radius (mm) and inner enclosure radius (mm) respectively.

$$E_{max} = \frac{V_{test}}{a * \ln(\frac{b}{a})} \quad (2\text{-}1)$$

2.4.2. Thermal Dimensioning

The thermal dimensioning design requires a trade-off between the cost and the current rating, which is responsible for the heat generated from the GIL conductor pipe [15], [19]. GIL's current rating depends on the wall thickness and the inner and outer diameter of the conductor and the enclosure.

A conductor with a large diameter means more current can be transmitted which require a larger enclosure pipe diameter to offer enough surface area to transfer the heat to the ambient air. This has a great impact on the total cost of the GIL pipe. According to (IEC 62271-1), the typical temperature of the insulators is 105-120^{0}C and the maximum allowed temperature for the enclosure pipe is 40-50^{0}C for directly buried and 60-70^{0}C for tunnel laid GIL [48], [52].

2.4.3. Gas Pressure Dimensioning

A GIL is filled with the insulation gas mixture at a relatively low pressure of about 0.7MPa, and so is seen as a low pressure vessel. The operation experience of the gas insulated system has shown that the GIL insulation gas pressure ranges from 0.4MPa to 0.8MPa depending on the percentage of the insulation gas

mixture [15]. When the gas pressure is increased to about 1.5MPa to 2.0MPa, the sensitivity toward internal failure is increased due to even small inhomogeneous areas [53]. At this pressure, the vessel can no longer be seen as a low-pressure vessel. Therefore, an increase in the conductor and the enclosure dimensions and wall thickness is required, which will add a further cost to the final price of the GIL.

2.4.4. High Voltage Tests Design

Three standard voltage tests Lightning Impulse Withstand Voltage (LIWV), Switching Impulse (SIWV) and Power Frequency (PFWV) are used when designing high voltage equipment. The design tests values are given by the related standards IEC 62271-204 [48], IEC 62271-1 [52] for different voltage levels. For 400 kV and 500 kV networks, the maximum voltage V_m is respectively 420 kV and 550 kV for the equipment during operation.

The PFWV is given by a factor of 1.5 for V_m = 420 kV and 1.36 kV for V_m = 550 kV. An increase the voltage behind these factors, increases the possibility of flashover. The ratio of LIWV to the rated voltage is 3.39 for V_m = 420 kV and 2.9 for V_m = 550 kV. For SIWV, the ratio is 2.5 for V_m = 420 kV and 2.18 for V_m =550 kV.

These test voltage ratios are standard values and reflect the experiences over the last 40 years. LIWV and SIWV tests are required to prove the design is suitable for the transient voltage that may come from the lightning strikes when connecting overhead lines to GIL or when a switching operation occurs in the network [54]. An example of the voltage tests is given in Table 2-5.

Table 2-5: High Voltage Dielectric Tests for Different Voltage Levels [52], [48]

Nominal voltage	400 kV	500 kV
Maximum voltage (V_m)	420 kV	550 kV
Power frequency withstand voltage (PFWV) 1 min	630 kV	750 kV
Lightning impulse withstand voltage (LIWV)	1425 kV	1600 kV
Switching impulse withstand voltage (SIWV)	1050 kV	1200 kV

2.4.5. Short Circuit Rating Design

When a short circuit fault occurs in a transmission system, the amount of current that flows toward that location depends on the source impedance of the system feeding that fault [19], [55]. The magnitude of the current that may flow when a fault occurs at a point in a transmission system is known as the fault level at that point. A high fault level is undesirable due to the heating effect and electromagnetic forces produced by the fault current. Thus, it is clear that the switchgear controlling the faulted circuit must be rated adequately to interrupt the fault current.

Depending on the network location, different levels of short-circuit ratings are found depending on how far the fault is from the power plant. Typical values of short-circuit ratings are found in the transmission network 50 kA, 63 kA and 80 kA. In some rare cases, 100 kA can be found [15], [19]. A GIL short circuit rating has to fulfil two requirements:

- To withstand the electromagnetic forces between conductor and ground
- To limit the maximum conductor temperature due to the high current.

In GIL, the enclosure is solidly grounded, and the electromagnetic forces are concentric around the conductor and so centralize the conductor in the enclosure. Therefore, the insulator does not need to withstand high mechanical forces. The solidly grounded system causes an induced current in the enclosure in the opposite direction, and both forces are subtracted from each other resulting in only a small force. The thermal heat caused by the high current rating is relatively low due to the large cross section of the GIL.

2.4.6. Internal Arc Design

The internal arc is the worst case of failure that may happen to a GIL. Therefore, the internal arc design is defined as a safety value for withstanding the internal arc before the failure occurs in the system [15]. The internal arc can be caused by particles inside the gas compartment or from failure at the conductor or enclosure pipes which can cause high electric field strength and a flash over through the insulating gas.

The arc generates high temperatures, which leads to an increase in the pressure inside the gas compartment. This increase in the pressure depends on the current and the volume of gas. The smaller the compartment, the higher the pressure; that is why small compartments use pressure interruption discs that break when a defined pressure is reached and so release the gas pressure. The second criterion which must be met for the safe operation of GIL is that the internal arc should not burn a hole in the enclosure wall [56].

For the development and design of the internal arc test, several tests were carried out in the IPH test field in Germany. The test set-up was built based on Siemens design which include all the major components of a GIL to prove the arc

withstand capabilities of the enclosure in case of an internal arc. The internal arc tests were designed according to the IEC requirements. The short-circuit arc current for example 63 kA is driven by an arc voltage of about 8000V, which results in a power of approximately 500 MVA [15].

The length of the GIL section was about 25 m, so the increase in gas pressure due to the heat generated by the arc remained within acceptable limits. The summary of the test results is as follows:

- No external influence during and after the internal arc test was noticed.
- No burn-through of the enclosure occurred and only very low material consumption was noticed on the enclosure and conductor.
- The increase in pressure within the enclosures during arcing was significantly low, so that even the rupture discs did not open.
- The arc characteristic was much smoother in terms of speed and the wider arc discharge canal compared with the characteristics when using pure SF_6 (wider arc diameter/lower arc travelling speed).
- The cast resin insulators were not seriously affected.

All these results indicate the safe operation of GIL; even in the very unlikely case of an internal arc, the environment is not affected. The results of the arc fault test also showed that in case of tunnel-laid GIL, no personal danger to people in the tunnel could be expected.

2.4.7. Mechanical Design

The mechanical design of a GIL depends on the installation type, that is, whether it is directly buried or laid in a tunnel. In operation, thermal expansion and gas

pressure generate the main forces that are influential on the enclosure. The differential expansion in the inner and outer pipes can be handled by using sliding contacts.

In the case of directly buried GIL, a high mechanical load is applied to the outer enclosure due to the friction with the soil. The further loads applied to the enclosure from the soil pressure and traffic load need to be considered. Moreover, banding stresses are another aspect of the mechanical design resulting from the condition of the installation, as it may be necessary to change direction within the 400 m bending radius. Such bending will introduce a tensile stress on the outside of the bend and a compressive stress on the internal side of the bend [15], [19], [21], [57].

2.4.8. Thermal Design

GIL forms a thermal system. The current circulating in both the conductor and the enclosure is the source of heat production. The generated heat is dissipated in a radial direction to the surrounding soil and then flows into the ambient air by convection. Many experimental and numerical works have been carried out to investigate the thermal behaviour of GIL under steady state and overload conditions [19], [58], [59], [60].

The thermal behaviour of GIL was studied in an experimental thermal test set-up [60]. The outer diameter of the conductor was 250 mm with a wall thickness of 16 mm. The inner diameter of the enclosure was 630 mm with a wall thickness of 10 mm. A gas mixture of SF_6 and N_2 was used as the insulating gas. The GIL pipes were heated by an electric current. The pipes were held at 12 m by insulators of epoxy cast resin. The outer pipe was thermally isolated by glass

wool. The temperatures of the conductor and the enclosure were measured at different angles: 0^o, 90^o and 180^o. The experimental data were collected 12 hours after the test started.

At the same time, a finite element thermal analysis was carried out [61]. Since the heat transfer occurs mainly in the radial direction, a 2D model was designed. A calculation domain of 40 m length and 20 m depth was modelled to take account of all the areas influenced by the heat coming from the GIL. The physical parameters were the same as the experimental model.

The temperature of the GIL conductor buried at 1.5 m remained at 65^oC, which is below the limit of 105-120^oC fixed by IEC 62271-1. The simulation shows that GIL can be overloaded by 150% with no time limitation without reaching the maximum allowed temperature, and they can be overloaded by 200% during 8.3 days to finally reach the maximum allowable temperature of the GIL (105◦C).

The thermal calculations have shown that with GIL, a high-power transmission system is available that, even under severe climatic and thermal conditions, can provide enough safety margins for reliable operation over the GIL's lifetime [62].

2.5. GIL Component Design

2.5.1. Technical Data

Similar to the bus sections and the bus bar arrangements on GIS, a GIL system can be described as a coaxial configuration consisting of an aluminium tubular conductor at high voltage inside an outer aluminium tube, which is usually grounded and which serves as encapsulation. The dimensions of the enclosure, the conductor pipes, and the wall thickness depend on the voltage rating, the gas

pressure, the rated current and the percentage of the gas mixtures. The main technical data of the GIL for 420 kV and 550 kV transmission networks are shown in Table 2-6.

Table 2-6: Technical Data for Different Voltage Levels [15]

Rated voltage	kV	420	550
Rated current	A	4000	4500
Rated power	MVA	3000	4500
Lightning impulse	kV	1425	1550
Power Frequency Voltage	kV	650	825
Short circuit current	$kA/3_s$	63	100
Gas pressure	MPa	0.7	0.7
Weight per metre	Kg	25	30
Gas mixture	%	20 % SF_6 80%N2	60%SF_6 40%N_2

2.5.2. Standard Units

In general, a GIL pipe consists of two basic units, namely, the straight unit and the angle unit, as shown in Figure 2-2. The straight unit consists of a single phase enclosure made of an aluminium alloy. The conductor is made from electrical aluminium that has 99.5% Al. The electrical aluminium has very high conductivity and low electrical resistance, which makes the power transmission losses very low. The surface of the conductor joint weld has to be very smooth to fulfil the high voltage requirements. The surface of the conductor pipes have to

be at a maximum surface roughness and should not have even small scratches or single spikes; thus, a special manufacturing process is required [63].

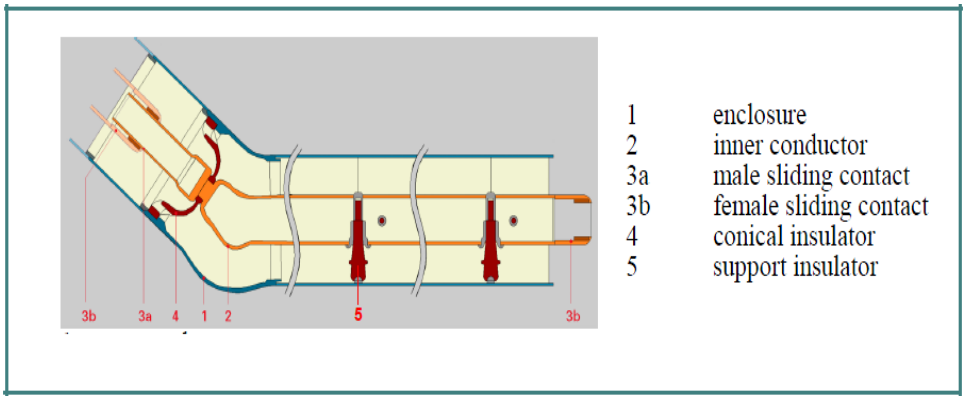

Figure 2-2: Straight Construction Unit with Angle Element [64]

The inner conductor is centred inside the outer enclosure by an insulator and lies on other support insulators. Different types of insulators were developed to fulfil the requirements of supporting the conductor and separating the gas compartment. Both post and conical insulators are used. The post insulators hold the conductor in the centre and enclose the conductor with insulating material. The insulators are made of tracking resistant cast resin mixtures which have a high mechanical strength [63].

The tracking resistance is important to prevent surface discharge during high voltage testing. There are two types of conical insulators in use: One forms a gas-tight enclosure pipe at the end of the GIL system and forms a gas compartment between two gas-tight conical insulators; The other type of conical insulator is non gas-tight and is used to fix the conductor towards the enclosure, and so is called the conductor fix point [63].

The thermal expansion of the conductor toward the enclosure is adjusted by the sliding contact system. One straight unit has a length up to 12-18 m comprising

several single pipe sections welded together by orbital welding machines. If a directional change exceeds what is allowed by the elastic bending, then the angle element is added to the straight unit by orbital welding. As mentioned previously, the angle element covers angles from 4^{o} to 90^{o}. Under normal conditions of the landscape, no angle units are needed due to the elastic bending, as a bending radius of 400 m is sufficient to follow the contour of the landscape. Disconnecting units are placed at distances from 1200 m to 1500 m to separate gas compartments and to connect high voltage testing equipment for the commissioning of the GIL [63].

A compensator unit is used to accommodate the thermal expansion of the enclosure in sections that are not buried in the earth. A compensator is a type of metallic enclosure with a mechanical soft section, which allows movement related to the thermal expansion of the enclosure. It compensates for the length of thermal expansion of the enclosure section. Thus, compensators are used in tunnel-laid GIL as well as in the shafts of directly buried GIL [63].

2.5.3. Electrical Parameters of GIL

The electrical parameters of GIL are related to the dimensions of the aluminium conductor and enclosure pipes, and the type of insulation gas. For single-phase GIL with the enclosures solidly bonded at both ends, each phase has series inductance and capacitance to earth. Coupling between phases is negligible due to the screening effect of the enclosures. The per unit length resistance depends on the conductor and enclosure dimensions and the electrical resistivity. The skin and proximity effects are negligible due to the thickness of the pipes and the space between them. Due to the cylindrical design and the solidly grounded

enclosure, the inductance is relatively small. More details of GIL's electrical parameters are given in Appendix 4.

2.5.4. Joint Technology

Different connection technologies are available for GIL. The choice of the right technology depends on the requirements. The flanges with bolts and a single O-ring sealing have been used in GIS for more than 40 years and show high quality and reliability. The only disadvantage when long distances have to be covered is the intensive manual handling on site when the GIL is assembled.

For long distances, an automated orbital welding system offers less manual handling. The clamp is also another manual technology used to connect the conductors. The clamp technology can be designed to standardize the connecting work step and minimize the manual work on site.

A new technology that has been introduced recently and that is very robust for on-site application is friction stir welding. This welding process uses a stir to generate heat to melt the aluminium and to make the connection. The advantages of this technology are higher speed and almost no impact from humidity and air movement [63].

2.6. Layout Methods

The layout options of GIL depend on the applications. When using GIL inside substations to connect different parts, the GIL are usually laid above the ground using steel structures or in concrete trenches. In some cases, the GIL is laid directly in the soil with corrosion protection on the outside. In hydropower plants, the GIL is installed in tunnels. Each case of layout has its own

requirements of thermal and mechanical stress that need to be taken into account [63], [65].

2.6.1. Above Ground Installation

GIL installation above ground is a trouble-free option. Most installed GIL are above ground even in extreme environmental conditions as GIL are unaffected by high ambient temperatures, intensive solar radiation, or severe atmospheric pollution, such as dust, sand or moisture. Corrosion protection is not always necessary for this type of installation. High transmission power can be achieved with above-ground installation [63].

2.6.2. Directly Buried

Directly buried GIL is the most economical and fastest method of laying options for long transmission distances. Directly buried GIL take the form of an "electrical pipeline" with the GIL layout method adapted from oil and gas pipeline laying techniques.

In addition, GIL laid in the soil are continuously anchored, so no compensation for additional thermal expansion is required, which makes the system more economical and reduces the time taken to complete the long distance installation. However, since the GIL is directly buried, the enclosure needs to be protected from corrosion using a polymer coating. As magnetic fields are marginal in the vicinity of all GIL applications, the land can be returned to agricultural use with very minor restrictions once the GIL system installation is completed [66].

2.6.3. Tunnel Installation

Tunnels made up of prefabricated structural elements are another method of GIL installation, and they open up the opportunity for high and compact electrical power transmission without being visible from above. Building a tunnel will add extra expense to the transmission project, but the cost depends on the way the tunnels are built. These can range from simple close to surface tunnels to those that are water tight or deep underground. With this method of installation, the land above the tunnel can be fully restored to agricultural use as only a negligible amount of heat is dissipated to the soil from the tunnel. The system stays accessible for easy inspection and high transmission capacity is ensured [67].

2.6.4. Vertical Installation

Gas-insulated tubular conductors can be installed easily at any gradient, even vertically. This makes them one of the best solutions, especially for cavern hydropower plants, where large amounts of energy have to be transmitted from the underground machine transformer to the switchgear and overhead line on the surface [67].

2.7. Advantages of GIL

2.7.1. High Transmission Capacity

A comparison has been made between different 400 kV transmission systems as they are used today. The technical data for the comparison are shown in Table 2-7.

Table 2-7: Technical Data for Different Transmission Systems [15]

	Overhead line 4*240/40Al/St	Cross-bounded Oil cable 1200 mm^2 Tunnel- laid	XLPE cable1600 mm^2 Tunnel -laid	GIL Tunnel laid Ø 600 mm grounded
Thermal power limit (MVA)	1790	1120	1150	3190
Thermal current limit (A)	2580	1610	1660	4600
Resistance R (mΩ/km)	30.4	23	19	6.9
Losses at limit current (W/m)	600	150	190	44
Losses at 1600 (A) (W/m)	230	145	177	53

2.7.2. Low Electrical Power Losses

GIL has the lowest electrical power losses compared to other transmission technologies. As can be seen in Table 2-7 the GIL resistance is lower than the resistance of other AC transmission technologies. The typical GIL resistance is 6.89mΩ/km for GIL outer diameter of 600 mm. The transmission losses are related to the square of the transmitted current as $P_{loss} = I^2 * R$. When the current rating is high as in this case 3190 A, the effect of low resistance on the transmission losses is high. This is a very important feature when it comes to calculating the total life cycle costs. Over the many years of service that can be anticipated, this represents a saving of millions of pounds.

2.7.3. High Level of Personnel Safety

The personnel safety level of GIL is very high due to the metallic enclosure, which provides reliable protection. Even in the rare case of an internal failure, the metallic enclosure is strong enough to withstand the stress of failure. The inherent safety of a GIL system, which contains no flammable materials, makes it suitable

for use in road or railway tunnels and on bridges. The use of existing tunnels has the obvious economic advantages of sharing the costs and solving some environmental problems because no additional overhead line is needed [63].

2.7.4. Natural Cooling Still Adequate at Over 3000 A

GIL needs no extra cooling when in service. The natural flow of air is sufficient to dissipate the heat losses when a transmission line is laid in a tunnel and the dissipation of the heat losses into the surrounding soil is sufficient when a GIL transmission line is laid directly in the ground. This is also the case even up to the maximum thermal current of 3150 A. As a comparison, in the case of cables buried in the ground, the thermal limit is usually well below 2000 A, while for overhead power lines that are operated at these high currents, the losses are very high [61].

2.7.5. Low Magnetic Fields

A high magnetic field can cause high interference and disturb electric equipment. For example, devices such as computer monitors can be influenced by magnetic field inductions of $\geq$2μT [63]. Moreover, magnetic fields may also harm human beings. The IRPA in Germany states a maximum exposure level for human beings of 100μT [68]. In UK the maximum exposure level is 20μT [69]. However, several countries have recently reduced this limit for power frequency magnetic fields.

For instance, in Switzerland, the maximum magnetic induction for the erection of new systems must be below 1μT in buildings [68]. Currently, some exceptions may be accepted. In Italy, 0.5μT has been proposed for residential areas in some

regions, with the goal of allowing a maximum of 0.2µT for the erection of new systems [68]. This trend suggests that, in the future, electrical power transmission systems with low magnetic fields will become increasingly important.

One of the advantages of GIL is the excellent electromagnetic compatibility. There is almost zero electric field outside the aluminium enclosing tube due to the solid grounded earth system. The currents flowing in the enclosing tube and the conductor tube for each phase are almost 180^{o} out of phase, which causes the two magnetic fields to be superimposed on each other and to cancel each other out. When a GIL is laid directly in the ground at a depth of one metre, the values of the magnetic field strength at ground level are less than 0.5µT. Figure 2-3 shows a comparison of the magnetic fields for different transmission systems [70].

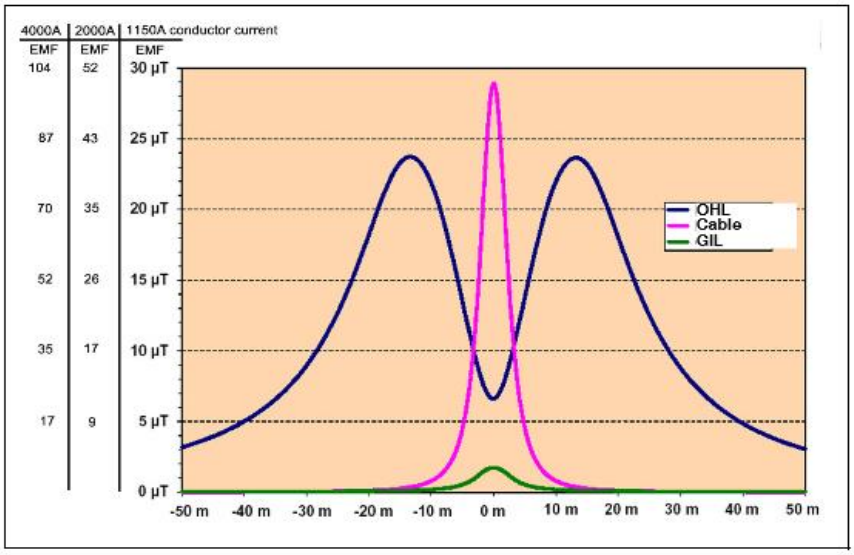

Figure 2-3: Comparison of Magnetic Flux Densities of Overhead Line, Cable and GIL [70]

2.8. Corrosion Protection

For most applications, the aluminium pipes are used above ground or in a tunnel; thus, the aluminium generates an oxide layer that protects the enclosure tube from

any kind of corrosion. The oxide layer of an aluminium pipe is very thin, but it is very hard and very resistive against environmental corrosion factors. Even in the case of outdoor application, no extra corrosion protection is required [71].

For directly buried systems, where the aluminium pipe has direct contact with the soil, corrosion protection is required. Two basic methods are used currently: passive corrosion protection and active corrosion protection.

Passive corrosion protection is an added layer of noncorrosive materials, usually, polyethylene (PE) or polypropylene (PP). In general, the process used to add coatings to the pipe as passive corrosion protection is similar to that for oil and gas pipelines. The surface of the enclosure aluminium pipe needs to be degreased, and the oxide layer needs to be removed using acid fluids or mechanical brushes. After the surface of the aluminium pipe has been prepared, the first layer of a corrosion protection fluid is applied onto the pipe to stop corrosion [71].

This first layer forms the active part of the passive corrosion protection and is only a few micrometres thick. On top of this layer, a 3 to 5 mm layer is added mainly for mechanical protection reasons. To apply this protective layer, two basic processes are used: the extruded layer and the tape wrapped layer methods.

The use of these passive corrosion protection methods has a long history and thousands of kilometres of experience as well as years of operating experience. After the pipe segments have been welded together, it is also necessary to protect the welded area by coating this area with passive corrosion protection [71].

In the active corrosion protection method, the induced current generates a voltage potential of the metallic enclosure toward the soil. If this voltage level is at a potential of around 1V toward a loss electrode, then the loss electrode corrodes instead of the aluminium enclosure.

The active corrosion protection system is a backup for the passive corrosion-protection system. It is installed as an additional quality insurance system if the passive corrosion protection fails. Failures in the passive corrosion protection can occur over the lifetime of the system due to outer damage through other earthworks or by cracks or voids in the protective material. If necessary, the active corrosion-protection system prevents corrosion in the event of cracks and voids in the passive corrosion-protection system [71].

Experience with directly buried pipe systems installed worldwide shows that, over the decades, some cracks or voids in the passive corrosion-protection system can occur, which increases the induced current of the active protection system.

The positive effect of the active corrosion protection system is that each passive corrosion-protection failure need not be repaired immediately, and the guaranteed lifetime of the passive corrosion protection system of 50 years can be extended by many more years. Repairs of passive corrosion protection systems can be planned for and concentrated on troublesome segments. Experience with oil and gas pipelines show that the lifetime can be extended significantly without any need to open the pipe.

The active corrosion protection system, also called cathodic corrosion protection, uses an induced current to adjust the protective voltage of approximately 1V against the lost electrode. To achieve this 1V protective voltage, an induced

current of approximately 100 μA is needed. The induced current is related to the total of the surface to be protected and increases with the length of the system and the number of failures. In practice, several kilometres can be protected with only one DC voltage source because the current is low.

Active corrosion protection can be easily installed along with an electrical transmission system, with no interference between electrical transmission and the corrosion protection voltage potential. Such electrical transmission systems have been operating for many years with no failures reported. The high reliability observed for pipelines and cables also applies to GIL systems [71].

2.9. System Control and Diagnostic Tools

In a complex insulation system such as a GIL system, a control and a diagnostic tool are necessary. It is important that gas density, partial discharge, and temperature be measured and monitored. The gas density needs to be monitored during operation, but partial discharge measurements are needed only for the commissioning process while temperature measurements are needed only at specific locations along the line where thermal overheating may be possible [72].

2.9.1. Gas Density Monitoring

The dielectric properties of the insulation gas are related to the gas density inside the enclosure. In turn, the gas density depends on the temperature and the pressure. Therefore, a temperature compensated pressure gauge is used to monitor the gas density level in the GIL.

The measured data are transmitted to the control centre, and a contact signal is used to give a warning of gas loss and to switch off the signal. The warning of gas

loss is given when the density is 5–10% lower than the minimum filling pressure [61].

If the gas density continues to drop below the safe dielectric level, the gas density monitoring system gives another signal to the control system to shut off the GIL system to avoid any internal flashover. The gas density monitoring system is a continuous measuring system of the GIL to ensure continued safe operation [61].

2.9.2. Partial Discharge Measurement

The partial discharge measurement is used during the commissioning process when the onsite test voltage is applied. This very sensitive measurement system is connected by internal antennae to detect any partial discharge and to give integrity to the electrical insulation system. Once these commissioning tests have been successfully completed, the partial discharge measuring system can be disconnected [73], [74]. Experience with gas-insulated technology (GIS and GIL) over the last 40 years has shown that once a gas compartment is free of partial discharges, it will remain that way. Only very few failures are related to increasing partial discharge intensities in gas-insulated systems. Once the partial discharges have disappeared during the high-voltage commissioning process, there is no need for continuous partial discharge measurement of the GIL. The UHF internal antenna to measure the electromagnetic radiation inside the GIL will stay in the GIL; only the external measuring equipment needs to be connected when required [75].

2.9.3. Temperature Measurement

During operation, the GIL may have different thermal locations because of external circumstances. Roadway tunnels, being buried at a greater depth, temporary soil dryness, or other reasons may cause thermal locations with a higher temperature. Control of such locations which are identified when the GIL route is studied can be monitored by external temperature sensors to avoid the GIL overheating [62], [61].

The design and layout of a GIL is made according to the worst-case scenario of an operation. The maximum temperatures are calculated for the laying conditions in a tunnel, trench, above ground or directly buried for operational conditions. Maximal load, maximal ambient and soil temperature, and expected load cycles are the calculation criteria for the thermal dimensioning of the GIL. If the conditions are not changing, no temperature measurements are required on a continuous basis. Only if conditions change, it is necessary to take control of the outside and inside temperatures of the GIL. Higher loads than expected, or temporary overload conditions, may be a reason for condition change.

2.10. Summary

Gas insulation transmission lines (GILs) are a high power transmission technology that can be installed above ground, directly buried in the soil, or placed in a tunnel. Since the first industrial application was built in 1974 using SF_6, more than 300 km phase length has been installed worldwide without a single failure.

Second step of GIL development was in 2001, when first second generation application was installed. Second generation of GIL was using a 70% N_2 and 30% SF_6 insulation gas mixture, which reduces the total cost of GIL system.

Today, GIL is adapted for many projects around the world especially when a high power transmission system is required. The size of projects is constantly increasing from some hundred metres in length to several kilometres. After more than 40 years in operation, the GIL has been proved very reliable technology. The flexibility of laying options offers large possible applications inside substations and power plants or even outside as cross-country installations.

GIL can be fitted into the high-power transmission network of voltage levels of typically 400 kV and higher with the availability of 500 kV, 800 kV and even 1200 kV GIL solutions. From an environmental point of view, GIL offers several advantages, such as being invisible underground, having lower transmission losses with very low electromagnetic fields, and having a high safety level concerning surrounding equipment or nearby personnel.

Moreover, it is possible to combine high-power transmission with roads and railways or as concentrated high-power underground electric pipes in a small corridor. The connection of large offshore wind farms and the landing of electrical energy are undergoing extensive investigation. After 40 years of very positive experiences with GIL, this technology is now ready to solve the high-power transmission requirements of the future.

CHAPTER 3: MODELLING OF GIL AND ASSOCIATED EQUIPMENT IN THE ELECTRICAL NETWORK

3.1. Introduction

The accurate representation of a power system component is essential to obtain correct and reliable results. The purpose of this chapter is to model GIL accurately in an EMTP simulation program for both steady state and transient state conditions. Moreover, models for other electrical network components such as circuit breakers, XLPE cables, overhead lines, transformers and equivalent wind farms are represented in order to identify the overvoltages that may occur along any point of the GIL during the energisation or disconnection of the wind farm. In this chapter, the approach and data used for the transient simulations and the data used in this research are described. A case is made for each choice of model and the source of data is given.

3.2. Line Models in EMTP

Representing a line or cable in an EMTP-ATP program is based on converting its physical characteristics (geometrical data and the material properties of the cable) to equivalent electrical parameters [70]. Depending on the phenomenon to be simulated, several line models can be used in EMTP-ATP. The lumped parameter model (PI) is usually used for steady state analysis. The distributed parameter model (Bergeron's model), which is based on travelling wave theory, can be used for both steady state and transient studies. The main limit of this model is that it was designed as a constant frequency model, and so its use is only for the cases when only one frequency is considered. The frequency dependent

parameter model (J-Marti) is also based on travelling wave theory, but the characteristic impedance Z_o and the propagation constant γ are calculated over a wide frequency range [76]. All these models require the same input parameters to calculate the series impedance matrix *Z* and the shunt admittance matrix *Y*. The following basic equations show the electrical characteristics of an insulated line:

$$\mathrm{Z}(\omega) = \mathrm{R}(\omega) + \mathrm{j}\omega\mathrm{L}(\omega) \tag{3-1}$$

$$\mathrm{Y}(\omega) = \mathrm{G}(\omega) + \mathrm{j}\omega\mathrm{C}(\omega) \tag{3-2}$$

Where *R* is the series resistance, *L* is the series inductance, *G* is the shunt conductance and *C* is the shunt capacitance per unit length of the line system. These quantities are [*n* x *n*] where *n* is the number of parallel conductors of the cable system. Both *Z* and *Y* are frequency-dependant quantities. The series impedance *Z* and the shunt admittance *Y* are calculated automatically by the cable constants routine (LCC) within the program, using cable geometry and material properties as input parameters[77].

The geometry required for simulation of the GIL line in EMTP-ATP is:

- GIL location of each conductor (x-y coordinates)
- GIL inner and outer radius of conductor and enclosure
- burial depth of the GIL system

The material properties required for simulation line is:

- resistivity ρ and relative permeability μ_r of the conductor material
- resistivity ρ and relative permeability μ_r of the enclosure material
- relative permittivity ε_r of the insulating gas

3.3. Transmission Line Modelling

3.3.1. GIL Modelling

The principle of representing GIL in an electromagnetic transient program is similar to representing conventional cables, but there are certain differences. The GIL is represented by three single core lines. Each line consists of an inner conductor and an outer enclosure both made of aluminium alloy with resistivity ρ = 2.8264E-8 and relative permeability μ_r = 1. The dielectric gas is a mixture of 70% CO_2 and 30% CF_3I with a relative permittivity of ε_r = 1.

The outer surface of the enclosure is coated by polyethylene or polypropylene of a thickness of 5 mm to give passive corrosion protection with a relative permittivity ε_r = 2.3. A soil resistivity of $1\Omega \cdot m$ was used to represent wet soil in the seabed. The geometrical characteristics of the GIL are given in Table 3-1[78] while Figure 3-1 shows a cross section of a single core GIL. The series impedance matrix Z and shunt admittance matrix Y were calculated internally using EMTP-LCC routines.

Table 3-1 Geometrical Characteristics of 420 kV GIL [78]

Phase cross-section area	mm^2	5340
Enclosure cross-section area	mm^2	10000
Phase outer diameter	mm	180
Enclosure inner diameter	mm	500
Phase thickness	mm	10
Enclosure thickness	mm	6.4
Protection layer	mm	5

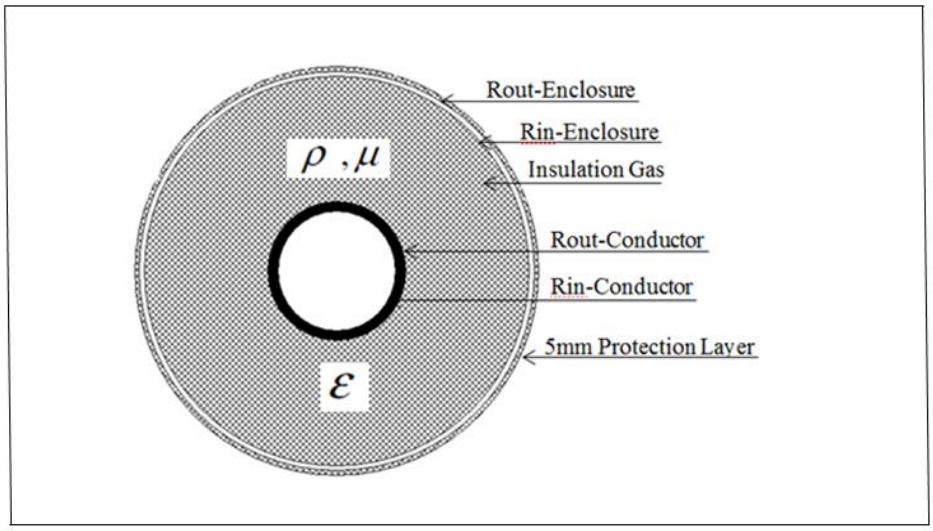

Figure 3-1: Cross Section of GIL Modelled in EMTP-ATP

The calculated electrical parameters are given in Table 3-2. It can be seen from Table 3-2 that the difference between the calculated electrical parameters at 50 Hz and the datasheet is relatively small. An example of the layout for three single core coaxial GIL pipes laid 100 m under the seabed is shown in Figure 3-2.

Table 3-2: Electrical Data and Parameters of a 420 kV GIL

Electrical Parameters		Units	Datasheet	Simulation results
Resistance per phase	r	mΩ/km	8.6	8.22
Inductance per phase	l	mH/km	0.204	0.201
Capacitance per phase	C	uF/km	0,0545	0.0521
Conductance per phase	g	nS/km	negligible	negligible
Characteristic Impedance	Z_0	Ω	61.46	62.11
Surge Impedance Loading at 420kV	SIL	MVA	2870	2840
Capacitive current related to $V_0 = 420\ kV/\sqrt{3}$	$Icap$	A/km	4.15	3.97

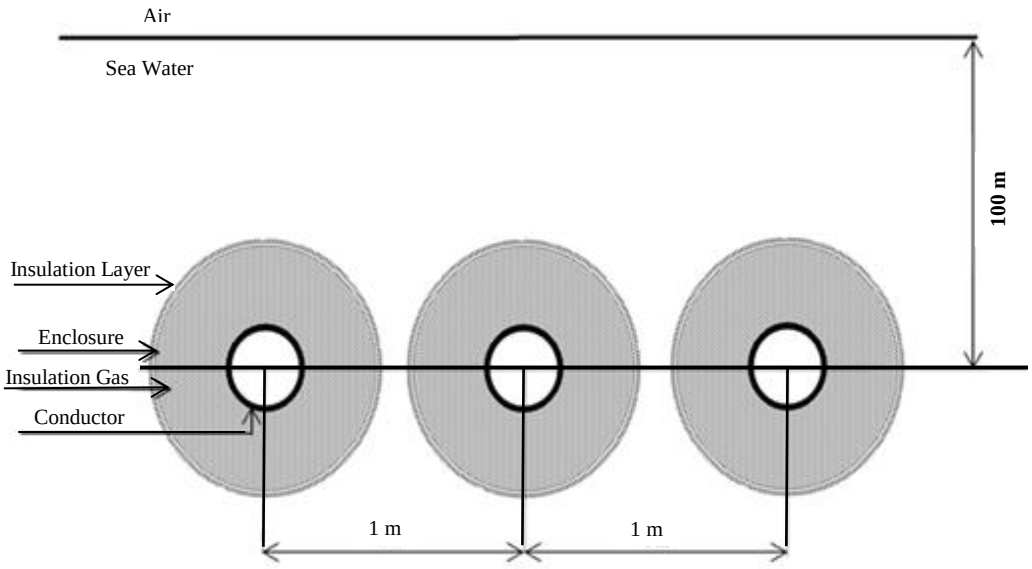

Figure 3-2: Layout for Three Single-Cores Coaxial GIL Pipes Modelled in EMTP-ATP

3.3.2. XLPE Cable Modelling

The EMTP-ATP simulation program cannot readily represent all details and layers of the XLPE cables. In practical terms, the core of the cables is designed using a segmented and stranded design. In addition, there are inner and outer semiconducting screens and a sheath that may be composed of a wire screen, which makes it difficult to specify these configurations directly into EMTP-ATP. However, a conversion method is combined with cable constants (CC) to take account of the effect of stranded conductors, semiconducting layers, and sheath in the model of the cable [79].

I. Cable Core:

CC routines require the core data to be given using the resistivity ρ and radius r_1. However, the core conductor is often of a stranded design, whereas CC routines assume a solid conductor. This makes it necessary to increase the resistivity of the core material to take into account the space between strands using Equation

(3-3). If the DC resistance (R_{DC}) of the core has been specified by the manufacturer, the resistivity can be alternatively calculated using Equation (3-4) [80]:

$$\rho_c' = \rho * \frac{r_1^2 * \pi}{A_c} \tag{3-3}$$

$$\rho_c' = R_{DC} * \frac{\pi * r_1^2}{l} \tag{3-4}$$

In [81], it was shown that either Equation (3-3) or Equation (3-4) can be used to calculate the core conductor resistance, as the small difference between the two does not affect the accuracy of the simulation results: ρ_c' is the increased resistivity, ρ is the resistivity of the stranded core, A_c is the nominal cross sectional area of the core, and r_1 is the radius of the core. The ρ_c of annealed copper wires is 1.7241E-8 Ω·m and from BS 60228 [82], $R_{DC} = 0.0072\ \Omega/\text{km}$, and l is cable length per km.

II. Insulation and Semiconducting Screen**:**

The different semiconducting layers of the cable cannot be automatically included in the cable model of EMTP-ATP. However, the effect of different semiconducting layers can be considered by changing the electrical permittivity of the insulation and keeping the capacitance between the conductor and the metal screen constant as shown in Equation (3-5) [80].

$$\varepsilon' = \varepsilon_r * \frac{ln\frac{r_2}{r_1}}{ln\frac{b}{a}} \tag{3-5}$$

Where r_1 and r_2 are the core radius and the sheath inner radius respectively, a and b are the inner and outer insulation radius respectively, and ε_r is the permittivity

of the insulating material (ε_r = 2.3 for XLPE). This neglects the possible attenuation caused by semiconducting screens, which affects the results for very high frequency transient simulations.

III. Inner Sheath:

It was not possible to specify a wire screen in EMTP-ATP, so the wire screen was replaced with a tubular conductor. The tubular conductor had a cross sectional area equal to the total wire area A_s . With an inner sheath radius of r_2, then the outer radius r_3 of the tubular conductor can be calculated from Equation (3-6) [80]. Figure 3-3 shows a single core XLPE cable modelled in EMTP.

$$r_3 = \sqrt{\frac{A_s}{\pi} * r_2^2} \tag{3-6}$$

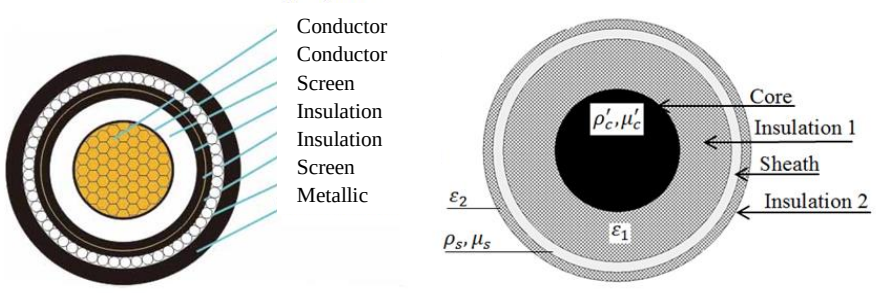

Real XLPE Cable EMTP Model

Figure 3-3: Single Core XLPE Cable Modelled in EMTP-ATP

The procedure outlined in the previous section is used to demonstrate the electrical characteristics of a 420 kV submarine XLPE cable with a cross section area of 2500 mm^2 [83], [84]. The conductor is made of copper. The converted data of the submarine cable used in the EMTP model is given in Table 3-3.

Table 3-4 shows the comparison between electrical parameters calculated at 50 Hz using the EMTP-LCC routine and the cable data sheath.

Table 3-3: Converted Data of 420 kV Submarine XLPE Cable Used in the EMTP-ATP Model

EMTP Model	Geometrical Parameters	Measurement
Conducting Layer	Outer Radius	33 mm
	Resistivity	2.36 E-8
	Relative Permeability	1
Insulation Layer 1	Outer Radius	62 mm
	Relative permittivity	2.72
	Relative permeability	1
Sheath	Outer radius	62.4 mm
	Resistivity	1.72E-8
	Relative permeability	1
Insulation Layer 2	Outer radius	71 mm
	Relative permittivity	2.3
	Relative permeability	1

Table 3-4: Electrical Parameters of XLPE Submarine Cable Modelled in EMTP-ATP [83], [84]

Cable parameters	Units	Simulation data	Datasheet
R	Ω/km	0.0188	0.0113
l	mH/km	0.422	0.41
C	uF/km	0.233	0.24
Z_o	Ω	42.46	41.5
SIL	MVA	4154.5	4250
Capacitive current related to $V_0 = 420\ kV/\sqrt{3}$	A/km	17.75	17.6

3.3.3. Overhead Line Modelling

A 420 kV double circuit overhead transmission line was modelled in the EMTP-ATP using L6 tower model. The conductors are numbered from 1 to 7 and their spacing, including average conductor sag relative to the centre of the tower and earth, are shown in Figure 3-4 [85].

A phase conductor is 4×400 mm^2 ACSR per phase 54/7 strands and the conductor outer radius is 14.31mm; the conductor ac resistance is 0.0684Ω/km. The earth wire conductor is 1×400 mm^2 ACSR 54/7 strands, the outer radius is 9.765 mm, and the ac resistance is 0.0643Ω/km. The earth resistivity is 20 Ωm, and the nominal frequency is 50 Hz [86].

Modelling of the overhead line in the EMTP-ATP was carried out following the same concept used for modelling the GIL and the XLPE cable. The electrical characteristics are calculated based on the geometry and the material properties of the conductor.

The overhead line input data were used with the line constant (LCC) calculation routine to calculate the line series impedance Z and shunt admittance Y matrices [79]. Table 3-5 shows equivalent electrical parameters of a 420 kV double circuit overhead line modelled in EMTP-ATP.

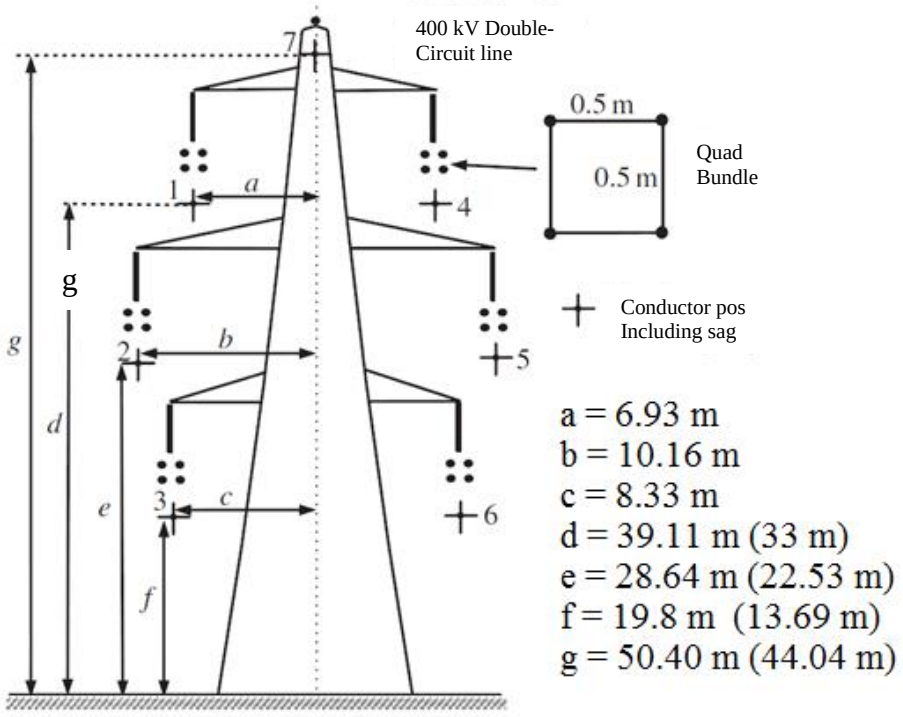

Figure 3-4: Double Circuit Overhead Line Modelled in EMTP [86]

Table 3-5: Equivalent Electrical Data and Parameters of a 420 kV Double Circuit Overhead Line

Cable parameters	Units	Simulation data
R	Ω/km	0.017
l	mΩ/km	0.8854
C	uF/km	0.0131
Z_0	Ω	260
SIL	MVA	678.5
Capacitive current related to $V_0 = 420\ kV/\sqrt{3}$	A/km	1

3.4. Transformer Modelling

Producing an exact representation of the transformer can be a significant challenge. Particular care has to be taken to model the transformer based on the requirement of the specific phenomena to be investigated. Therefore, a modelling guideline was developed by CIGRE [87] for the importance of representing different transformer parameters of the four main frequency ranges. Table 3-6 shows the modelling guideline.

Table 3-6: Modelling Guideline for Representation Transformer Parameters [87]

Transformer parameter	**Group 1** **0.1 to 3kHz**	**Group 2** **50/60 to 3kHz**	**Group 3** **10kHZ to 3MHz**	**Group 4** **100kHz to50MHz**
Short circuit impedance	Very Important	Very Important	Important only for surge transfer	Negligible
Saturation	Very Important	Very important for transformer energising	Negligible	Negligible
Hysteresis and iron losses	Important only for resonance phenomena	Important only for transformer energising	Negligible	Negligible
Frequency dependent series losses	Very Important	Important	Negligible	Negligible
Capacitance coupling	Negligible	Important for surge transfer	Very Important for surge transfer	Very Important for surge transfer

The energisation of offshore wind farm transformers falls under the second category of low frequency transients. Table 3-6 shows the parameters that have to be taken into account when modelling a power transformer. Several transformer models are available in the EMTP, such as BCTRAN, Hybrid and Saturable models [77]. Given to the data available, the BCTRAN model has been modelled in this thesis. The detailed representation of the BCTRAN model is explained in the following sections.

3.4.1. BCTRAN Model

The BCTRAN model consist of two parts: a linear part to represent the transformer short circuit characteristics and a nonlinear part to represent the transformer core saturation characteristics, which consist of a set of delta connected nonlinear inductors located at the low voltage (LV) side of the BCTRAN model. Moreover, the transformer capacitances must be represented as they determine the voltage distribution across the internal windings when a transformer is subjected to the transient.

A supporting routine BCTRAN can be used to derive a linear [R]-[ωL] representation for a single or three phase, a two or three winding, or for an autotransformer; using tests data of both the open exciting test and the short circuit test at the rated frequency [77].

The input data required for the BCTRAN model consist of rated power MVA, rated voltage, winding connection, grounding, impedance, losses, frequency, short circuit, and open circuit tests. More required parameters can be obtained from the transformer name plate, such as the number of phases, number of windings, frequency test, rated power, line-to-line voltage, and the winding connection, and all phase shifts are supported [77].

3.4.2. Linear BCTRAN Part Modelling

The transformer that is modelled in this thesis is a 783MVA, 420/33 kV three-phase two-winding Yd transformer. Under the open circuit tab, it can specify how the real factory test has been performed and where to connect the excitation branch. In this model for the factory, tests were performed at the HV winding,

and the excitation branch was connected at the low voltage side. Usually, the excitation branch is connected to the lowest voltage side of the transformer, but in some cases, the delta connected excitation branch is connected to the Y connected winding due to stability problems [88].

Depending on available data, up to 6 points on the magnetizing curve can be specified under the open circuit tab. The excitation voltage and current must be specified in % and the losses in kW [77]. Figure 3-5 [89] shows the open circuit test characteristics value of the excitation current Curr (%) and the power losses for two winding three phase transformers in relation to the rated apparent power MVA. At 100% excitation voltage, a 0.4% IEXPOS = Curr (%) excitation current was specified and the power loss was 900 kW. The zero sequence open circuit test data can be neglected for three phase low reluctance transformers [88].

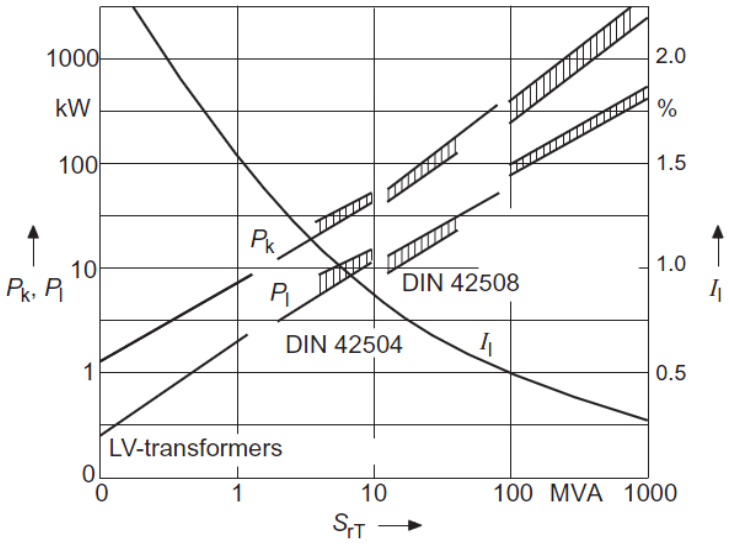

Figure 3-5: Characteristic Values for Excitation Current Curr (%) and Power Losses P_k versus S_{rT} of Two Winding Transformer [89]**.**

Under the short circuit tab, the positive sequence data can be specified. The positive sequence short circuit impedance Imp [%], rated power for the short

circuit test [MVA] and the power losses [kW] at short circuit test. These three values are specified for all the windings. Imp [%] is 15.13%, which was taken from Figure 3-6 [89]; this is a characteristic value of the impedance voltage of two winding transformers. The short circuit power losses are 2800 kW. Figure 3-7 [89] shows the short circuit power losses. The zero-sequence short circuit factory test data are not specified due to a lack of data.

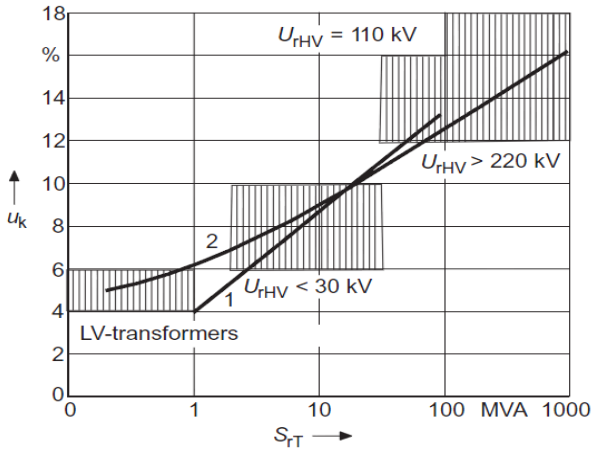

Figure 3-6: Characteristic Value of Impedance Voltage of Two Winding Transformer [89]

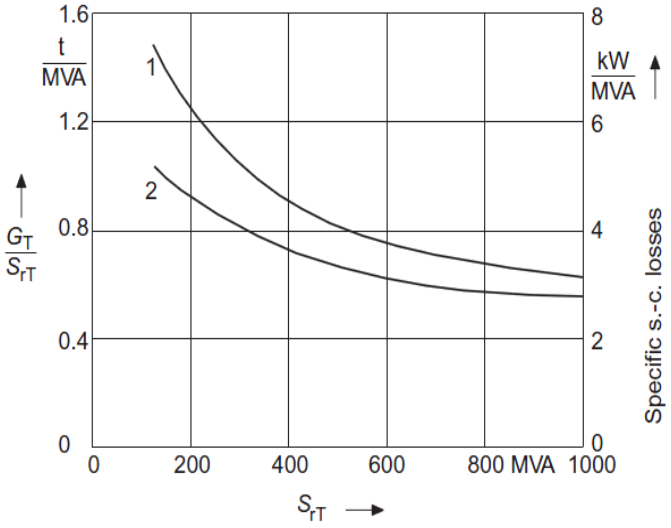

Figure 3-7: Short Circuit Losses (Lower Curve) of Transformers with Rated Voltages above 115 kV [89].

3.4.3. Nonlinear BCTRAN Part

The nonlinear behaviour of the transformer's core, which accounts for the saturation effect, has been modelled externally using element type 96. This can be accomplished by selecting the external Lm under the positive core magnetization tab. The core is then represented by three nonlinear inductors connected in delta as shown in Figure 3-8, which are connected externally at the secondary terminals of the BCTRAN model.

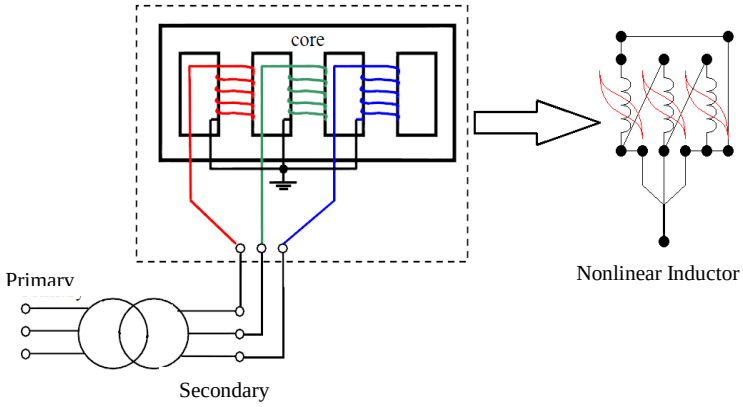

Figure 3-8: Modelling of Transformer Core in BCTRAN

3.4.4. Estimation of Core Saturation Curve

The open circuit data is used to approximate the saturation curve. The open circuit data voltage and current are usually given in RMS values, which are converted to peak value. Then, the SATURA supporting routine is used internally to calculate the flux linkage λ versus current i curve. According to the data available, the saturation knee point is reached at 1.13 from the 100% open circuit excitation voltage level, which will generate a λ/i characteristic curve consisting of only two points. The phase peak flux leakage λ_{peak} and the I_{RMS}

for the knee point are calculated from Equations (3-7) and (3-8). The saturation slope part in the saturation range is unknown, and so it has been approximated. Figure 3-9 shows the magnetising characteristic for a 420/33 kV transformer which is calculated based on the open-circuit test data of 100% excitation voltage.

$$\lambda_{peak} = \frac{\sqrt{2}\cdot 1.13\cdot V_{RMS}}{k\cdot\omega} = 186 \text{ (Wb-T)} \quad (3\text{-}7)$$

$$I_{peak} = \frac{\sqrt{2}\cdot P_{loss}}{\sqrt{3}\cdot 1.13\cdot V_{RMS}} = 61.3 \text{ A} \quad (3\text{-}8)$$

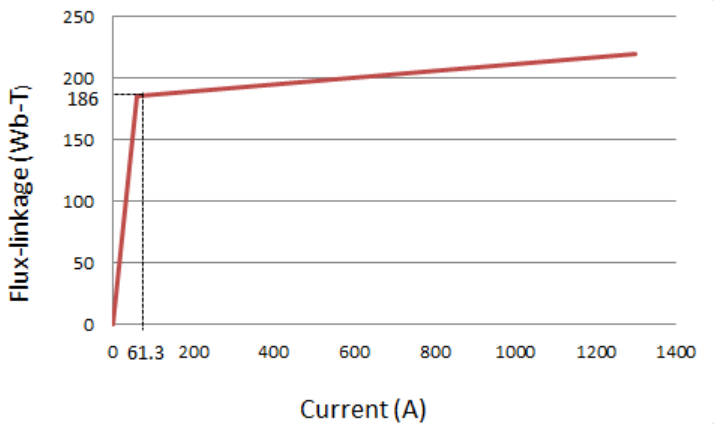

Figure 3-9: Magnetising Characteristic for 420/33 kV Transformer

3.4.5. Capacitances of the Transformer

The external and internal coupling capacitive effects of the transformer are taken into consideration in the BCTRAN model; the capacitances between windings: primary to ground, secondary to ground, and primary to secondary are included. Figure 3-10 shows a 420/33 kV BCTRAN transformer model modelled in EMTP.

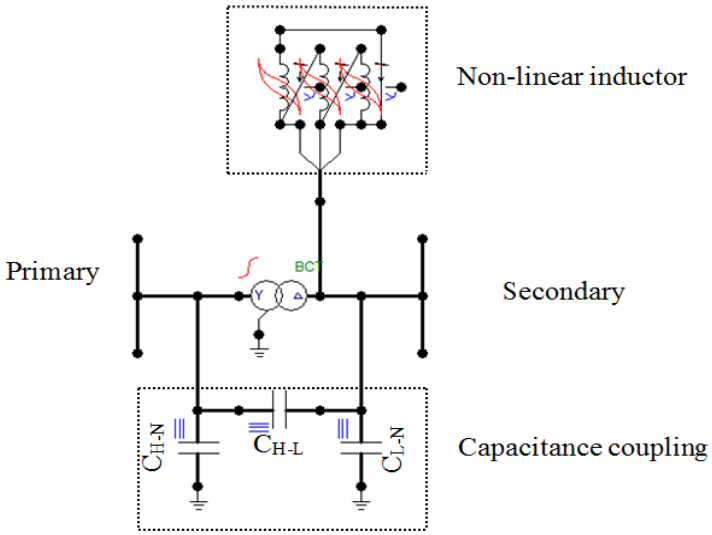

Figure 3-10: 420/33 kV BCTRAN Transformer Modelled in EMTP-ATP

3.5. Wind Farm Modelling

Large scale wind farms were undertaken by several researchers. This wind farms can consist of up to hundreds of wind turbines, which are interconnected by a complex collector system. The impact of single turbines on the large power system network is minimal and beyond the scope of this study, while large wind farms can have a significant impact on the power system during a severe disturbance, such as a nearby fault.

A power flow study is commonly performed during the different development stages of the wind farms. Therefore, it is important to model the wind farm as closely as possible to the real implementation, which will give reliable results. However, representing hundreds of turbines and branches is not practical in terms of the amount of time required. Therefore, modelling the wind farms as an equivalent model especially for transient studies is essential.

3.5.1. Effect of Wind Turbine Converter Model on Switching Transient

For simulations involving faults such as Transient Recovery Voltage (TRV) study, the model used for the wind turbine should represent the short circuit (SC) current contribution from this turbine. With the different types of wind turbine generators, the task of calculating SC current is not simple task as in case of a synchronous generator in a conventional power plant [90].

The fault current contribution from a wind power plant (WPP) depends on the wind turbines are they fixed speed induction machines (FSIG), doubly-fed induction generators DFIG or fully rated converter machines (FRC). The calculation of a wind farm's short circuit current contribution is not only important for the rating of switchgear but also for the coordination of network protection.

First generation of wind turbines generator is a fixed speed turbine with a squirrel-cage induction generator (SCIG) which is directly coupled to the grid. The equivalent machine impedance for fault calculations is the sum of the stator and rotor reactance. The fixed speed induction machines (FSIG), are able to contribute significantly in the fault current. The contribution during the initial cycle of the fault can be as high as six times the rated current or more [91].

For doubly-fed induction generators DFIG there is a power converter between the rotor windings and the grid. In case of short circuit in the DFIG wind turbine generator a large current will flow in the rotor circuit and through the generator-side converter during system faults. The response of a DFIG can be divided into two phases [92]. During the first phase, which lasts approximately 2 to 3 cycles, it

can be considered to operate as an FSIG. In the second phase, the current on the rotor side of the converter is limited by a control function or crowbar protection and the short circuit current contribution for three-phase fault is about 3pu from the rated current [91].

For FRC machines the wind turbine generator is decoupled from the grid through a power converter that is rated to the full output of the turbine. The short circuit current contribution of a three-phase fault is limited to its rated current of the converter or a little above its rated current. After a fault in the system is detected by the fully rated generator, the grid side converter rapidly limits the output to 1pu. The FRC can therefore be approximated as a constant current source [91].

3.5.2. Equivalent Model of Wind Farm

The wind turbines induction generators are directly connected to the grid or decoupled from the grid using power electronics. These topologies have different short circuit characteristics than conventional power generation machines. Therefore, appropriate short circuit studies are necessary to determine the maximum short circuit contribution from the wind farm. For short circuit studies at the transmission level, it is not practical to model the entire wind farm in detail; it is more appropriate to represent the wind farm by 1pu voltage source behind the equivalent impedance.

According to IEC 60909 [93], to determine the maximum short circuit current contribution from induction generators, it is possible to represent the induction generators of the wind farm by a 1pu voltage source in series with the equivalent sub-transient impedance. In [94], an equivalent circuit is used to represent a 50 MW wind farm consisting of Fixed Speed Induction Generator (FSIG) for short

circuit calculations. In [95], a method for calculating the equivalent wind power plant for short circuit studies was described in detail.

3.5.3. Models Used in This Thesis

To represent a large-scale wind farm energised or referenced to voltage source in series with equivalent impedance, the basic concept of wind farm connections has to be understood. Current wind turbines generate electrical power at LV levels of typically 575 V or 690 V, and the power ratings range from 1.5 MW to 5 MW up to 10 MW per turbine.

Several turbines are connected to each other to form a single feeder. Several feeders are connected to the MV bus at 33 kV that is connected to the offshore power plant transformer substation, which steps up the voltage to the transmission voltage level.

In this research programme, the total capacity of the wind farm that needed to be simulated was based on the full load for the GIL transmission system, which is 2.3 GVA. This wind farm is quite large, and it would be time consuming to represent each topology. Therefore, according to Seven Year Statement (SYS), the fault level contribution from the wind farm network was assumed to be about 5.7 kA, which is typical for 33 kV network in the UK transmission system [4]. According to IEC 60909, the X/R ratio is about 8%. Figure 3-11 shows the equivalent circuit of the wind farm represented by the voltage source and equivalent short circuit impedance.

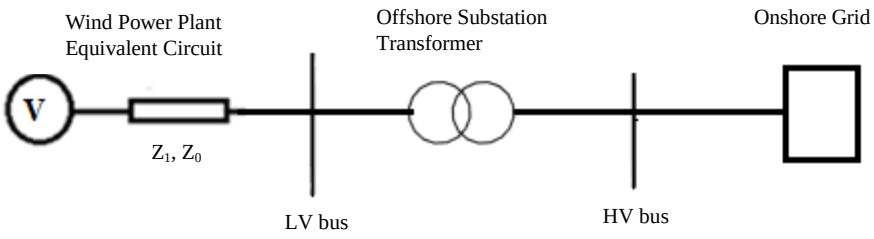

Figure 3-11: Equivalent Circuit of Wind Farm Represented by Voltage Source and Equivalent Short Circuit Impedance

3.6. Circuit Breaker Modelling

A circuit breaker is a mechanical switching device that is capable of breaking or connecting currents under normal or abnormal conditions, such as a short circuit. The level of modelling for the circuit breaker depends on the transient analysis required. Therefore, a guideline was developed by CIGRE to represent the circuit breaker's closing and opening operations for studying transients in different frequency ranges, as shown in Table 3-7 [96].

In the simplest model, the circuit breaker is assumed to be an ideal switch whose impedance changes instantaneously from an infinite value for the open switch condition to a zero value at the closing switch condition. This performance can be represented at any point of a power cycle.

A closing operation can produce transient overvoltages whose maximum peaks depend on several factors, such as the closing instant, the network representation on the source side of the breaker, or the trapped charge on transmission lines in a reclosing operation. The closing instant, which can be different for every pole of

a three-phase breaker, has more influence on the maximum peak of the overvoltages subjected to the power system.

Table 3-7: Modelling Guidelines for Circuit Breakers Proposed by CIGRE [96]

OPERATION	Low Frequency Transient	Slow Front Transient	Fast-Front Transient	Very Fast-Front Transient
Closing				
Mechanical pole spread	Important	Very important	Negligible	Negligible
Prestrikes (decrease of spark overvoltage versus time)	Negligible	Important	Important	Very important
Opening				
High current interruption (arc equation)	Important only for interruption capability studies	Important only for interruption capability studies	Negligible	Negligible
Current chopping (arc instability)	Negligible	Important only for interruption of small inductive currents	Important only for interruption of small inductive currents	Negligible
Restrike characteristic (increase of sparkover voltage versus time)	Negligible	Important only for interruption of small inductive currents	Very important	Very important
High frequency current interruption	Negligible	Important only for interruption of small inductive currents	Very important	Very important

For the closing time span, in general, there is small time delay from the moment at which the contacts start to close to the moment that they finally closed. Transient program allows analysing the influence of this factor and obtaining a statistical distribution of switching overvoltages, usually provided in the form of a cumulative distribution function. Two types of switches can be used to obtain the statistical distribution of the overvoltages:

- Systematic switch, in this switch the closing time is systematically changed from a minimum to a maximum instant in equal increments of time. This switch has been used in this thesis.

- Statistical switch, the closing time is randomly changing according to either a normal (Gaussian) or a uniform distribution. Data required to represent these switches are the mean closing time, the standard deviation, and the number of switching operations.

3.7. Summary

A model for GIL transmission line has been developed in EMTP for both steady state and transient studies. The electrical characteristics of the GIL are frequency dependent. The range of the frequency at which the electrical characteristics will be calculated depends on the phenomena studied. Moreover, XLPE cable and overhead line models were required to build offshore electrical network connected to onshore grid using GIL as the main transmission system.

For transient studies, the way of representing various component of different transmission systems have strong impact in the simulation results. Unlike XLPE cables, the simple coaxial homogenous configuration of the GIL made it possible to represent the model without the conversion procedure used for modelling the XLPE cable.

For switching transient in the offshore wind farm, the terminal behaviour of transformers is required. Therefore, the transformer model has been designed. The magnetizing characteristic, which has a strong influence on the energisation studies, was estimated as accurately as possible. In addition, the capacitance effect of the transformer winding, which is important for surge transfer, was taken into consideration.

The switching transient studies considered in this thesis do not include the medium voltage collector system. This means that the entire wind power plant (WPP) can be represented by an equivalent model that consists of voltage source in series with its equivalent impedance. The impedance was chosen based on the current fault level contribution from the WPP.

CHAPTER 4: STEADY STATE OPERATION FOR LONG GAS-INSULATED TRANSMISSION LINES (GIL)

4.1. Introduction

The rapid growth of renewable energy sources of electrical power, such as offshore wind farms, has brought transmission technology into focus. Proposing GIL as an alternative transmission option not only for short links but also for power transmission over long distances requires extensive investigation. This is necessary to prove the functionality of the planned GIL link in any case and condition during operation. A steady state power flow is one of these studies.

Power flow studies are used to calculate various bus voltages, current, and active and reactive power flow along the transmission system. Power flow analysis is used to determine the condition of a power system operating at steady state [97]. This study is very important in the planning stages for any transmission network.

In this chapter, a model of 420 kV gas-insulated transmission line (GIL) was built using EMTP to carry out a steady state power flow study for different line lengths of a GIL. The electrical characteristics of the GIL are calculated for different factors affecting the steady state conditions. The maximum transmission capacity of the GIL is studied, and a brief comparison with other AC transmission technologies is provided. Moreover, the electrical transmission characteristics under different line lengths are explored. In addition, the effect of different load conditions for line lengths of 300 km and 500 km is studied. Finally, the effect

of variation power factors at the receiving end for line lengths of 300 km and 500 km are examined.

4.2. Effect of Line Length in GIL on Maximum Real Power Transmission

The maximum power flow through a transmission line can be limited by electrical or thermal factors [98]. The electrical limitation factor includes the voltage drop limit and the stability limit. The main reason for the electrical limitation factor in AC transmission systems, such as cables and overhead lines, is their electrical capacitance. As the length of the AC transmission system increases, the capacitive charging current increases; this, in turn, reduces the ability to transmit real power and causes a voltage drop at the load bus.

To determine the maximum transmission power limit against line length for a GIL without reactive power compensation, the method applied was that originally proposed by St. Clair [99] and later analytically derived by Dunlop et al. [100]. The method offers a good approximation for quickly estimating the maximum transmission power limit. Previous papers have shown that the maximum transmission power limit for uncompensated high voltage transmission lines depends only on the line length.

In order to evaluate the maximum length of GIL line for transmitting the thermal power limit, let us refer to the GIL line represented in Figure 4-1. The GIL is connecting two identical voltage sources at both ends. The voltage at the sending end is Vs = $420\angle 0^{o}$kV, and the voltage at the receiving end is Vr = $420\angle \delta^{o}$kV.

The rated current is $3180\angle 0^{o}$ A, corresponding to a thermal power limit "S" of about 2300 MVA at 420 kV.

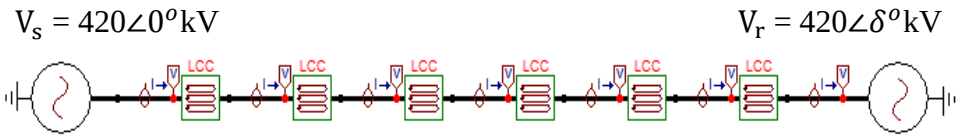

Figure 4-1: GIL Line Model Connecting Two Voltage Sources Modelled in EMTP-ATP.

By adjusting the load angle δ to have maximum power at the receiving end for different line lengths, and since the line is connected between two equal voltage sources, the highest voltage will be seen at the middle of the GIL line.

As the load angle increases, the voltage at the middle of the GIL line increases to reach the voltage limit, which is +5% and –10% as stated by SQSS for the voltage limits in planning and operating the offshore transmission system [101]. Figure 4-2 shows the voltage profile along the 800 km line, which is the maximum length at which the GIL reaches its voltage limit. The maximum active power transmitted through the line is plotted in Figure 4-3.

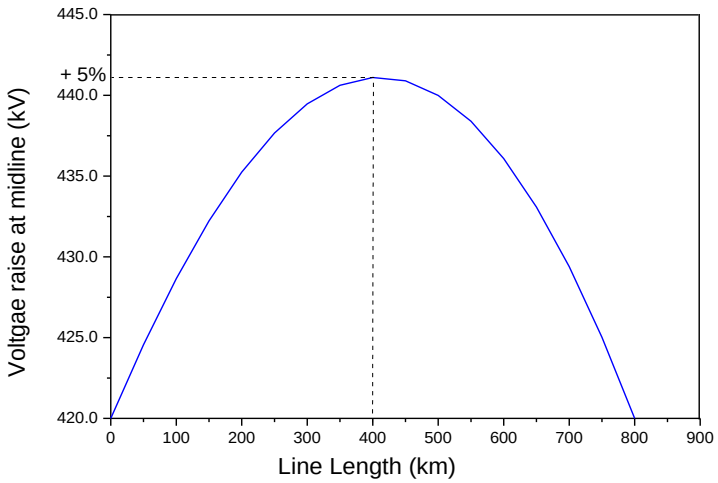

Figure 4-2: Voltage Profile for 800 km GIL Connected between Two Equal Voltage Sources

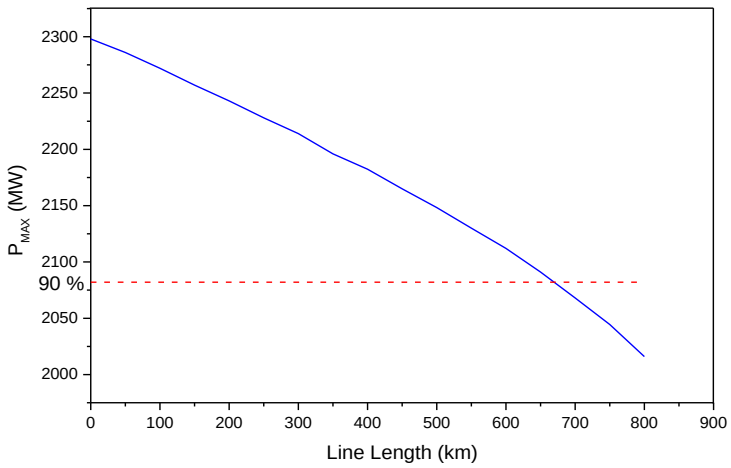

Figure 4-3: Maximum Active Power Transmitted through the GIL Line versus Line Length for 800 km GIL Connected between two Equal Voltage Sauces

It can be seen from Figure 4-3 that the maximum active power transmitted through the line decreases as the line length increases, up to about 800 km where the voltage limit +5% has been reached at the middle of the GIL line. It can be seen also that the GIL can carry active power of up to 2070 MW, which equates to 90% of its thermal power rating for distances of up to 680 km without any shunt reactive power compensation; this demonstrates the high transmission capability of GIL.

4.2.1. Comparison of Maximum Transmission Capacity with other AC Transmission Technology

The production of a large amount of reactive power is the main limitation factor for utilizing HVAC transmission systems over long distances. This can be mitigated by installing reactive compensation at both ends of the transmission line. Increasing the line length beyond this distance requires additional shunt compensation to be installed at the middle of the line length. In an offshore application, it is very expensive to install shunt compensation at the middle of the

line as it requires additional offshore platforms; therefore, economic transmission distances are limited [102], [103].

A comparison study for maximum real power transmission against line length has been made between three different AC transmission systems, with each of the three AC transmission systems transmitting its maximum thermal power limit XLPE cable, overhead line, and GIL, all of them operating at 420 kV.

Long XLPE cables and overhead lines require permanently connected inductive shunt compensation, in order to suppress undesired effects of their reactive power output. Therefore, 50/50% inductive shunt reactors were installed at both terminals for XLPE cable and overhead line to compensate their reactive power output. No reactive power compensation is used for the GIL line. Figure 4-4 shows a comparison of maximum real power transfer for the different transmission systems.

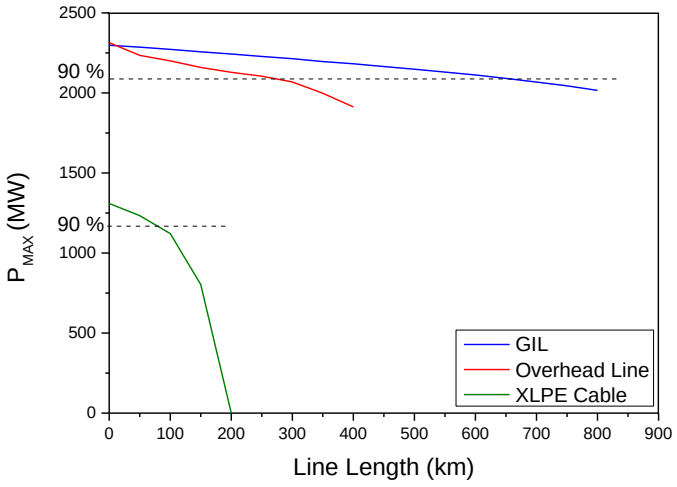

Figure 4-4: Comparison of Maximum Real Power Transfer for Uncompensated 420kV GIL Transmission Line with 50/50 Compensated Overhead Line and XLPE Cable Transmitting their Thermal Power Limit versus Line Length.

As can be seen in Figure 4-4, even though the GIL line is operating without reactive power compensation a big difference is evident between the GIL and

other AC transmission technologies in both the amount of real power that can be transmitted and in the distances. The reason for this is the large cross section of the GIL conductor, which allows transmission of a high amount of real current. At the same time, the reactive current generated by the line capacitance is still small and will not reach the amount of real current transmitted by the GIL even with an increase in the line length.

In the case of XLPE cable, Figure 4-4 shows that the critical distance is achieved before the voltage drop limit. When the reactive current produced by the cable reaches the nominal current at the end of the cable, there is no transmission capacity left for active power transmission; this is called the critical line length [104]. For the considered cable, the critical distance is achieved at 200 km. It can be seen also that 90% of the thermal rated power was reached at about 85 km with 50/50 shunt reactive power compensation connected at both ends.

For the considered overhead line, the voltage drop limit was reached before the critical line length was reached. It can be seen that the voltage drop limit was reached at 435 km and 90% of the thermal rated power was reached at about 280 km also with 50/50 shunt reactive power compensation connected at both ends.

4.3. Electrical Transmission Characteristics for GIL under Different Line Lengths

In this section, the effect of the line length on electrical transmission characteristics for a 100% load condition and a 0.8 typical power factor is studied. A computer model was developed using EMTP-ATP to quantify the voltage, current and power transfer characteristics for different line lengths. In addition, an

analytical method using MATLB was used to calculate the voltage, current and power profiles for GIL line lengths ranging from 200 km to 500 km.

4.3.1. EMTP Simulation Model

The GIL is represented by three single-core GIL lines using a π model. It is divided into sections of 50 km length each. Figure 4-5 shows a GIL model constructed in EMTP-ATP and an assumed sending end voltage of Vs = $420\angle 0^{o}$kVrms. In order to achieve the thermal current limit 3180A at the receiving end with a power factor of 0.8, the load at the end of line was specified as given in Table 4-1. The voltage and current profiles are plotted in Figure 4-6 (a) and (b) respectively and the corresponding real and reactive powers are plotted in Figure 4-6 (c) and (d).

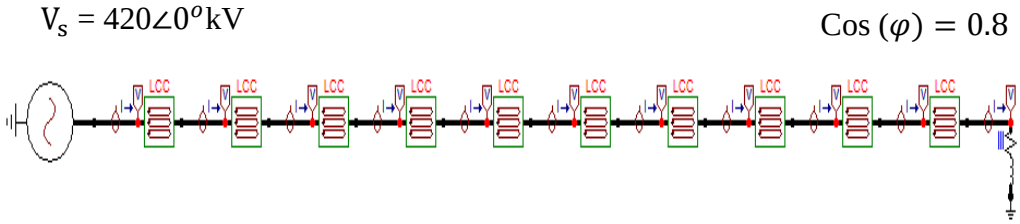

Figure 4-5: GIL Model in EMTP Sectionalized to 50 km each Connected by Load Operating at 0.8 Power Factor.

Table 4-1: Load Connected to the End of Each Line Operating at 0.8 Power Factor

Line Length (km)	Z_{Load} (Ω)
200	55 + j 39.9
300	52 + j 38
400	49.35 + j 36.3
500	47+ j 34.54

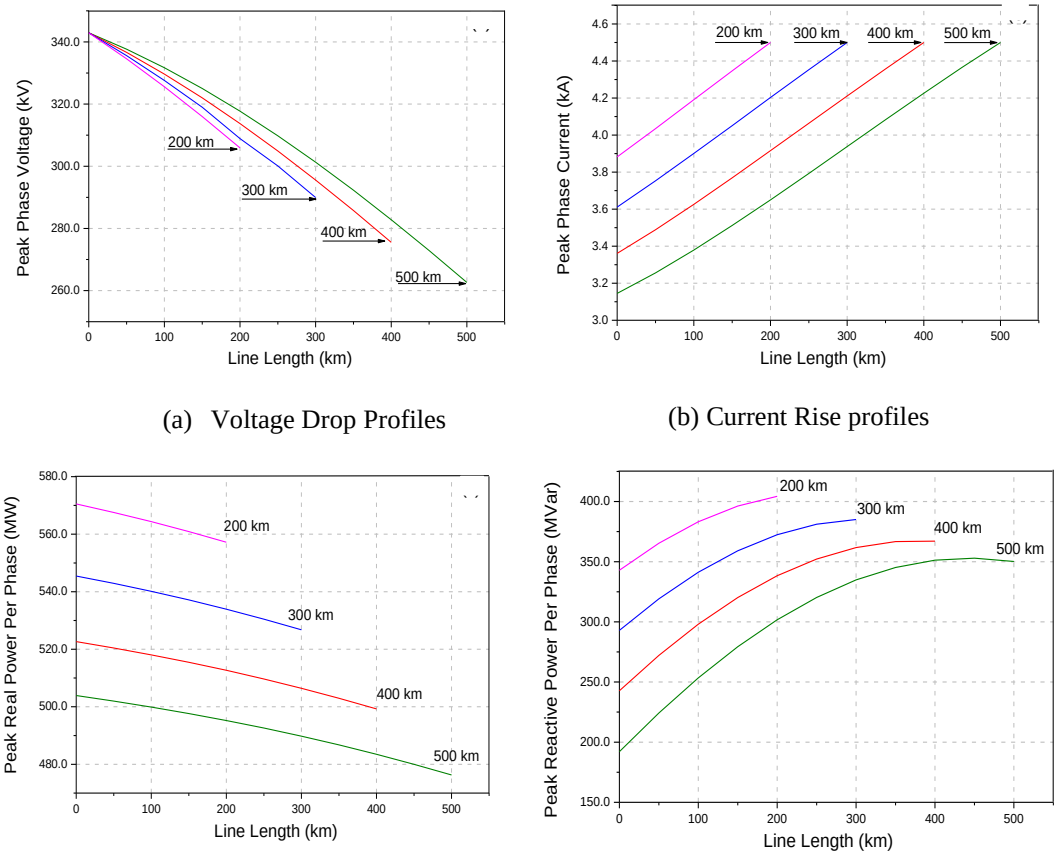

(a) Voltage Drop Profiles

(b) Current Rise profiles

(c) Real Power Losses Profiles

(d) Reactive Power Gain Profiles

Figure 4-6: EMTP-ATP Simulation Results for Electrical Transmission Characteristics of Different GIL Line Lengths Ranging from 200 km to 500 km.

4.3.2. Analytical Method

The analytical method was based on the long transmission line equations that are used to calculate the voltage, current and power profiles for different GIL line lengths [105]. The total series impedance Z and the total shunt admittance Y per phase are calculated based on the per unit line length parameters shown in Table 3-2, and their values are shown in Table 4-2 together with the characteristic impedance, propagation constant, and surge impedance loading.

Table 4-2: The Electrical GIL Line Parameters Used in the Analytical Method.

Longitudinal impedance	$Z = r + j\omega l$	mΩ/km	8.616+j64
Shunt admittance	$Y = g + j\omega c$	mS/km	0 + j0.017
Characteristic Impedance	$Z_0 = \sqrt{Z/Y}$	Ω	61.64 - j 4.1
Propagation Constant	$\gamma = \sqrt{Z*Y}$	1/km	0.0001 + j0.001
Surge Impedance Loading at 420 kV	$SIL = (420kV)^2 / \lvert Z_0 \rvert$	MVA	2893.6

The *ABCD* generalised circuit constants were obtained using the electrical parameters shown in Table 4-2 The relationship between the sending and receiving end quantities given in Equations (4-1) and (4-2) were adopted assuming a maximum sending end voltage of Vs = $420\angle 0^o$kVrms, a maximum receiving end current as determined from the EMTP simulation method shown in Table 4-3, and a power factor of 0.8 at the receiving end. The MATLAB equations are shown in Appendix 5.

$$V_R = A * V_s - B * I_S \tag{4-1}$$

$$I_R = D * I_S - C * V_S \tag{4-2}$$

Table 4-3: Maximum Sending End Current as Determined from the EMTP-ATP Simulation Model.

Line Length (km)	Sending End Current (A)
200	$3145\angle 20.9^o$
300	$3361\angle 24.9^0$
400	$3611\angle 28.2^0$
500	$3882\angle 31^0$

Figure 4-7 (a) and (b) respectively show the calculated voltage and current profiles along the GIL. The active and reactive power flow can be calculated at any point along the GIL using Equations (4-3) and (4-4). Figure 4-7 (c) and (d) respectively show calculated active and reactive power flows on the line where $(\theta_V - \theta_I)$ is the angle by which the current is lagging the voltage.

$$P_R = |V_R| * |I_R| * \text{Cos}\,(\theta_V - \theta_I) \quad (4\text{-}3)$$

$$Q_R = |V_R| * |I_R| * \text{Sin}\,(\theta_V - \theta_I) \quad (4\text{-}4)$$

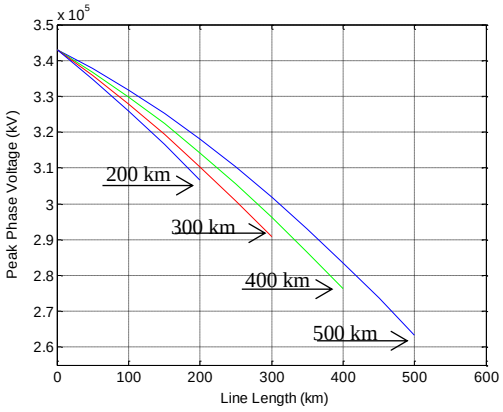

(a) Voltage Drop Profiles

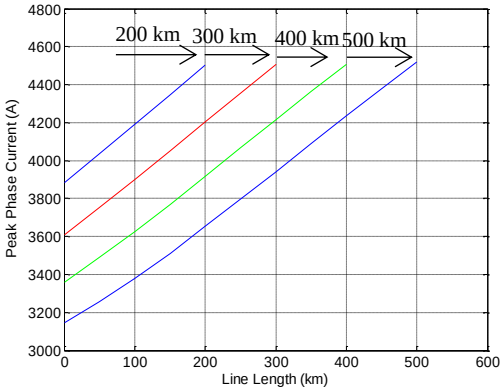

(b) Current Rise profiles

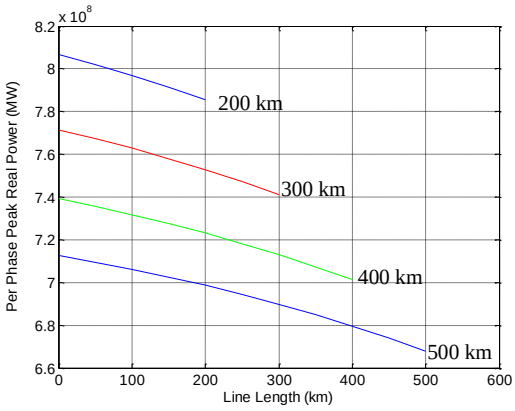

(c) Real Power Losses profiles

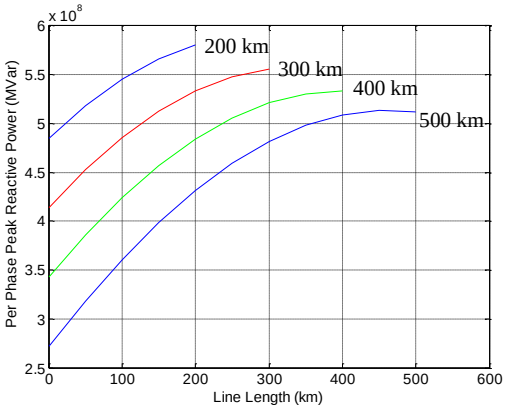

(d) Reactive Power Gain Profiles

Figure 4-7: MATLAB Calculation Results for Electrical Transmission Characteristics of Different GIL Line Lengths Ranging from 200 km to 500 km.

4.3.3. Comparison of Simulation and Analytical Results

The electrical power transfer characteristics of GIL have been studied for lengths ranging from 200 km to 500 km. The electrical power transfer characteristics were calculated using Equation (4-5).

$$\% = (\frac{Receiving\ end}{sending\ end} - 1)*100 \quad (4\text{-}5)$$

A summary of the results obtained is given in Table 4-4. As can be observed, the results of the analytical model agree very closely with the results obtained from the EMTP-ATP simulation method.

Table 4-4: Electrical Power Transfer Characteristics of GIL for Length Ranging from 200 km to 500 km.

Line Length (km)	Voltage Drop ΔV (%)	Current Rise I (%)	Real Power Losses P P (%)	Reactive Power Gain Q (%)
200	-11	+13.9	-2.48	+17.4
300	-15.64	+19.9	-3.33	+30.87
400	-19.81	+25.3	-4.41	+50
500	-23.58	+43.5	-5.6	+82

The voltage profiles along the GIL are shown in Figure 4-6 (a) (EMTP) and Figure 4-7 (a) (analytical equations) for line lengths ranging from 200 km to 500 km. From the figures, it can be seen that there is a fall in the voltage from the sending to the receiving end. The voltage drop percentage increased from -11% for 200 km to -23.58% for 500 km. The voltage drop percentages fall outside of the voltage drop limit + 5% and – 10% stated by SQSS for voltage limits in planning and operating the offshore transmission system [101].

The voltage drop percentage for each line length with this load condition is due to the heavy inductive load. Therefore, in order to maintain the load bus voltage

with the voltage drop limit, shunt capacitor compensation has to be connected to the load bus.

Examination of the current distribution across the line shows that current increases from the sending end to the receiving end until it reached its thermal current limit for each line ling with 100% assumed load condition and a lagging power factor of 0.8 as can be seen in Figure 4-6 (b) and Figure 4-7 (b). The current rise percentage for this load condition increased from +13.9% for 200 km to +43.5 for 500 km. This can be explained by the reactive current generated by the line capacitance being injected into the line.

Real power losses in the GIL are relatively low, as shown in Figure 4-6 (c) and Figure 4-7 (c); for the assumed load condition the percentage real power losses increased from -2.48% for 200 km to -5.6% for 500 km.

Reactive power profiles for different line lengths are illustrated in Figure 4-6 (d) and Figure 4-7 (d). From the figures, it can be seen that there is a reactive power gain from the sending to the receiving end of each line. The reactive power gain from the line shunt capacitance exceeds that consumed by the series inductance. The percentage reactive power gain increased from +17.4% for 200 km to +82% for 500 km. Different line lengths and different load conditions lead to different distribution profiles.

The results shown in Table 4-4 were obtained for 0.8 load power factor and 100% load condition. This load condition results high voltage drop exceeding the voltage drop limit stated by SQSS for all line length considered in this study. Moreover, there is high reactive power gain due to the line shunt capacitance. Therefore, to operate the GIL at this load condition with this load power factor,

reactive power compensation has to be connected to the load bus to maintain the load bus voltage within the voltage drop limit and to reduce the reactive power gain for the line.

Pervious results lead to investigate the effect of different load condition on the electrical transmission characteristics, as well as the effect of different load power factor. Two different line lengths were chosen to carry out these studies 300 km as this length can fulfil transmission distances required for an offshore development scenario in the North Sea and 500 km for future need.

4.4. The Effect of Different Load Conditions for 300 km, 500 km GIL Line Lengths

4.4.1. EMTP-ATP Simulation Model

The EMTP-ATP model shown in Figure 4-5 was used to study the effect of different load conditions on the transmission characteristics for GIL at line lengths of 300 km and 500 km. The load impedances were adjusted as specified in Table 4-5 to have 0% up to 120% load conditions from the 3180 A thermal rated current at the receiving end of the GIL with a typical power factor of 0.8. The sending end voltage is set to Vs = $420\angle 0^{o}$kV. Figure 4-8 shows the effect of different load conditions on the transmission characteristics for GIL at line lengths of 300 km and 500 km.

Table 4-5: Impedance Connected to the End of the 300, 500 km GIL Line for Different Load Conditions.

% Loading	0 %	20 %	40 %	60 %	80 %	100 %	120 %
Z_{Load} (Ω) 300 km	0	312.7 + j234	147.5 + j113	95 + j71.1	67.8 + j51	52 + j38	40.3 + j30.3
Z_{Load} (Ω) 500 km	0	330 + j248.1	158 + j113	95 + j61.1	65 + j48.4	47.3+ j34.5	34.3+ j25.3

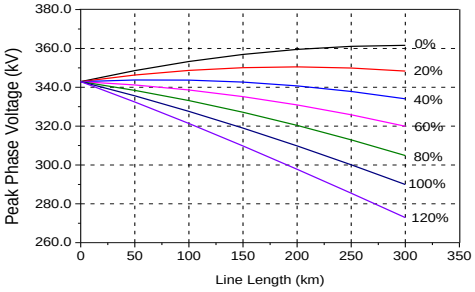

(A) Voltage Profiles for 300 km GIL Line

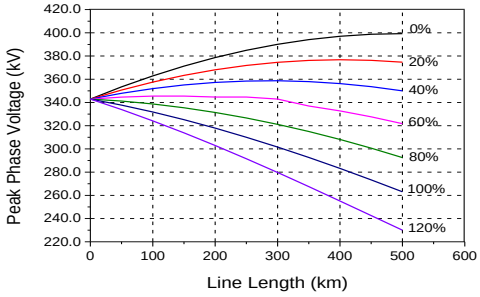

(B) Voltage Profiles for 500 km GIL Line

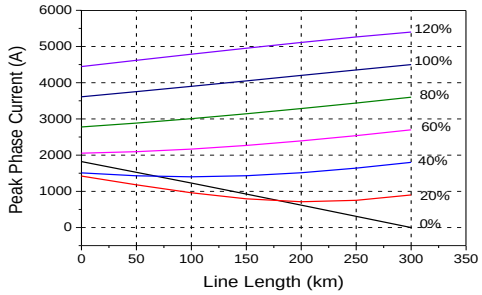

(C) Current Profiles for 300 km GIL Line

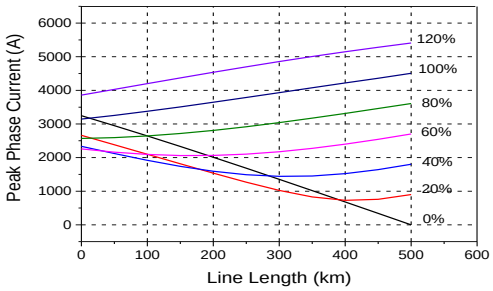

(D) Current Profiles for 500 km GIL Line

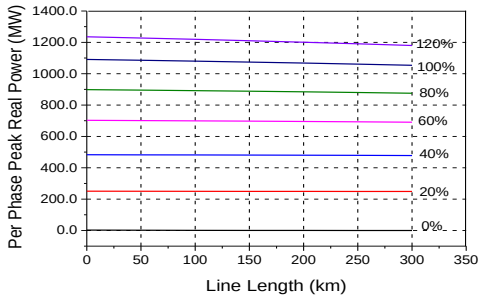

(E) Real Power Profiles for 300 km GIL Line

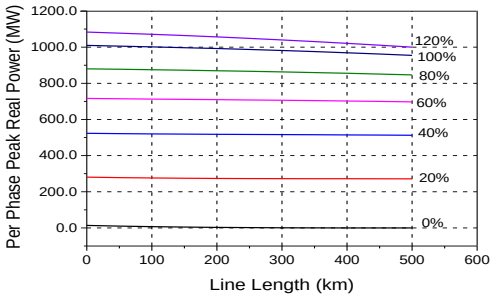

(F) Real Power Profiles for 500 km GIL Line

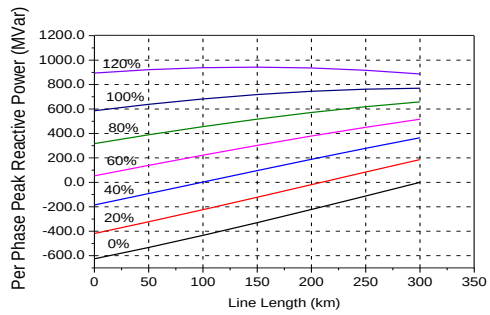

(G) Reactive Power Profiles for 300 km GIL Line

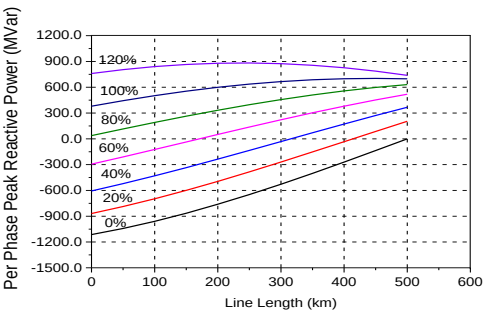

(H) Reactive Power Profiles for 500 km GIL Line

Figure 4-8: Effect of Different Load Conditions on the Transmission Characteristics for GIL at Line Lengths of 300 km and 500 km.

The electrical power transfer characteristics of 300 km and 500 km GIL have been studied for different load conditions. Figure 4-8 (A, B) show the voltage profiles for both line lengths. It can be seen from the figures that the highest voltage were seen at the receiving ends are at 0% load condition which is +5.44% for 300 km and +16.4% for 500 km.

By increasing the load from 20% up to 120%, the voltage continues dropping until it reaches -20.4% voltage drop for 300 km and -32.9% voltage drop for 500 km for 120% load condition and 0.8 power factor.

It should be noted that during the change in the voltage from the case of no load condition to the 120% load condition, the voltage crosses the voltage drop limit +5% and -10%, but at very low load conditions, which are considered non-economic load conditions to operate such a transmission line. Table 4-6 shows the voltage drop at the receiving end of GIL line lengths of 300 km and 500 km for different load conditions.

Table 4-6: Voltage Drop at the Receiving End of 300 km and 500 km GIL Line Lengths for Different Loads.

Length (km)	0 %	20 %	40 %	60 %	80 %	100 %	120 %
300	+ 5.44%	+ 1.57%	- 2.6%	- 6.708%	- 11.1%	-15.63%	- 20.4%
500	+ 16.4%	+ 9.2%	+ 2.05%	- 6.3%	-1 4.7%	- 23.28%	- 32.9%

Figure 4-8 (C, D) show the current profiles for different load conditions. It can be seen that for the case of no load condition, there is no current flow through the line at the receiving end. By increasing the load from 20% to 120%, the current starts increasing from the sending end to the receiving end due to the reactive current generated by the line capacitance until it reaches 18.7% for 300 km and

40% for 500 km at a 120% load condition and a 0.8 power factor. Table 4-7 shows the current increase at the receiving end of GIL line length of 300 km and 500 km for different load conditions.

Table 4-7: Current Rise at the Receiving End for 300 km and 500 km GIL Line Lengths.

Length (km)	0 %	20 %	40 %	60 %	80 %	100 %	120 %
300	0%	-36.7%	19.3%	31.4%	27.6%	20.3%	18.7%
500	0%	-66%	-22.9%	19.7%	48.4%	43.1%	40.1%

The real power profiles are shown in Figure 4-8 (E, F). It can be seen that the real power losses are relatively low; even for a 120% load condition and a 0.8 power factor, the power losses are 4.5% for a line length of 300 km and 7.7% for 500 km, which confirms that the power losses are very low in the GIL transmission line. Table 4-8 shows the real power losses at the receiving end of the 300 km and 500 km GIL for different load conditions.

Table 4-8: Real Power Losses at Receiving End of 300 km and 500 km GILs.

Length (km)	0 %	20 %	40 %	60 %	80 %	100 %	120 %
300	0%	0.8%	1.1%	1.7%	2.5%	3.4%	4.5%
500	0%	2.1%	2.29%	2.51%	3.86%	5.54%	7.75%

The reactive power profiles are shown in Figure 4-8 (G, H). It can be seen that there is an increase in the reactive power from the sending end to the receiving end for every load condition at a 0.8 power factor, except for the 120% load condition.

The highest increase in the reactive power is at the 60% load condition with 355%, which is the worst load condition for 300 km. For 500 km, the worst load

condition was seen at the 80% load condition, with a 213% increase in the reactive power.

For the 120% load condition, the big inductive load connected at the receiving end absorbs all the reactive power generated by the line capacitance. The reactive power generated by the line capacitance is not enough to feed this inductive load. Therefore, the reactive power starts decreasing at the receiving end for both line lengths.

Table 4-9 shows the reactive power at the receiving end of the 300 km and 500 km GILs. Table 4-9 shows that when the GIL is fully loaded, the increase in reactive power at the receiving end is reduced to lower levels.

Table 4-9: Reactive Power at Receiving End of the 300 km and 500 km GILs.

Length (km)	0%	20%	40%	60%	80%	100%	120%
300	0%	145%	279%	355%	108%	31%	-0.8%
500	0%	123%	160.5%	183%	213%	83%	-2.9%

4.5. Effect of variation in Receiving End Power Factor on Transmission Performance for a 300 km and 500 km GIL Lengths

4.5.1. Effect of Lagging Power Factors on Transmission Performance

In this section, the effect of different lagging power factors on the transmission characteristics has been studied for 300 km and 500 km GIL line lengths. The

EMTP model shown in Figure 4-5 was used, and the sending end voltage was set to Vs = $420\angle 0^{o}$kV.

Different inductive loads were adjusted at the receiving end to achieve a load of 3180A, which represents a 100% load condition. The loads connected at the receiving end of GIL as a function of the lagging power factors are shown in Table 4-10. Figure 4-9 shows the effect of the lagging power factors on the transmission performance of 300 km and 500 km GILs.

Table 4-10: Load Connected to the Lines End for Different Lagging Power Factors

Power factor	Z_{load} (Ω) for 300 km	Z_{load} (Ω) for 500 km
Unity	77.31 + j0	87.57 + j0
0.98	69.75 + j14.13	68 + j13.424
0.95	65.5 + j21.67	62.5 + j20.41
0.9	60 + j29.52	56.5 + j26.69
0.8	52 + j37.994	47.3 + j34.54

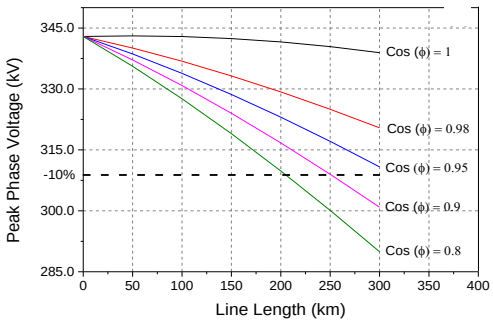

(A) Voltage Profiles for 300 km GIL Line

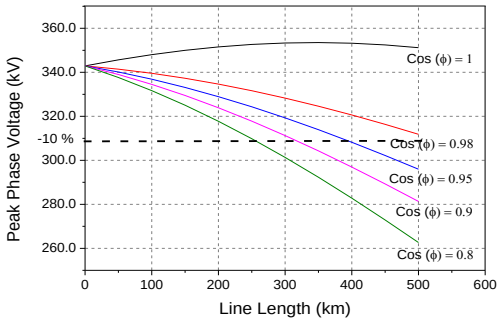

(B) Voltage Profiles for 500 km GIL Line

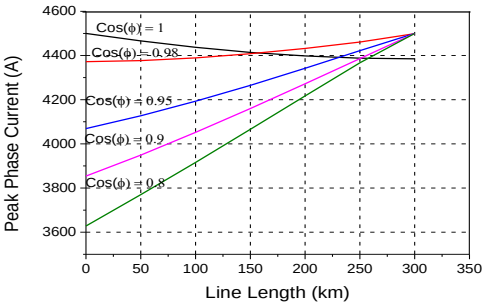

(C) Current Profiles for 300 km GIL Line

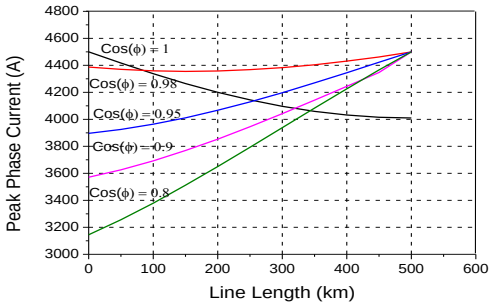

(D) Current Profiles for 500 km GIL Line

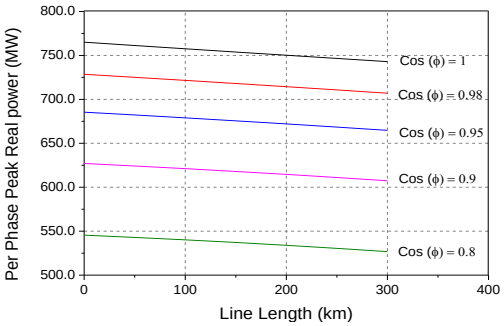

(E) Real Power Profiles for 300 km GIL Line

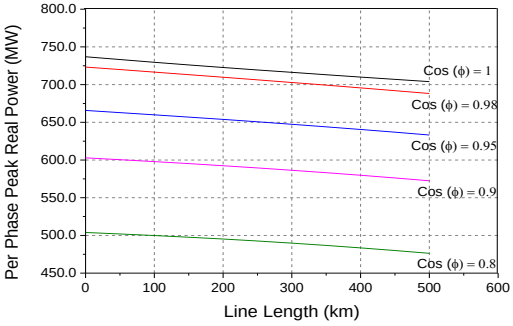

(F) Real Power Profiles for 300 km GIL Line

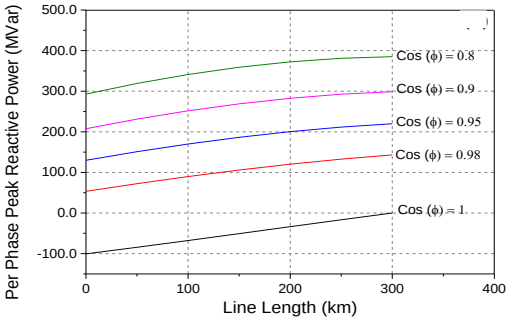

(G) Reactive Power Profiles for 300 km GIL Line

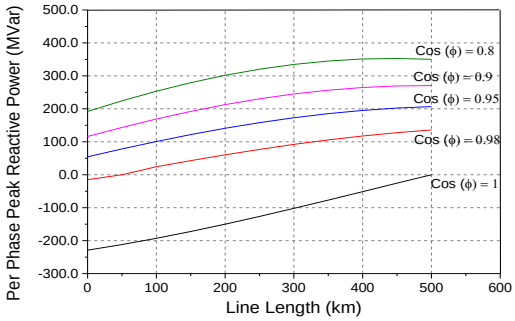

(H) Reactive Power Profiles for 300 km GIL Line

Figure 4-9: Effect of Different Lagging Power Factors on Electrical Transmission Characteristics for 300 km and 500 km GIL Line Lengths.

The relationship between the voltage drop and the different lagging power factors for both line lengths is shown in Figure 4-9 (A, B). From the voltage profile of 300 km, it can be seen that there is drop in the voltage from the sending end to the receiving end. This drop increased from -1.2% for a unity power factor to a -15.45% voltage drop for a 120% load condition and a 0.8 lagging power factor.

According to the voltage drop limit stated by SQSS, which is +5% and -10% for planning and operating offshore transmission systems [101], 300 km GIL can be operated as an offshore transmission system with a lagging power factor limit between unity and 0.95 without the need for any reactive power compensation support at the load bus.

For 500 km, the drop in the voltage increases from +2.4% for a unity power factor to -23.4% for a 0.8 lagging power factor. From the voltage profiles, it can be seen that the limit of the lagging power factor to operate the 500 km GIL as an offshore transmission system without the need for any reactive power compensation support is between unity and 0.98. Table 4-11 shows the voltage drop at the receiving end of 300 km and 500 km due to the variation in the lagging power factors.

Table 4-11: Voltage Drop at Receiving End of 300 km and 500 km for Different Lagging Power Factors.

Length (km)	Cos (φ) = 1	Cos (φ) = 0.98	Cos (φ) = 0.95	Cos (φ) = 0.9	Cos (φ) = 0.8
300	-1.2%	-4.9%	-9.2%	-12%	-15.45%
500	2.4%	-8.78%	-13.7%	-17.2%	-23.4%

Figure 4-9 (C, D) show the current distribution profiles for both line lengths. It can be seen that for a unity power factor, there is a 2.9% loss in the current flow from the sending end to the receiving end for the 300 km line length, which means that the real current flows through a mostly resistive impedance.

For other power factors, it can be seen that there is an increase in the current from the sending end to the receiving end. This increase starts from +3.26% for a 0.98

lagging power factor to +20.62% for a 0.8 lagging power factor due to the reactive current generated by the line capacitance.

For 500 km GIL line length at a unity power factor, there is a loss in the current from the sending to the receiving end of -10.88%. For a 0.98 lagging power factor, the current increases from +7.67% to +43.1% for a 0.8 lagging power factor as shown in Table 4-12.

Table 4-12: Current Gain at Receiving End of 300 km and 500 km for Different Lagging Power Factors.

Length (km)	Cos (φ) = 1	Cos (φ) = 0.98	Cos (φ) = 0.95	Cos (φ) = 0.9	Cos (φ) = 0.8
300	-2.56%	3.26%	10.59%	16.28%	20.62%
500	-10.88%	7.76%	15.5%	26%	43.1%

The real power profiles for the 300 km and 500 km line lengths are shown in Figure 4-9 (E, F). It can be seen that the percentage real power losses are relatively low; even for 500 km and a 0.8 power factor, the power losses are 5.5%. The figures show the effect of the variation in power factors on the amount of real power that can be transmitted through the GIL. Table 4-13 shows the real power losses for the different lagging power factors for both line lengths.

Table 4-13: Real Power Losses for Different Lagging Power Factors for 300 km and 500 km GILs.

Length (km)	Cos (φ) = 1	Cos (φ) = 0.98	Cos (φ) = 0.95	Cos (φ) = 0.9	Cos (φ) = 0.8
300	2.88%	2.95%	3.05%	3.016%	3.31%
500	4.47%	4.89%	4.91%	4.97%	5.55%

The reactive power profiles along the 300 km and 500 km lines GIL are shown in Figure 4-9 (G, H). For the 300 km line, it can be seen that for unity power factor, the reactive power received at the receiving end is zero.

For the remaining power factors considered here, it can be seen that there are positive reactive power flows out from both ends of the GIL line, which means there is a demand for capacitive reactive power compensation. The reactive power demand is decreased by reducing the power factor, which means increasing the line capacitance. Even though there is a high demand for capacitive reactive power compensation, the voltage at the load bus is still within the voltage drop limit from 0.95 lagging up to unity power factor.

For 500 km, it can be seen that the demand for capacitive reactive power compensation increases as the line length increases. The power factor operating limit decreases between 0.98 and unity power factor. Table 4-14 shows the reactive power demand for different lagging power factors for 300 km and 500 km GIL.

Table 4-14: Reactive Power Demand for Different Lagging Power Factors for 300 km and 500 km GIL.

Length (km)	Cos (φ) = 1	Cos (φ) = 0.98	Cos (φ) = 0.95	Cos (φ) = 0.9	Cos (φ) = 0.8
300	0%	+180%	+72%	+45%	+31%
500	0%	+700%	+280.5%	+161.4%	+82.3%

4.5.2. Effect of Leading Power Factors on Transmission Performance

In this section, the effect of different leading power factors on the transmission characteristics is investigated for 300 km and 500 km GIL line lengths. Different capacitive loads are adjusted at the receiving end to achieve a load of no more than 3180 A, which represents a 100% load condition.

The loads connected at the receiving end of the GIL as a function of the leading power factors are shown in Table 4-15. Figure 4-10 shows the effect of leading power factors on the transmission performance of 300 km and 500 km GIL line lengths.

Table 4-15: Load Connected to the Line End for Different Leading Power Factors.

Power factor	Z_{load} (Ω) for 300 km	Z_{load} (Ω) for 500 km
Unity	77.31 – j0	87.57 – j0
0.98	88.25 – j0.0568	127 – j0.03925
0.95	93.5 – j0.0327	152.75 – j0.0201
0.9	97.5 – j0.0214	176 – j0.01224
0.8	98 – j0.01365	204 – j0.00659

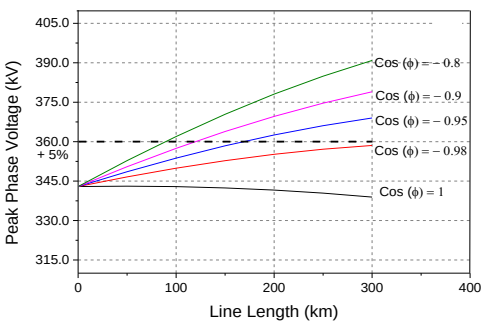

(A) Voltage Profiles for 300 km GIL Line

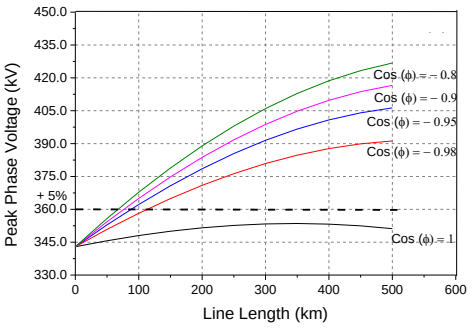

(B) Voltage Profiles for 500 km GIL Line

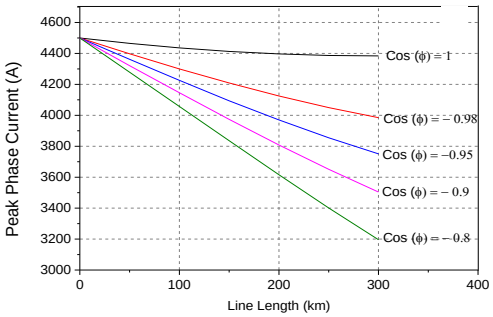

(C) Current Profiles for 300 km GIL Line

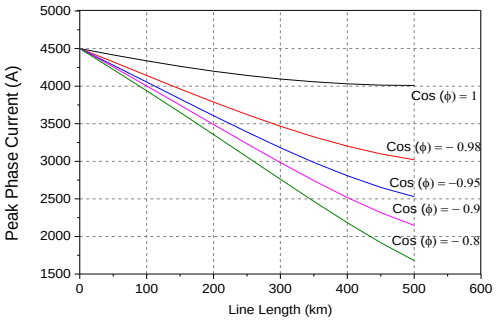

(D) Current Profiles for 500 km GIL Line

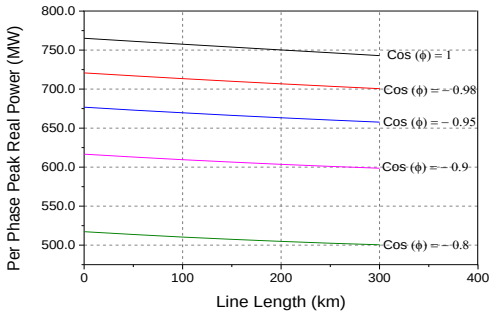

(E) Real Power Profiles for 300 km GIL Line

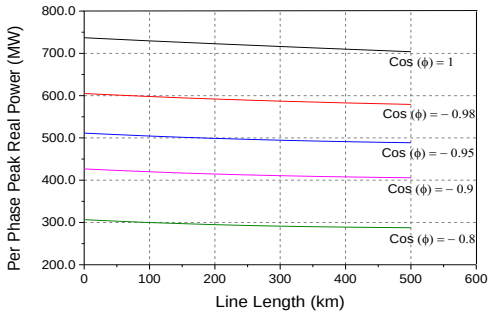

(F) Real Power Profiles for 300 km GIL Line

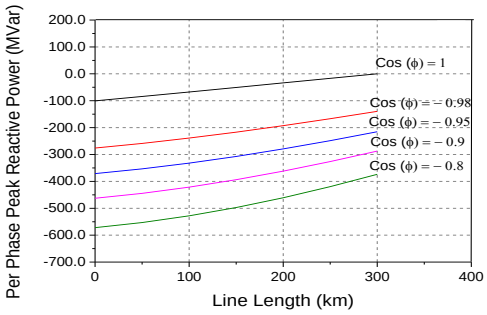

(G) Reactive Power Profiles for 300 km GIL Line

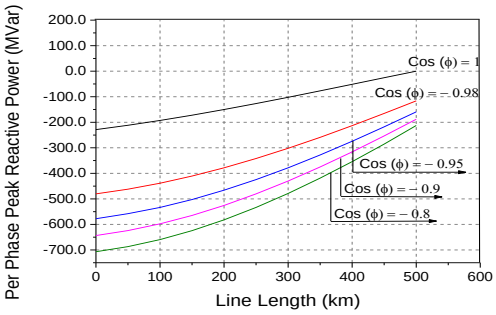

(H) Reactive Power Profiles for 300 km GIL Line

Figure 4-10: Effect of Different Leading Power Factors on Electrical Transmission Characteristics for 300 km and 500 km GIL Line Lengths.

Leading power factors cause an increase in the voltage from the sending end to the receiving end of the line, as shown in Figure 4-10 (A, B). For 300 km, the increase in the voltage starts from -1.2% for unity power factor to +14% for 0.8 leading power factor.

For 500 km, the increase in the voltage is increased from +2.4% for unity power factor to +24.5% for a 0.8 leading power factor. Table 4-16 shows the voltage drop at the receiving end of the 300 km and 500 km lines for different leading power factors.

The voltage drop limit stated by SQSS for planning and operating offshore transmission systems is +5% and -10**%.** Table 4-16 shows that the operating power factor ranges from unity to a 0.98 leading power factor for the 300 km line length, where the voltage at the load bus falls within the voltage drop limit, which is +5%. For the 500 km line length, the voltage increase falls out of the voltage drop limit except for unity power factor.

Table 4-16: Voltage Drop at Receiving End of 300 km and 500 km for Different Leading Power Factors.

Length (km)	Cos (φ) = 1	Cos (φ) = -0.98	Cos (φ) = -0.95	Cos (φ) = -0.9	Cos (φ) = -0.8
300	-1.2%	4.55%	7.6%	10.5%	14%
500	2.4%	14.1%	18.5%	21.5%	24.5%

Operating GIL with leading power factor will lead to the highest current being seen at the sending end as shown in Figure 4-10 (C, D). For the 300 km line length, the current losses increased from the sending end to the receiving end by -2.65% for unity power factor to -29% for a 0.8 leading power factor. For the 500 km line length, the current losses increased from the sending end to the receiving end by -10.88% for unity power factor to -62.7% for a 0.8 leading power factor as shown in Table 4-17.

Table 4-17: Current Losses at Receiving End of 300 km and 500 km for Different Lagging Power Factors.

Length (km)	Cos (φ) = 1	Cos (φ) = -0.98	Cos (φ) = -0.95	Cos (φ) = -0.9	Cos (φ) = -0.8
300	-2.56%	-11.45%	-16.6%	-22%	-29%
500	-10.88%	-32.89%	-43.5%	-52.3%	-62.7%

The real power profiles for the 300 km and 500 km line lengths operated at different leading power factors are shown in Figure 4-10 (E, F). Table 4-18 shows real power losses at the receiving ends of both line lengths. It can be seen that the percentage real power losses is relatively low even for the 500 km line length where the power loss is 5.5% at a 0.8 leading power factor.

Table 4-18: Real Power Losses for Different Leading Power Factors for 300 km and 500 km GIL.

Length (km)	Cos (φ) = 1	Cos (φ) = -0.98	Cos (φ) = -0.95	Cos (φ) = -0.9	Cos (φ) = -0.8
300	2.88%	2.8%	2.81%	2.9%	3.3%
500	4.47%	4.5%	4.7%	4.9%	5.5%

The reactive power profiles are shown in Figure 4-10 (G, H) for leading power factors. It can be seen that the percentage of the reactive power gain decreases by the decreasing leading power factor from -49.5% for a 0.98 leading power factor to -34.7% for a 0.8 leading power factor for the 300 km line length.

For the 500 km line length, the reactive power gain decreases from -75.8% for a 0.98 leading power factor to -69.8% for a 0.8 leading power factor. Table 4-19 shows the reactive power gain for different leading power factors at the receiving ends for both line lengths. It should be noted that the reactive power gain in the

case of a leading power factor is smaller than the reactive power gain in the case of a lagging power factor due to the local capacitive reactive power supply at the load bus.

Table 4-19: Reactive Power Gain for Different Leading Power Factors for 300 km and 500 km GIL line lengths

Length (km)	Cos (φ) = 1	Cos (φ) = -0.98	Cos (φ) = -0.95	Cos (φ) = -0.9	Cos (φ) = -0.8
300	0%	-49.5%	-42%	-37.9%	-34.7%
500	0%	-75.8%	-72.2%	-70.7%	-69.8%

4.6. Summary

AC transmission technologies such as overhead line and XLPE cable are limited in their transmission capacity and transmission distances. The main reason for this limit is their high shunt capacitance. As the length of the AC transmission system increases, the capacitive charging current increases; this, in turn, reduces the ability to transmit real power and causes a voltage drop at the load bus. Shunt reactive power compensation has to be connected to the load bus to regulate the voltage within acceptable voltage drop limit and to transmit more real power for these transmission technologies.

This limit for utilizing AC transmission technologies for long distances without any need for reactive power compensation can be addressed by introducing GIL as a transmission system. GIL has lower shunt capacitance than XLPE cable by four times which make the reactive power generated by the GIL shunt capacitance less by four times than the reactive power generated by XLPE cable for the same voltage level. The high amount of real power that can be transmitted by a single

circuit of GIL is another advantage of utilizing GIL over other underground or submarine transmission technology.

The effects of different factors on the transmission characteristics, such as line length, load conditions, and variable power factors, have been studied for 420 kV gas insulted transmission line and with no reactive power compensation. It can be concluded from the results obtained that to operate the voltage profile of long GIL transmission line within the voltage drop limit of +5% and -10% stated by SQSS for planning and operating offshore transmission systems without any need for reactive power compensation, the acceptable operating power factor at the receiving end is ranging from 0.95 lagging to 0.98 leading power factor for a 300 km line length with 100% load condition.

As the line length increases, the range of acceptable power factors decreases. For operating a 500 km gas insulated transmission line with no reactive power compensation, the operation power factor at the receiving is ranging from 0.98 lagging to 0.98 leading power factor. Both line lengths were operated at a 100% load condition to reduce the reactive power produced by the line to the lower level.

Due to the fact that wind farms have a variable output and they will not operate at their full nameplate capacity, so the GIL transmission line in this case will not be operated at its 100% load condition. Therefore, for lower load condition higher voltage drop will be seen at the load bus which may require reactive power compensation to be connected to the load bus to maintain the bus voltage within the acceptable voltage drop limit.

CHAPTER 5: SWITCHING TRANSIENTS IN LONG GIL CONNECTING OFFSHORE WIND FARMS

5.1. Introduction

The electrical transient is a short period of oscillation in a system caused by a sudden change in voltage, current or load due to the switching operation or a fault occurring on the system [79]. The transient duration is short compared to the operating period of the system under steady-state conditions, but it is in the course of such events that network components are subjected to high stress from extreme currents or voltages, which may lead to permanent equipment damage.

Switching overvoltages are a result of the operation of switching devices during normal conditions or are a result of fault clearings. These transients last from ten to thousands of microseconds [106]. In an extra high voltage (EHV) transmission line, the switching impulse withstand voltage (SIWV) is generally lower than the lightning impulse withstand voltage (LIWV). It is the SIWV that governs the insulation design of an EHV transmission line, as the overvoltage caused by lightning strikes is independent of the power system voltage.

Moreover, the transmission line insulation has its lowest breakdown strength under surges whose fronts fall in the range 50-500 μs which is typical for switching surges [107]. According to (IEC) recommendations, all equipment designed for operating voltages above 245 kV should be tested under switching impulses [106]. The specification of an insulation level capable of withstanding switching surge overvoltages has a significant influence on the capital cost of

transmission lines. Therefore, an accurate estimate of the switching overvoltages expected under various operating conditions is an important stage in the design of new transmission systems.

Offshore wind farms are steadily increasing in capacity and distance from the shoreline [108]. GIL is proposed as an alternative transmission system to the conventional submarine cables for offshore wind farms. GILs are coaxial gas insulated pipes that must be capable of withstanding the electrical field caused by transient conditions. During transient conditions, electromagnetic waves are propagated and reflected throughout the system, negatively affecting the insulation gas, in some extreme transient conditions, this may lead to a failure in the insulation medium.

The aim of this chapter is to carry out studies on the behaviour of the transients due to the energisation of a 300 km 420 kV GIL connecting offshore wind farms to the onshore transmission system. The two major objectives of this research are now presented.

First, development of a computer model, using the EMTP-ATP transient simulation program, of a GIL connecting offshore wind farms to the onshore transmission system. This includes models for circuit breakers, XLPE cable, overhead line, transformers and equivalent offshore wind farm.

Secondly, an extensive study of gas insulated transmission line (GIL) is carried out with a view to provide useful information on switching overvoltage distribution based on the statistical method, as suggested by the IEC standards[106], [107]. The modelling of the offshore and onshore power system

networks employing the statistical evaluation of overvoltage data is to be carried out.

5.2. Analysis of Switching Transient Overvoltages

5.2.1. An Overview of Statistical Switching Studies

Switching overvoltage studies are of primary importance in electric power insulation co-ordination. Studies are normally performed with particular interest in avoiding breakdown, or minimising transient stress on the insulation systems as well as the transmission and distribution equipment. In general, characterisation of overvoltage stress may be performed by the following means [112]:

- The maximum peak values;
- A statistical overvoltage of the peak values;
- A statistical overvoltage generated by particular events with a peak value that has a 2% probability of being exceeded.

The latter method has been used in studying the influence of the cable length and the risk of insulation failure of the transmission on MV and HV lines.

5.2.2. Switching Phenomena and Statistical Methods

Switching surges are random in nature as they are affected by many different factors. Two factors to be further investigated in this work are:

- The pole span of the circuit breaker (CB) which refers to the time between the first and the third pole to close.
- The point-on-wave (POW) of switching angles on the 3-phase closure.

In practice, the breaker poles will not close simultaneously. There will be a small time gap between poles during the 3-phase closure. The high speed closing of contacts and their closing time are governed by their mechanical tolerances.

The second parameter considered is the closing angle, which refers to the point-on-wave where the CB starts to close. If a contact initiates a close at the peak of the power frequency (50 Hz) voltage, the corresponding phase will experience higher transient magnitude.

Due to the random behaviour of CB poles during switching, probability analysis is the most practical way in providing useful data on switching overvoltgaes. In practice, there are several analytical methods. However, the statistical study approach is the most common which was adapted in this study. Random closing of contacts can be assumed to follow the normal distribution.

In the statistical approach, statistics are used to evaluate the switching surges to obtain relevant data such as those suggested by IEC standards for insulation coordination. The range of values required include the maximum value, 2% probability value, mean amplitude as well as the standard deviation. Scattering characteristics of CB poles, normally assumed as normal distribution (Gaussian). Cumulative probability distribution of overvolatges is calculated and compared with the ability of the system to withstand transient overvoltages.

5.3. Description of Electrical Network Modelled in EMTP

Figure 5-1 shows a model for the interface between offshore and onshore transmission networks using a 300 km 420 kV submarine GIL, consisting of three single-core coaxial lines. The model described here was created to explore the

level of overvoltages seen when energizing the long GIL transmission system connecting the main offshore platform substation to the first onshore connection point (PCC).

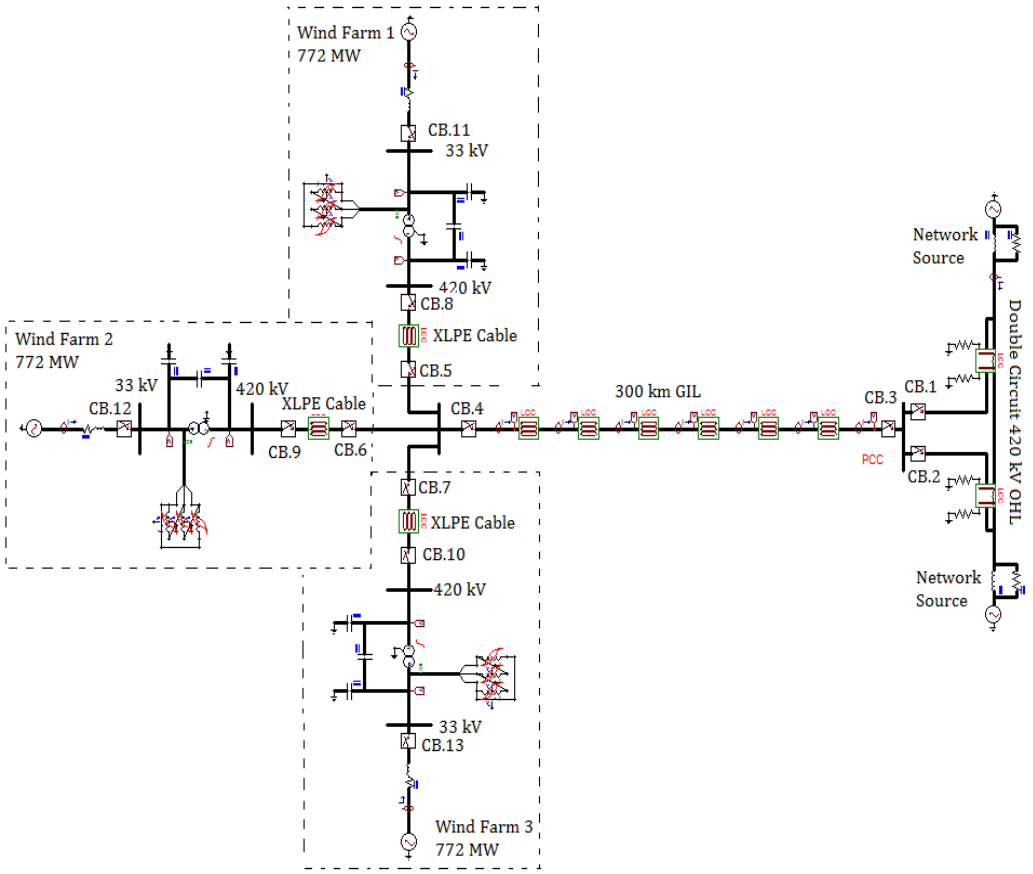

Figure 5-1: Interface Model between 420 kV Offshore and Onshore Networks

The onshore transmission system is represented using two network equivalents connected by a 420 kV double circuit overhead line with 60 km length each. Each network equivalent is a voltage source behind impedance. The impedance consists of the inductance representing the network fault level in parallel with a resistance representing the network surge impedance [88].

It is assumed that the fault level contribution is shared equally between the two equivalent sources. According to the Seven Year Statement (SYS), the network fault level is assumed to be 19.85GVA, which is typical for the UK transmission

system [113]. It should be noted that a detailed description of the network model components is presented in Chapter 3.

The 420 kV bus bar at the PCC is connected to one of the double circuit overhead lines through one of the circuit breakers CB1, CB2. The GIL system is represented by a three-phase single core line using a JMarti frequency-dependant model, with modal transformation matrices calculated at 20 kHz. It is divided into six sections with 50 km each and connects the main offshore substation to the onshore interface substation through CB3 and CB4.

The wind farm is divided into three clusters, each with a capacity of 772 MW. Three XLPE cables, each 10 km in length and having CSA 2,500 mm^2, are also modelled using the JMarti model with modal transformation matrices calculated at 20 kHz. The XLPE cables connect the three offshore wind farm substations to the main offshore platform substation through three circuit breakers CB5, CB6 and CB7.

The 420/33 kV (Yd) transformer at the offshore substations is modelled using the BCTRAN component. The saturation effect is included using nonlinear inductors connected externally to the lowest voltage winding. Core losses are modelled as resistance within each BCTRAN component. Winding capacitances are connected externally. Three circuit breakers CB8, CB9 and CB10 connect each wind farm substation to the main offshore substation through the XLPE cables.

Each wind power plant is represented by a voltage source behind the impedance representing the short circuit current contribution from the wind farm. According to (SYS), the short circuit current is assumed to be 5.7 kA [113].

Three 33 kV circuit breakers CB.11, CB.12 and CB.13 are used to connect the equivalent wind farms to the collection of offshore substations. The 420 kV and 33 kV circuit breakers are represented as ideal switches.

5.4. Circuit Breakers Sequences Operation Study

The following scenarios are considered:

- Energisation of GIL submarine transmission line
- Energisation of main offshore platform
- Energisation of XLPE cables connecting the offshore wind farm substation to the main collection platform.
- Energisation of 420/33 kV offshore wind farm transformers

The energisation scenario assumes that, since the circuit breakers isolate the network components from each other, the circuit may be energised in sections. This happens by first energising the GIL submarine transmission line by closing the 420kV circuit breaker (CB3).

Closing the 420 kV offshore circuit breaker (CB4) will energize the main offshore collection platform. Through the 420 kV offshore circuit breakers CB5, CB6 and CB7, the XLPE cables will be energised.

The 420/33 kV wind farm transformers will be energized through the 420 kV offshore circuit breakers CB8, CB9 and CB10. The offshore wind farms will be connected to the offshore substations through the 33 kV circuit breakers CB11, CB12, and CB13.

5.5. Energisation Scenario

Energisation of the 300 km GIL causes a transient overvoltage with amplitude dependent on the pole-closing instant in each phase. If energisation occurs at a moment when the voltage across the open CB terminals is high, a large amplitude travelling wave will be injected into the transmission line. When this wave reaches the open far end of the line it is reflected, and a transient overvoltage may thus be experienced [101].

To investigate the maximum overvoltage generated during energisation of the 300 km GIL without taking the pole-span delay between phases in consideration, an ideal circuit breaker model was used. The pole-span between the closing of the circuit breaker phases was selected to be zero. The GIL was energized at 20ms where the voltage for phase A at the source side was at its peak value and the line-side voltage is initially zero. Figure 5-2 shows voltage in phase A at the sending and the receiving end of the 300 km GIL, when the circuit breaker is closed at the instant of peak voltage.

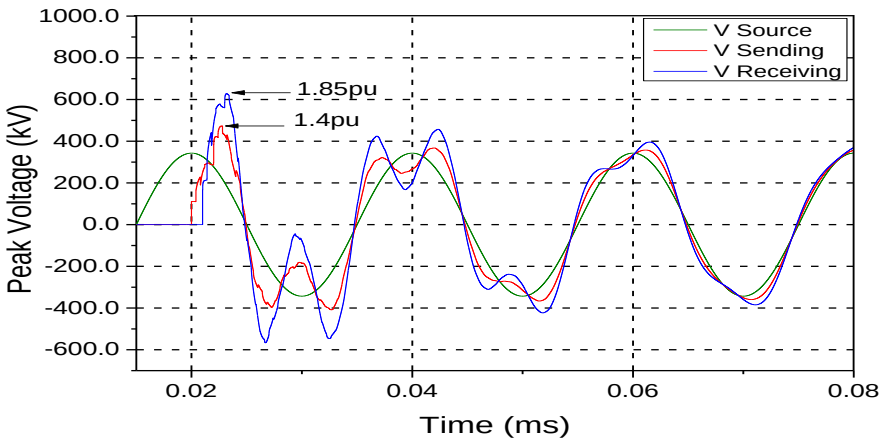

Figure 5-2: Voltage at Sending and Receiving End of a 300 km GIL, Circuit Breaker Closed at Instant of Peak Voltage

As can be seen from Figure 5-2, the highest peak overvoltage recorded at the sending end of the 300 km GIL is 1.4pu and at the receiving end is 1.85pu. The three phases of the circuit breaker were assumed to close at the same time with no pole-span. In practice, however, the three poles of a circuit breaker close with a delay, due to mechanical dispersion and the occurrence of pre-strikes. The pole span is defined as the time between the closing times of the first and the last poles.

5.5.1. Sensitivity of Switching Transient to Pole Span

All switching surges are products of circuit breaker operations. As results of random variations in the circuit breakers poles, a higher transient overvoltage may occur in the power system. The worst-case values of these transient overvoltages depend on several factors, such as the closing instant of each circuit breaker pole, the network configuration on the source side of the circuit breaker, and the amount of trapped charge remaining on the transmission line to be energised [102].

Therefore, the sensitivity of the transient overvoltages distributed as a function of the circuit breaker closing time was studied. A systematic switch was placed at the interface point between the onshore and the offshore networks (PCC) to determine the range of overvoltages from different circuit-breaker pole closing times in the energisation of the 300 km GIL. The combination of switching times at which the highest overvoltage occurs is thus determined.

Switching across one third or half of the waveform would probably be acceptable if symmetry is assumed; however, trapped charge is explored by simulating a single breaker opening event prior to statistically re-closing the circuit breaker. In

this case, switching across the whole waveform is required. The switching time varied from 20ms to 40ms in time increments of 2ms giving 1000 switching operations with different pole closing times. For each simulated switching operation, the maximum phase voltage was recorded at each node, giving 3,000 recorded voltages per node.

The switching overvoltages distributed across the network for three different measurement points are shown in Figure 5-3. The frequency of occurrence shown in Figure 5-3 is the number of simulated switching events walling into each overvoltage range.

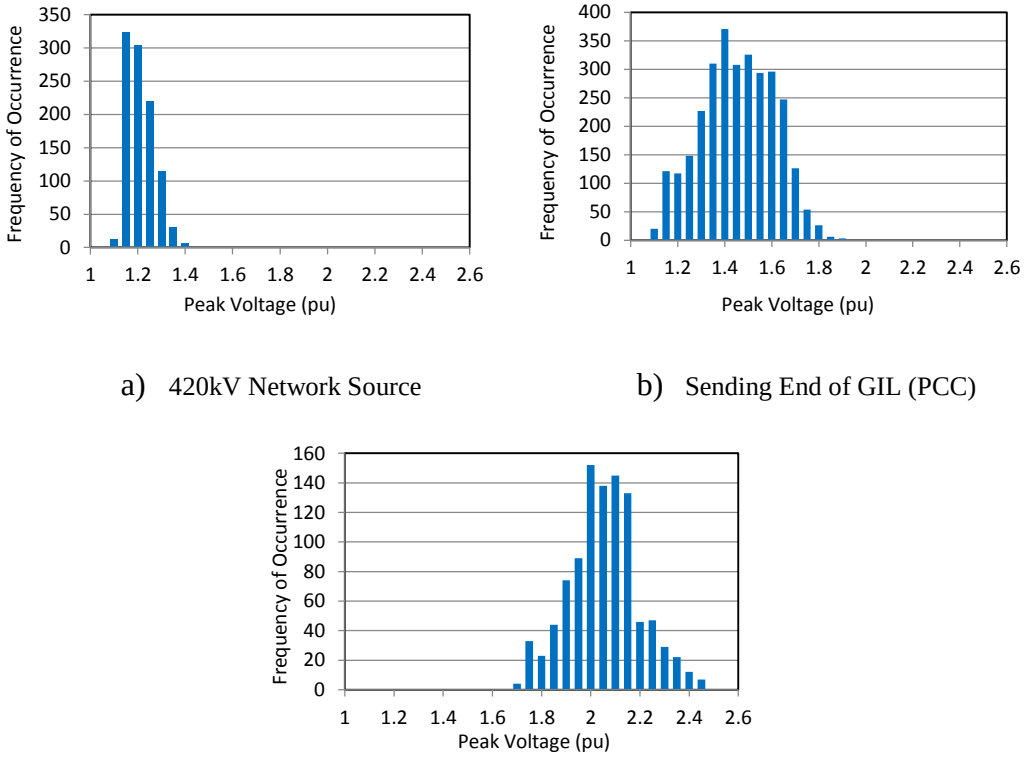

Figure 5-3: Range of Peak Overvoltage Over all Phases for 1000 Systematic CB Closing Combinations (Energisation of the 300 km GIL).

The over-voltages were calculated in per unit for peak phase voltage. Figure 5-3 (a) shows that there is impact on the 420 kV network sources where the highest

overvoltage recorded is 1.4pu. In addition, it can be seen that the most frequently occurring voltage is in rang between (1.15-1.20pu).

Figure 5-3 (b) shows the overvoltage distributed at the sending end of the GIL where the highest overvoltage recorded is 1.9pu and the most frequently recurring voltage is in range (1.4-1.45pu). It should be noted that the overvoltage increases by about 35% at the sending end (from 1.4pu to 1.9pu) when pole-span is taken into consideration.

The highest overvoltage seen at the open receiving end of the GIL is 2.45pu, and the most frequently recurring voltage is in range (2.0-2.1pu) as shown in Figure 5-3 (c). The highest overvoltage was increased also by about 30% from 1.85pu to 2.45pu when the pole-span was taken into consideration.

5.5.2. Energisation of XLPE Cables Connecting Offshore Wind Farm Substations to the Main Offshore Substation

Energisation three 10 km XLPE cables from the already energised 420 kV bas bar at the collecting offshore platform can be done by turning on CB5, CB6 and CB7. To determine the highest overvoltages that may occur at the receiving end of the XLPE cables due to the effect of pole-span and the combination of switching times at which the highest overvoltage occur a systematic study similar to previous study is carried out by replacing CB5 with systematic switch. The switching overvoltages distributed across the network for four different measurement points are shown in Figure 5-4.

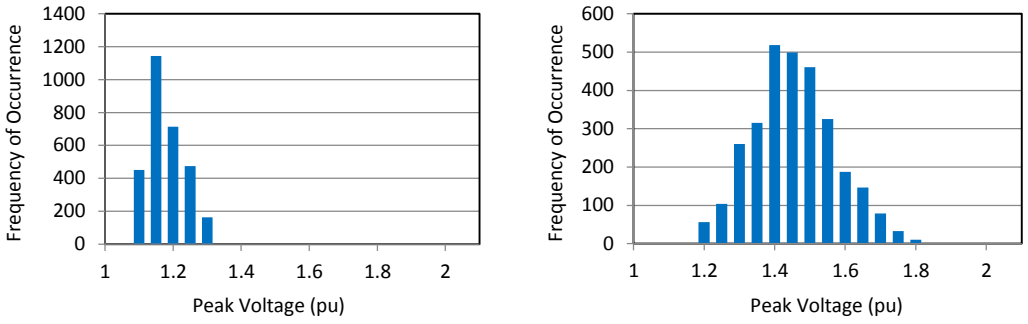

a) 420kV Network Source

b) Sending End of GIL (PCC)

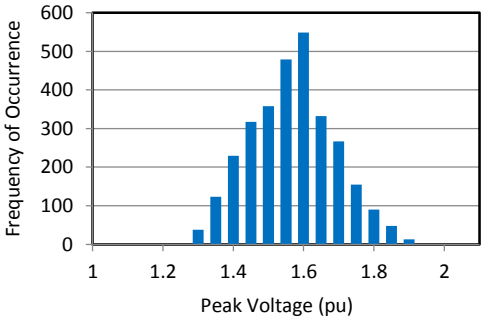

c) Receiving End of GIL

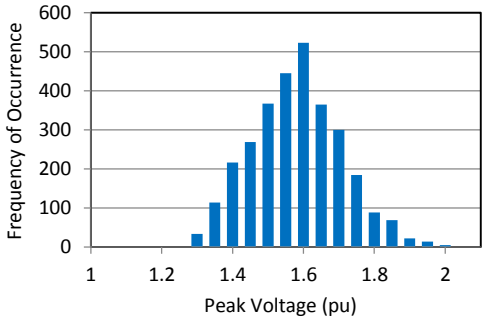

d) Open Receiving End of XLPE cable

Figure 5-4: Range of Peak Overvoltage Over all Phases for 1000 Systematic CB Closing Combinations (Energisation of Three 10 km XLPE Cables).

Figure 5-4 (a) shows that there is a small impact on the 420 kV network sources where the highest overvoltage recorded is 1.3pu and the most frequently occurring voltage is in rang between (1.15-1.2pu). Figure 5-4 (b) shows the overvoltage distributed at the sending end of the GIL where the highest overvoltage recorded is 1.8pu and the most frequently recurring voltage is in range (1.4-1.5pu). The highest overvoltage seen at the receiving end of the GIL is 1.9pu, and the most frequently recurring voltage is in range (1.55-1.6pu) as shown in Figure 5-4 (c). The highest overvoltage was recorded at the open receiving end of XLPE cable is 2.0pu and the most frequently recurring voltage is in range (1.55-1.6pu).

5.5.3. Energisation 420/33 kV offshore wind farm transformers

To determine the highest overvoltages that may occur at the transformer terminals during energization of the 420/33 kV offshore wind farm transformer, a systematic study is carried out by replacing CB9 with systematic switch. The switching overvoltages distributed across the network due to the effect of the pole-span for five different measurement points are shown in Figure 5-5.

A standard SIWV for the low voltage transformer terminals 33kV is not directly listed in IEC 60071-1. The SIWV needs to be calculated applying a test conversion factor to the standard corresponding to the lightning impulse withstand voltages LIWV which is 170 kV for the insulation used on the 33 kV transmission network [106].

This test conversion factor depends on the insulation type. By dividing the LIWV by the test conversion factor of 1.25 for GIS, and then a safety factor of 1.15, we can calculate the SIWV which is equal to 4.4pu. The highest overvoltage seen at the low voltage terminal of the transformer is 5.94pu which is exceeded the SIWV limit by about 35%.

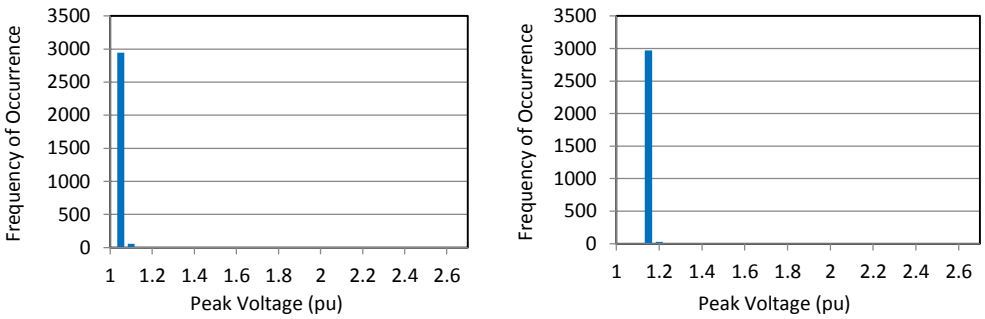

a) 420kV Network Source

b) Sending End of GIL (PCC)

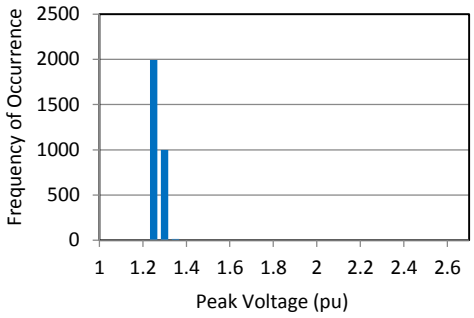

c) Receiving End of GIL

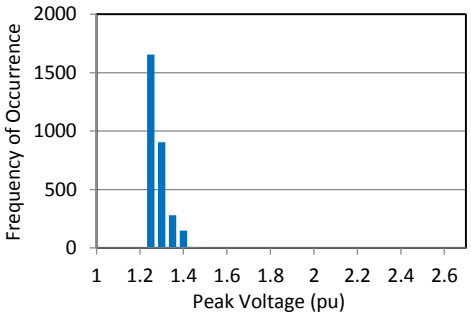

d) Receiving End of XLPE Cable

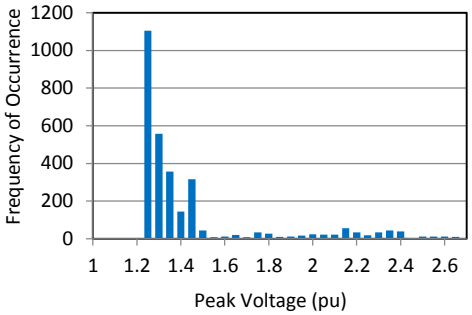

e) High Voltage Terminal of 420/33 kV Transformer

Figure 5-5: Range of Peak Overvoltage Over all Phases for 1000 Systematic CB Closing Combinations (Energisation of 420/33 kV Offshore Wind Farms Transformers).

5.5.4. Energisation of 420 kV GIL with Trapped Charge

Reclosing the circuit breaker can produce a significantly higher transient than the transient produced by the first energisation action. When the transmission line is disconnected, there is a high chance of leaving a trapped charge in the line when there is no in-circuit component to provide a discharge path to earth.

Due to an increase in the potential difference across the open CB terminals prior reclosing the CB a large amplitude travelling wave will be injected into the transmission line. When this wave reaches the open far end of the line, it is reflected, and a high transient overvoltage of up to 4pu may be experienced, which will likely damage the insulation medium.

Due to an increase in the potential difference across the open CB terminals prior reclosing the CB a large amplitude travelling wave will be injected into the transmission line. When this wave reaches the open far end of the line, it is reflected, and a high transient overvoltage of up to 4pu may be experienced, which will likely damage the insulation medium.

For this reason, a systematic switch is used to study the influence of the trapped charge on the switching overvoltage. A trapped charge was introduced to the system during energisation of a 300 km GIL. The trapped charge was modelled by three single-phase current sources connected to the line. By specifying the special code for the TSTART = 5432 rather than -1, the trapped charge sources serve to initialise the phase conductor voltage, but are disconnected at the start of the time-domain solution [88].

Moreover, for the steady state phase solution, the current sources were treated as a voltage sources having amplitude of +1pu for phase A, -1pu for phase B and +1pu for phase C. The three sources were disconnected at the circuit-breaker closing time. The switching overvoltages distributed across the network due to the effect of the pole-span for five different measurement points are shown in Figure 5-6.

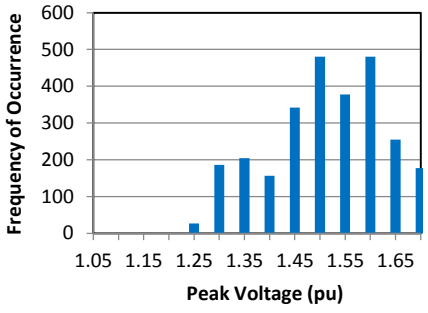

a) 420 kV Network Source

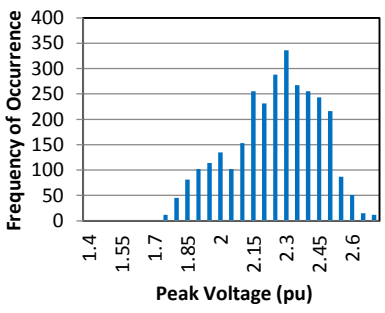

b) Sending End of GIL

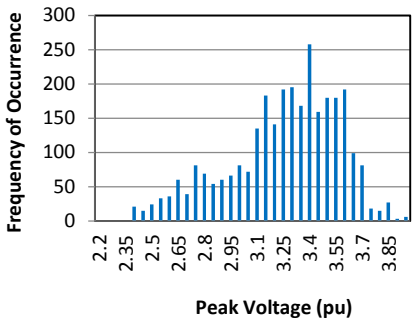

c) Receiving End of GIL

Figure 5-6: Range of Peak Overvoltage Over all Phases for 1000 Systematic CB Closing Combinations (Re-energisation 300 km GIL Line).

Reclosing the circuit breaker produce very high overvoltages during re-energistion unloaded 300 km GIL line. The highest overvoltage seen at the receiving end of the GIL was 3.95pu with low probability of occurrence less than 5%. This overvoltage exceeded the SIWV limit by about 27%. This overvoltage is high enough to cause a failure in the insulation medium. Therefore, connecting a shunt reactor during energisation of the line is required to provide a path for the cable to discharge to earth.

5.6. Evaluation of the risk of failure of a GIL due to switching transient overvoltages

The risk of failure caused by the switching surges is always viewed as the switching impulse flashover rate, which is the probability that an unwanted stress along the line exceeds the insulation strength. For self-recovering insulation the overvoltages and the insulation strength show probabilistic behaviours. A rigorous calculation of the risk of failure requires the frequency distribution of the transmission line insulation strength and switching overvoltage stresses. Assume that an overvoltage V_k is having a probability of occurrence $Po\ (V_k)\ dV$, whereas the probability of insulator breakdown at this

voltage is $P_b\ (V_k)$. Therefore the probability that the insulator will fail at an overvoltage V_k is:

$$dR = Po(V_k)*P_b(V_k)\ dV \tag{5-1}$$

For the overall range of the overvoltages, the total probability of the insulator failure or "risk of failure" is given by:

$$R = \int_0^\infty P_0(V_k).\ P_b(V_k)\ dV \tag{5-2}$$

This integral can be evaluated numerically provided that the point-by-point distribution is available for both $Po\ (V_k)$ and $P_b\ (V_k)$. For a particular network, the probability of occurrence $Po\ (V_k)$ as well as the probability of insulator breakdown $P_b\ (V_k)$ can be obtained using EMTP with the capability of statistical switching overvoltage calculation.

5.6.1. Determining the Probability of Insulator Breakdown

The task of co-ordinating the electrical stresses with electrical strengths requires representing the overvoltage distribution in the form of a probability density function and the insulation failure probability by a cumulative distribution function. For this reason, statistical switching was used to determine the range of overvoltages from different circuit breaker pole closing times across the 20ms/50Hz waveform. The parameters required to perform the simulations are the point of circuit breaker closing aiming point of 22ms and the standard deviation σ. To cover the entire range of a 50 Hz cycle, the standard deviation for a uniformly distributed switch must be $20/(2\sqrt{3})$ = 5.77ms.

If a normal distribution is truncated at −4σ and +4σ, more than 99.99% of the switching times will range within a cycle centered at the aiming instant;

therefore, for a 50 Hz cycle, the selected standard deviation is 20/10 = 2ms. A total of 500 operations were simulated for each circuit breaker operation studied. The 2% value which is defined as the value of the overvoltage having a 2% probability of being exceeded as proposed by IEC 60071-2 can be directly obtained as well as the 90% value which is defined by the voltage corresponding to a 10% probability of breakdown. Figure 5-7 shows the cumulative probability curves of overvoltages calculated for different measurement point on the network using the statistical energisation studies.

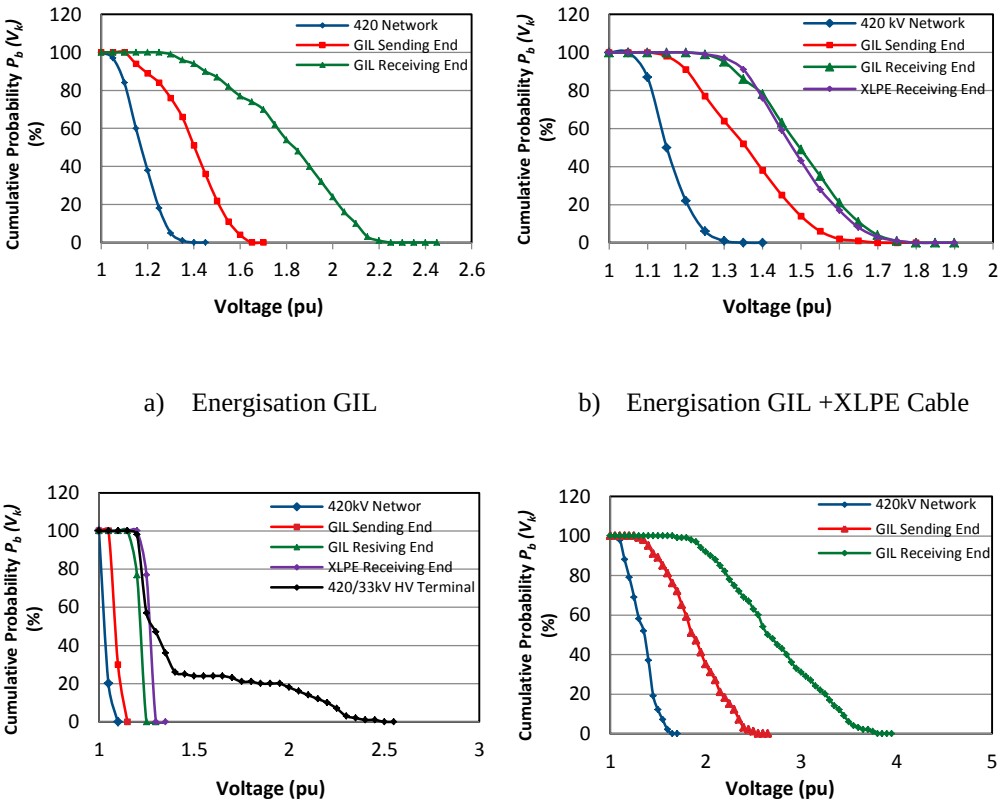

a) Energisation GIL

b) Energisation GIL +XLPE Cable

c) Energisation GIL +XLPE Cable + 420/33 kV Transformer

d) Energisation GIL with Tripped Charge

Figure 5-7: Cumulative Probability Curves of Overvoltages Calculated for Different Measurement Point on the Network Using the Statistical Energisation Studies.

5.6.2. Simplified Method for calculating Risk of Failure

IEC60071-2 proposed simplified method to calculate the risk of failure which

was used in this study. The risk of failure is related to a statistical safety facto (K_{CS}) which is defined as the ratio of statistical overvoltage to statistical withstands voltage. The overvoltage distribution is identified by the statistical overvoltage, which is the overvoltage having a 2 % probability of being exceeded. The insulation strength distribution is identified by the statistical withstand voltage, which is the voltage at which the insulation exhibits a 90 % probability of withstand or the voltage corresponding to a 10% probability of breakdown.

Table 5-1 shows statistical overvoltages results for 2% and 10% value obtained from the cumulative probability curves for every considered configuration as well as the calculated statistical safety factor. The risk of failure can be directly determined from the graph given by IEC 60071-2 which shows the correlation between risk of failure and statistical safety factor for 1050 kV switching impulse withstand voltage.

Table 5-1: Statistical Overvoltages Results for V2% and V10% Value Obtained from the Cumulative Probability Curves.

Energisation Scenario	**300 km GIL**	**GIL + XLPE Cable**	**GIL + XLPE Cable +420/33 kV Transformer**	**Re-energisation GIL with tripped charge**
Main Value	2.45	2	2.65	3.95
2% value	2.57	2.05	2.61	3.65
10% value	2.35	1.68	2.45	4.33
K_{CS}	1.20	1.22	1.06	0.84
Risk of failure	1.0E-4	6.0E-4	4.0E-2	-

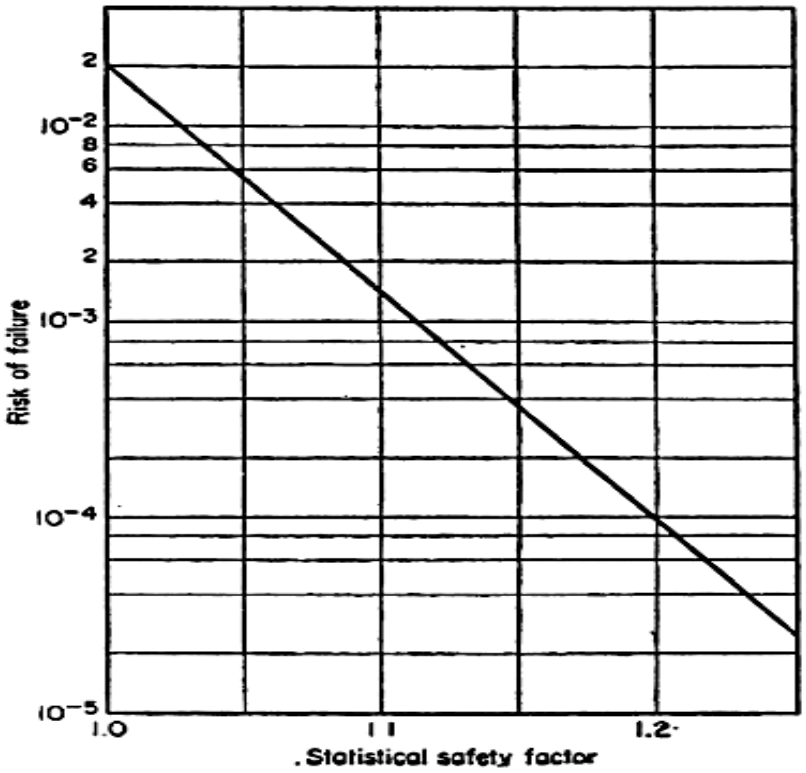

Figure 5-8: Correlation between Risk of Failure and Statistical Safety Factor IEC 60071-2

It can be seen from table 1 that the statistical safety facto (K_{CS}) for the three energistion scenario 300 km GIL, with XLPE cable and with XLPE and 420/33 kV transformer is at good level $K_{CS} > 1$. This safety factor result low risk of failure rate, which means there is no need for extra protection equipment to deal with the switching overvoltages during energistion action.

For re-energistion 300 km GIL line the statistical safety facto is low $K_{CS} < 1$ this factor means the overvoltage caused by re-energisation the line is at high level that may cause breakdown to the insulation. Therefore, temporary shunt reactor has to be connected to offer path to the tripped charge to the earth.

5.7. Switching Transient Waveform

5.7.1. Energisation of GIL Submarine Transmission Line

Figure 5-9 shows the three phase voltage waveforms during energisation of the open end 300 km GIL from the 420 kV onshore network for three measurement nodes. The circuit-breaker pole closing times were taken from the results of previous systematic study. The corresponding highest overvoltage is found on the randomly switching operation 90 and at times 20.0ms, 26.03ms and 25.36ms. The time span between the first and third pole to close is 6.03ms.

It can be seen from the waveforms that the distortion of the wave at the network source where the highest overvoltage was recorded is 1.4pu. The voltage at the grid took 45ms to settle and return to study state condition due to the damping effect of the network surge impedance.

Figure 5-9 (b) shows the voltage wave form at the sending end of GIL (PCC). It can be seen that the highest overvoltage was recorded is 1.9pu. The voltage at the sending end took longer time 65ms to settle to study state condition.

Figure 5-9 (c) shows the voltage wave form at the receiving end of GIL. The simulation results show that highest overvoltage of 2.45pu was recorded at the receiving end of the GIL. The voltage took 80ms to settle when the GIL only was energized. The current waveform during energisation of the GIL that flowed through CB3 is shown in Figure 5-10.

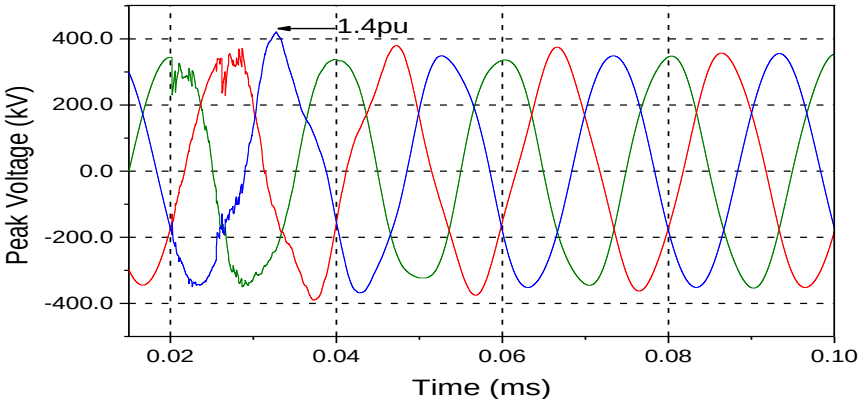

(a) 240 kV Network Source

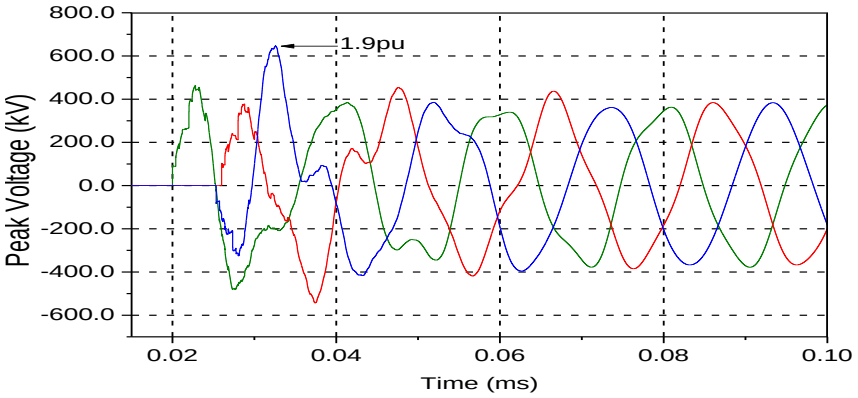

(b) Sending End of GIL (PCC)

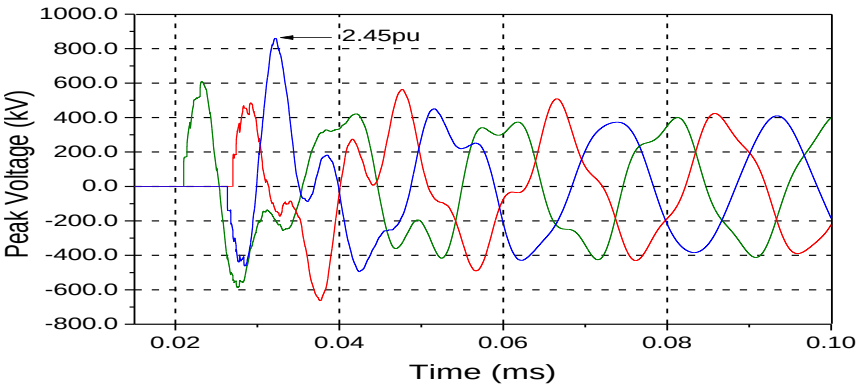

(c) Receiving End of GIL

Figure 5-9: Voltage Waveforms at Different Nodes during Energisation of 300 km GIL.

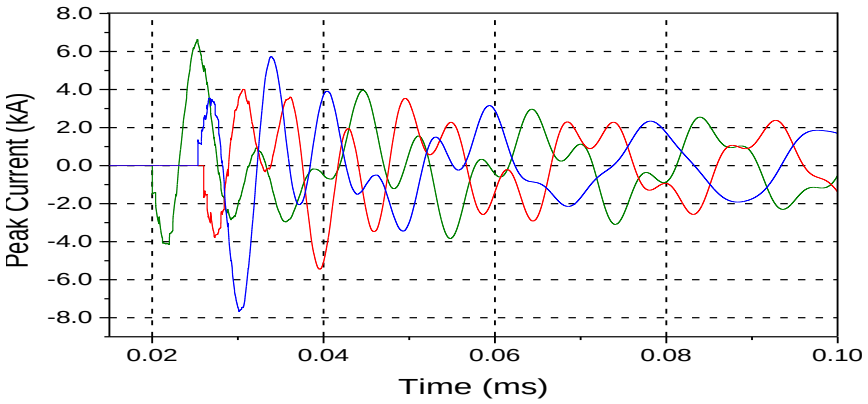

Figure 5-10: Three-Phase Current at the Onshore Connection Point (PCC) during Energisation of a 300km GIL

5.7.2. Energisation of XLPE Cables Connecting Offshore Wind Farm Substations to the Main Offshore Substation

Figure 5-11 shows the voltage waveform for different measurement point. Figure 5-11 (d) shows the voltage waveform at the receiving end of XLPE cable where the highest overvoltage recorded is 2pu. The voltage at the grid took 65ms to settle and return to study state condition. It can be notes that the voltage wave form took longer time to settle than when energisation GIL alone. The current waveform during energisation of the XLPE cable that flowed through CB5 is shown in Figure 5-12.

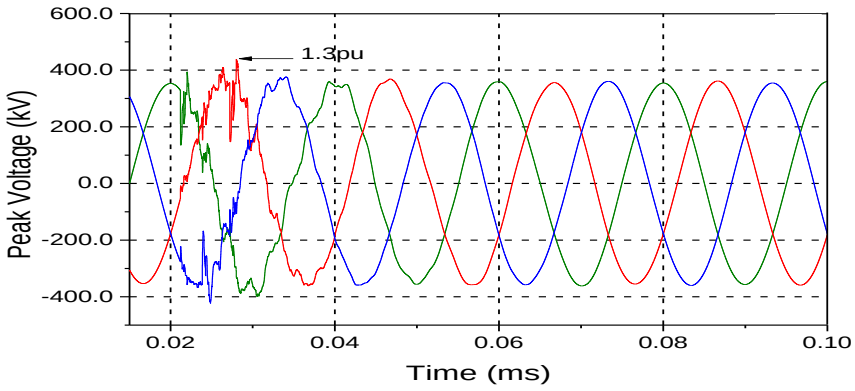

(a) 420kV Network Source

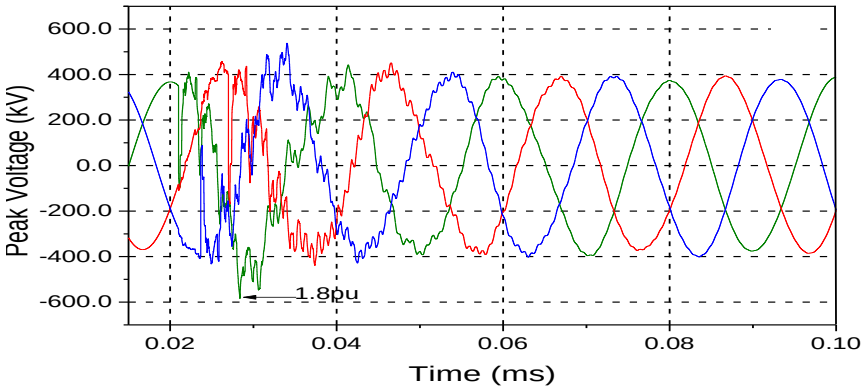

(b) Sending End of GIL (PCC)

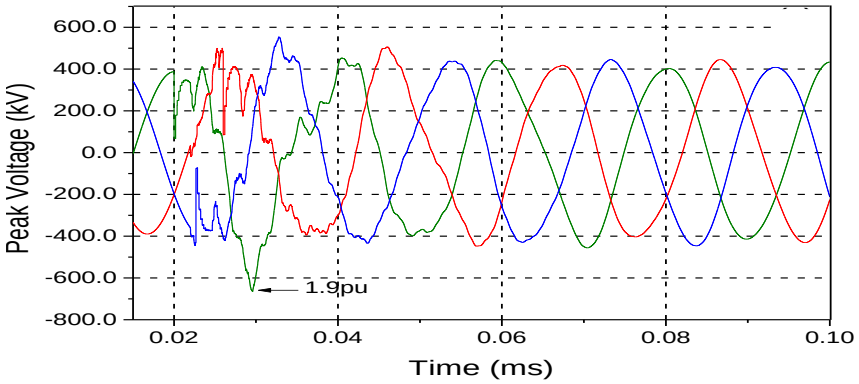

(c) Receiving End of GIL

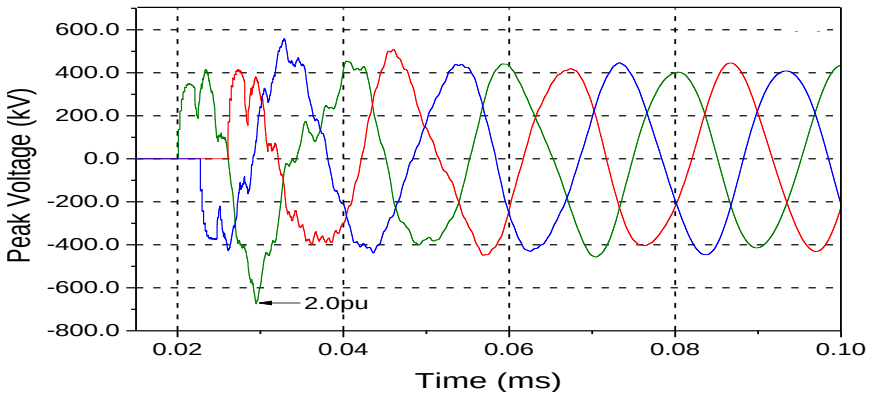

(d) Receiving End of XLPE cable

Figure 5-11: Voltage Waveforms at Different Nodes during Energisation of 10 km XLPE Cables.

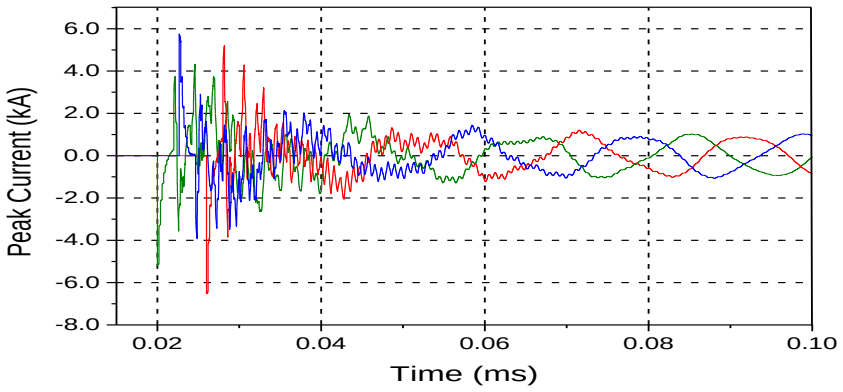

Figure 5-12: Current through CB5 during Energisation XLPE Cable

5.7.3. Energisation 420/33 kV Offshore Wind Farms Transformers

Figure 5-13 shows the voltage waveforms during the energisation of the 420/33kV transformers at the offshore wind farm platforms. Closing the three circuit breakers CB8, CB9 and CB10 connects the already energised XLPE cables to the 420/33 kV offshore transformers.

The closing time of the circuit breakers was taken from the systematic study. The corresponding highest overvoltage was found on the randomly switching operation 101 and at times 20.67ms, 26.67ms and 20.0ms. The current waveform during energisation of the XLPE cable that flowed through CB5 is shown in Figure 5-14.

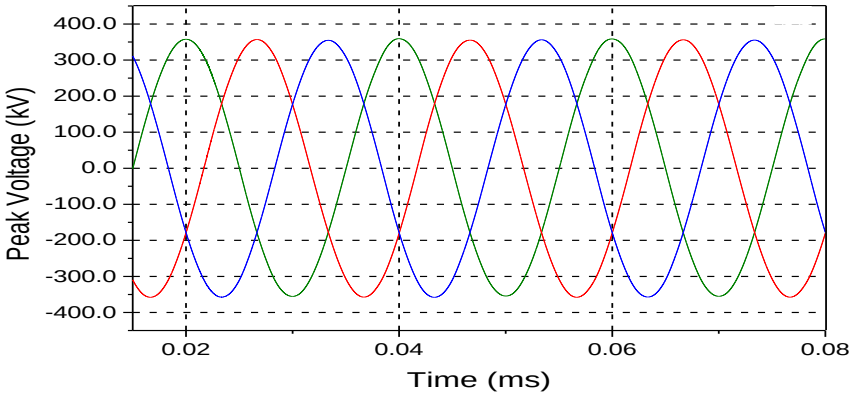

(a) 420kV Network Source

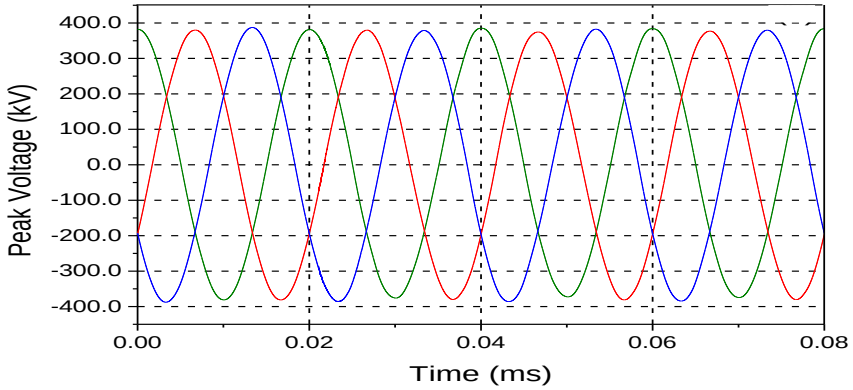

(b) Sending End of GIL (PCC)

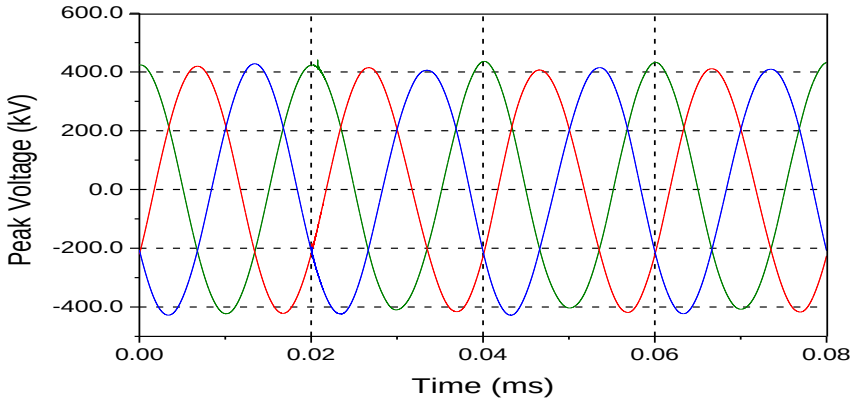

(c) Receiving End of GIL

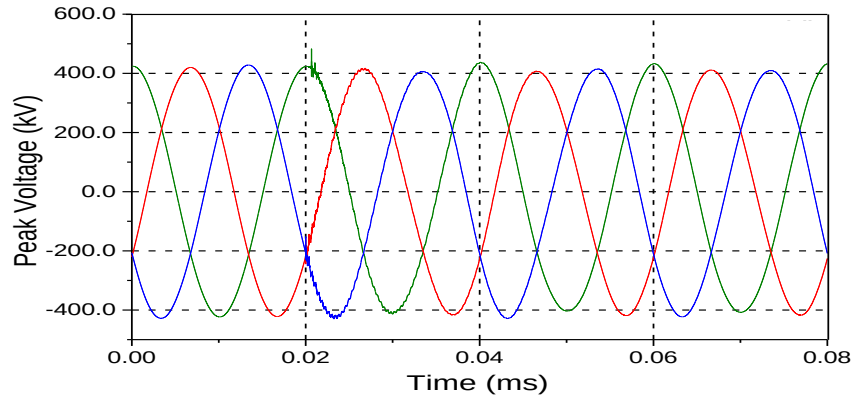

(d) Receiving End of XLPE Cable

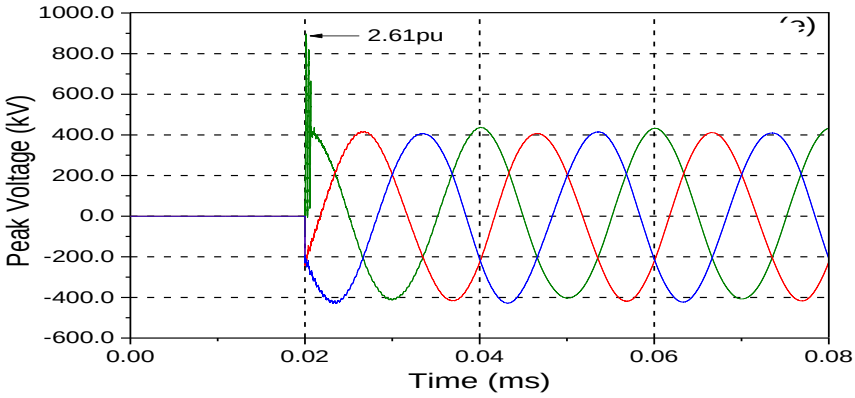

(e) High Voltage Terminal of Transformer

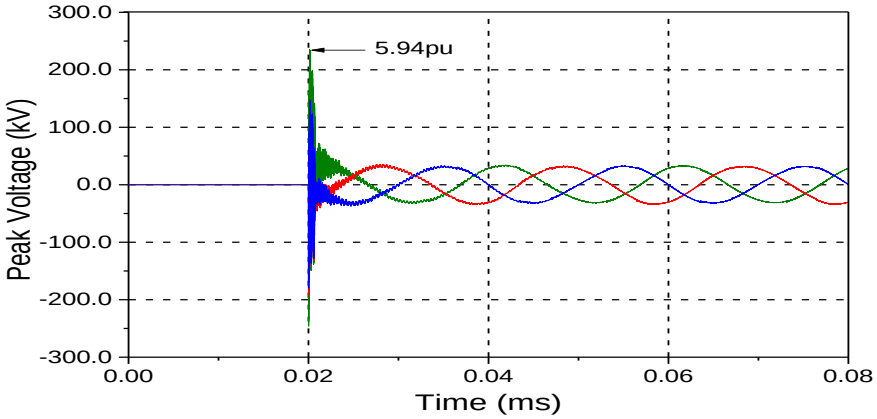

(f) Low Voltage Terminal of Transformer

Figure 5-13: Voltage Waveforms at Different Nodes during Energisation of 420/33 kV Offshore Wind Farm Transformer.

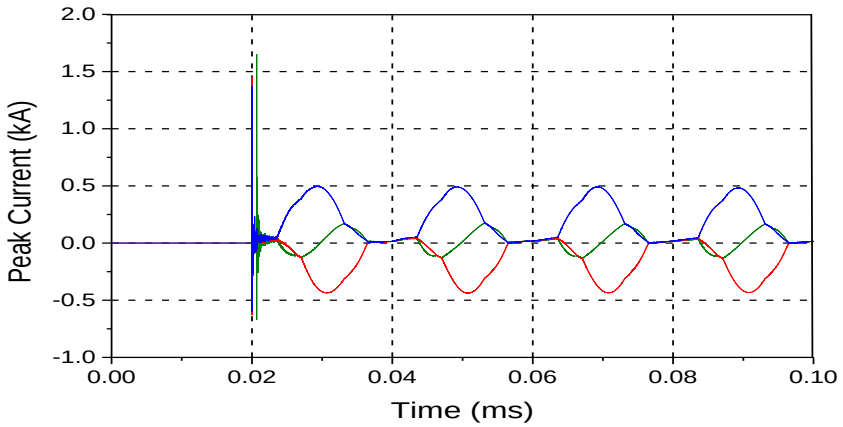

Figure 5-14: Current through CB9 during Energisation 420/33 kV Offshore Wind Farm Transformer

5.7.4. Energisation of 420 kV GIL with trapped charge

Figure 5-15 shows the voltage waveform during the reclosing operation on an unloaded 300 km GIL for different measurement points.

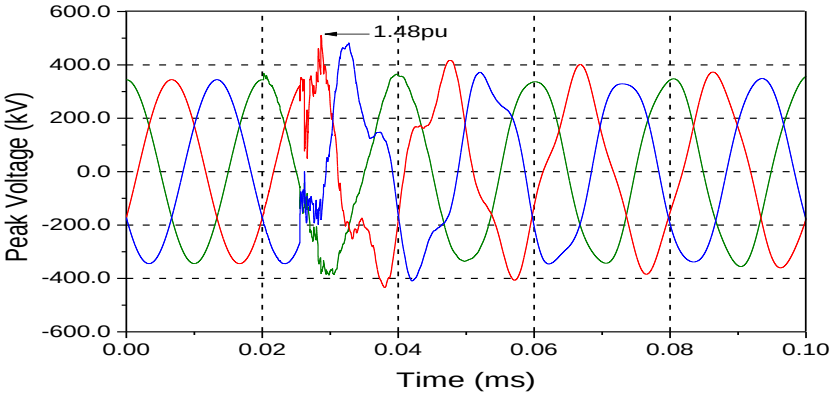

(a) 420kV Network Source

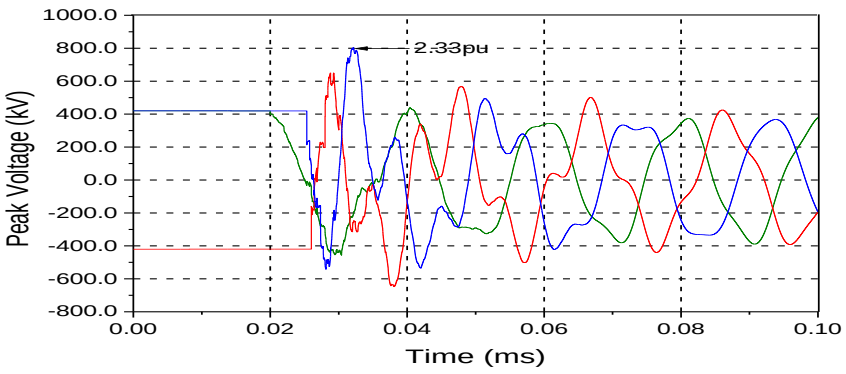

(b) Sending End of GIL (PCC)

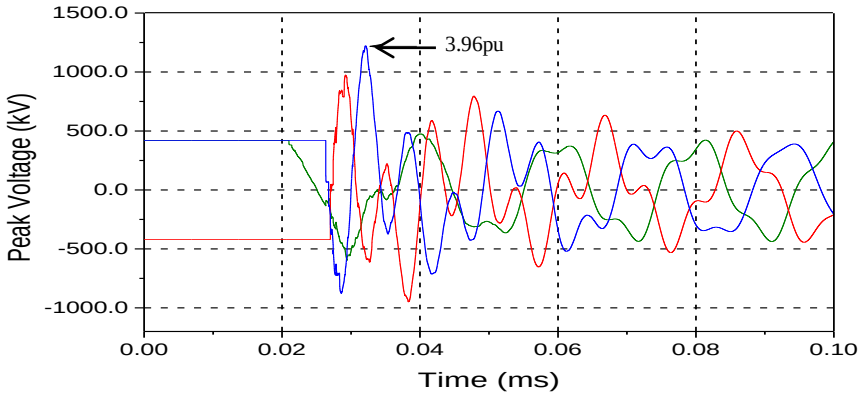

(c) Receiving End of GIL.

Figure 5-15: Three-Phase Voltage during Re-closing Operation on Unloaded 300 km GIL

5.8. Effect of GIL Line Length on the Switching Transient

The overvoltage amplitudes due to line energization depend on several factors including type of circuit-breaker nature, short-circuit power of the bus bar from which the line is energized and the transmission line length. Therefore, this section illustrates the effect of different GIL length on the overvoltages generated during energisation of the GIL under the no load condition. Figure 5-16 shows respectively the effects of the line length on the maximum overvoltages and 2% values in 3000 line energizations. Different colours in the figures show different feeding networks.

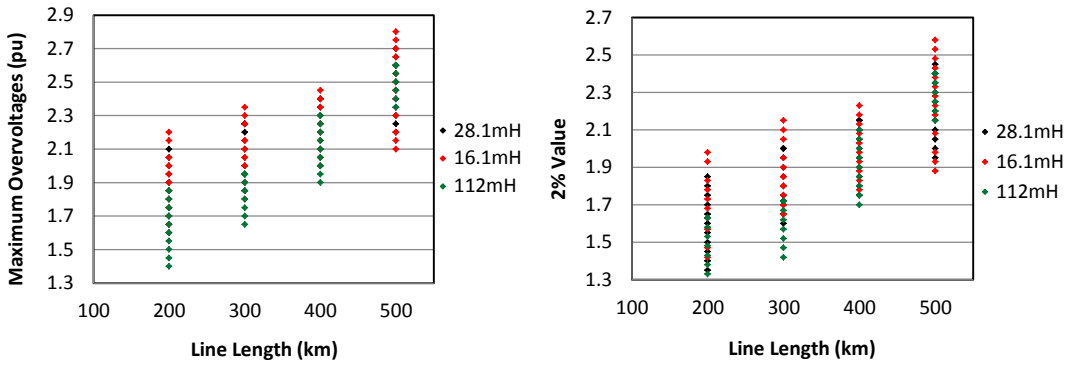

Figure 5-16: Effect of Different GIL Line Lengths on the Occurrence for Maximum Overvoltage at the Receiving End for Different Feeding Network Including 2% Value.

As can be seen from Figure 5-16, the overvoltages on GIL lines are more dependent on the line length. Increase the line length means longer travelling time for the transient surge to reach the open far end of the line. This increase in the travelling time will lead to increase the transient surge amplitude. When this surge gets reflected a higher transient overvoltage will be experienced. From Figure 5-16 it can be seen that the highest switching overvoltage recorded at the receiving end of 500 km was 2.80pu which is still within the SIWV limit of 3.1pu.

5.9. Effects of Feeding Network on the Switching Transient

It has been established, from the literature, that the overvoltage amplitudes due to line energization depend on several factors including type of circuit-breaker (closing resistor or not), nature and short-circuit power of the bus bar from which the line is energized. There for in this section the effect of a different feeding network on the switching transient during energisation different GIL line length was carried out. Figure 5-17 shows respectively the effects of the feeding network on the maximum overvoltages and 2% values in 3000 line energizations. Different colours in the figures show different line lengths.

The figures show that the overvoltages in cables have a clear dependence on the feeding network. The overvoltage level becomes lower for larger source impedance (weaker feeding network). From Figure 5-17, it is clear that the overvoltages are more dependent on the line length and the feeding network than on the line type.

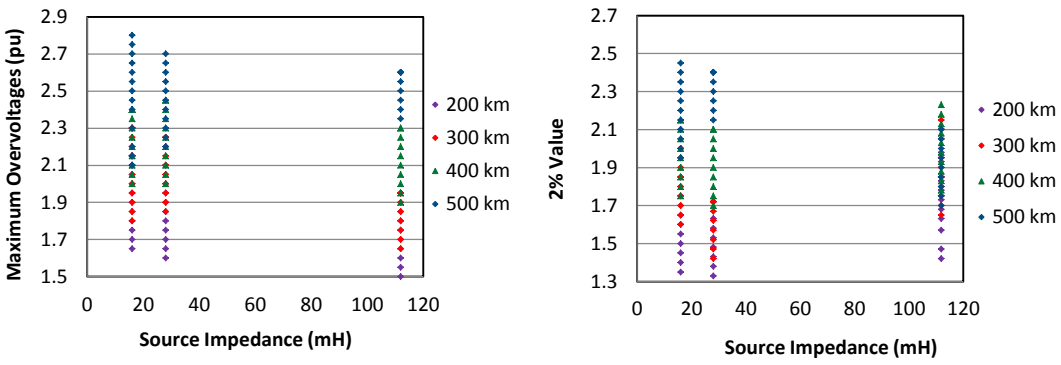

Figure 5-17: Effect of Feeding Network on Maximum Overvoltage for Different GIL Line Lengths Including 2% Value.

5.10. Summary

The energisation of an unloaded gas insulated transmission line causes high overvoltage transient and stresses the insulation systems. The level of overvoltage experienced is governed by many factors, in particular, the problem underlying sensitivity of CB contacts as well as the characteristics of switching operation. In this case, attention has been given to the CB pole closing span as well as the point-on-wave where the contacts initiate their closure.

According to the statistical analysis to the overvoltages distribution data obtained from simulation approaches for different energisation scenario of 300 km GIL with offshore transmission network using different pole spans, the switching transient overvoltage magnitudes are at average level compared to the values

indicated by IEC standard. Overall, for the cases studied using different pole spans, the range of overvoltages value obtained including the 2% probability of failure values are within acceptable level and considered to comply with the standards. Moreover, the risk of insulation failure due to the switching transient stress applied to the insulation medium was calculated using simplified method proposed by IEC60071-2. The results have shown that the risk of failure is at low level which means the risk of insulation is negligible.

The transient overvoltage caused by the trapped charge during re-closing on the unloaded GIL results in the worst overvoltages at the remote end of the 300 km GIL. The transient overvoltages was recorded at the receiving end has exceeded the value specified by IEC by about 27%. The overvoltage is high enough to cause a failure in the insulation gas. This overvoltage can be avoided by providing a path for the line to discharge to earth, by connecting a temporary shunt reactor during energisation of the line.

The overvoltage stress affecting the insulation medium of gas insulation line increases as the line length increases for different feeding network. Up to 500 km line length, all the overvoltage magnitudes were within the average level compared to the values indicated by IEC standard. The network source impedance also has a strong impact on the overvoltage seen at the receiving end during energisation of the unloaded GIL. The energisation overvoltages of GIL become lower for a weaker feeding network

CHAPTER 6: THE PRACTICAL SIDE OF INSTALLING A "GIL" BASED ON POWER TRANSMISSION PIPLINE "PTP" TECHNOLOGY

6.1 Introduction

Grid connection for offshore wind farms presents a significant challenge, especially because of the planned capacities, environmental considerations, technical constraints, and limited experience regarding offshore power pipeline projects. Moreover, design power transmission routes complicate the network development in some subsea areas. This has led to calls for the development of a new infrastructure solution that can support and advance the development of offshore wind energy. A new technology based on GIL, which meet the electrical requirements of connecting large-scale offshore wind farms, has recently received attention. This technology is known as 'power transmission pipelines' or (PTP) [118].

The construction and operation of a PTP system and other tubular structures offshore presents great challenges and unique design needs, which sometimes require the development of new technologies, such as new underwater surveying technologies, a variety of methods and associated vessels for installing pipelines in increasingly deeper waters, new corrosion protection methods and insulation materials, submarine welding and monitoring methods and facilities, seafloor trench digging methods, remotely controlled vehicles, and equipment for deep water operations [119], [120].

Oil and natural gas pipelines are usually the longest and the most advanced technology for transmitting oil and gas through submarine pipes. Oil and gas pipelines often cross countries and sometimes continental borders; such pipeline projects require long and careful planning [119]. Therefore, building the PTP necessitate adapting the equipment and utilizing the long experience gained from gas and oil pipeline technology.

This chapter will explain the practical side of installing PTP technology and the special design required for offshore wind farms. The PTP component, the maximum transmission capacity of the PTP system, and the laying technology will be addressed. In addition, the challenges facing this technology will be illustrated.

6.2 Power Transmission Pipelines (PTP)

PTP is a total system for transporting electrical power generated far away from the load centre based on approaches from offshore oil and gas pipeline technology using GIL as a power transmission system. The system includes a main collecting platform for the feed-in of electrical power from different offshore wind farm substations. Moreover, the laying technology for the transmission system is via directly buried GIL aluminium pipes coated with a thick layer of polyethylene or polypropylene for corrosion protection or via tunnel construction [118].

The PTP theory is based on connecting the accumulated and clustered power produced by a number of offshore wind farms located within optimised distances from the main collecting platform. The voltage is likely to be transferred from a medium voltage level of 33 kV to a high transmission voltage level of 420 kV at

each collecting wind farm platform in order to reduce the losses to the lower level during the transmission of electrical power to the main collecting platform for feed-in [121].

At the main collecting platform, the bundled power is connected to the transmission system, that is, the GIL, to transmit the power to the onshore connecting point. The GIL form the core for the PTP technology as a transmission system lay in a tunnel under the seawater or coated with a thick passive corrosion protection layer for carrying power to the shore. Figure 6-1 shows a visualisation of the PTP offshore transmission solution.

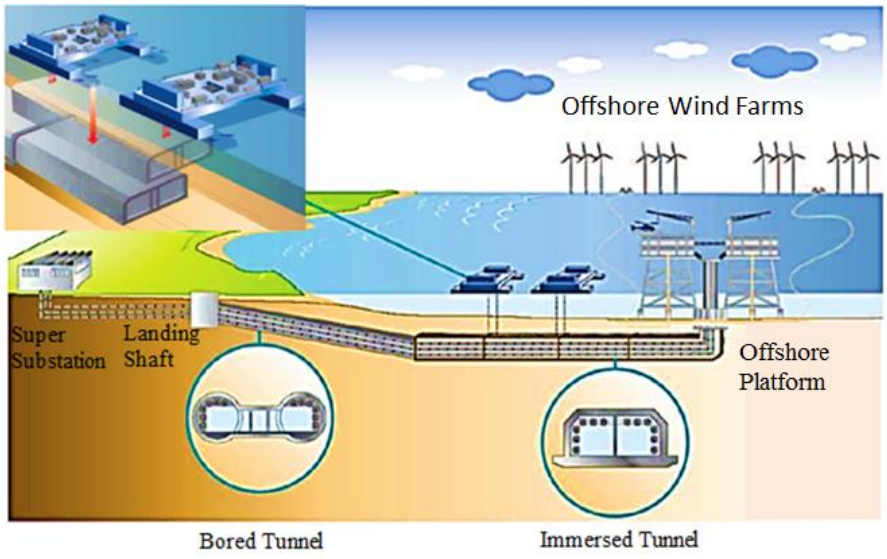

Figure 6-1: Visualisation of PTP Offshore Transmission Solution [122]

6.3 PTP Offshore Design Consideration

The construction of an offshore PTP requires the involvement of several engineering disciplines. A survey of the installation site has to be commissioned before the route of the pipelines is selected. The water depth and sea floor tenacity

for the pipelines route define the load that can be applied to the sea floor as well as the installation method chosen for the project.

Furthermore, several impediments that may affect the final route selection need to be taken in consideration, such as political issues in the case of crossing other countries territorial waters; geological hazards, such as earthquakes and volcanos; physical factors along the prospective route; and other users of the seabed in the selected area. This task starts with a survey of geological maps, fishing charts, and aerial and satellite photography, as well as information from navigation authorities [119].

6.3.1 Physical Factors

The physical factors that need to be considered at the beginning are the state of the seabed, that is, whether it is relatively flat or rough with high hills. If the sea floor has high hills, the PTP will include free spans. When the PTP is placed on high points, there will be unsupported sections between these points. If the unsupported sections are too long, the bending stress applied to them due to their weight may cause the PTP to bend. Therefore, corrective measures for unsupported PTP spans with post installation support, such as berm or sand infilling below the PTP, are very important. The solidity of the sea floor is another important factor; if the soil is not strong enough to withstand the weight of the PTP, the PTP may sink into it [120].

6.3.2 Other Users of the Seabed

Western Europe, including the North Sea, falls into the International Council for exploration and monitoring of human activities in the seas [123]. Therefore,

proper planning of a PTP has to take in a wide range of human activities that may affect the seabed along the proposed route or that are likely to do so in the future, such as other pipelines, fishing vessels, ships anchors, and military activities. The offshore PTP pipelines are major structures with costs that run into the hundreds of millions of pounds; thus, they need and deserve to be designed carefully with all the care and attention that modern engineering tools can provide [120].

6.4 PTP System Design

6.4.1 Model of an AC Offshore Solutions

Each feeder consists of a number of turbines; these will be connected to an offshore collector platform, located in an appropriate place to minimise the feeder cable lengths required. At the offshore collector platform, the generated power will be transformed from a medium voltage level to a higher voltage level to transmit the generated power to the PTP main collection platform with minimum power loss using AC cables as the connection medium. The cross section and the number of cables will be determined based on the amount of power generated and the transmission voltage level. The voltage level will be determined by detailed studies, but it is likely to be 420 kV or 550 kV [121].

The number of collector substations for the project will be determined based on detailed studies. An immersed tunnel is one of the laying technology options for the PTP system design, not only from the economic point of view but also for safety and reliability reasons; the tunnel should have at least two three-phase transmission circuits. The special design of the tunnels can give a space for four three-phase systems with a total power of 4*3000 MW. Figure 6-2 shows a

model of an AC offshore solution. The foundation type for the collector substations is likely to comprise different types of foundation, but this will be confirmed in the following design section.

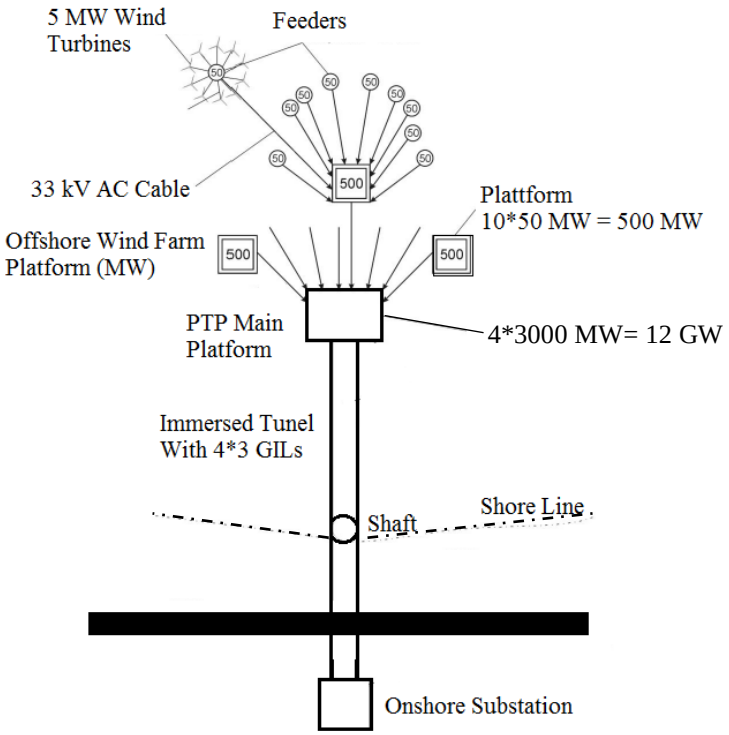

Figure 6-2: Model of an AC Offshore Solution

6.4.2 Offshore Substation Size and Distance to the Main Substation

In addition to the economic decision of using a PTP as an offshore transmission system, there are a number of technical factors that have to be considered; these include, for example, not only the wind farm's distance to the shoreline, but also the total capacity of offshore wind power generation and whether the offshore wind farm's platform is at reasonable distance from the PTP main substation.

The maximum power transmission capacity is limited by the cross section of the AC cables and the amount of reactive power generated by the cable shunt capacitance where the reactive power is proportional to the square voltage level. Based on the ABB and Prysmian models [124], [125], the 2500 mm^2 XLPE cable for offshore application can transmit up to 800 MVA at 420 kV per three-phase system.

The technological advancement of the PTP system, which utilizes GIL as a main connection medium, reconfirmed that, based on the conductor and enclosure cross sections, a single three-phase circuit of GIL can transmit power up to 4000 MVA at 420 kV [78]. The largest distance from the individual wind farms to the PTP main substation is generally less than 20 km as stated in the report [121]. Beyond a certain distance from the main PTP substation, AC cables lose their attractiveness as an option and are no longer economically viable for the connection of the wind farms to the PTP main substation.

6.5 PTP Laying Technology

Constructing a subsea tunnel for such line lengths is not an easy task. A subsea tunnel represents the biggest percentage of the cost of the overall system cost, but in some cases, it is still central to the PTP system for a variety of reasons. Unlike the oil and gas pipelines, which are made from steel pipes, the PTP pipe is made from an aluminium alloy, which is weaker than steel and has a low corrosion resistivity. Strength and corrosion resistivity are required characteristics for offshore pipelines to resist collapse due to external pressure and to extend the pipeline's life.

The wall thickness of the gas and oil pipelines ranges from 11.4 mm to 38 mm depending on the type of goods and the water depth [119], whereas the wall thickness of the GIL ranges from 6.4 mm for 420 kV to 9.5 mm for 1200 kV[78]. Therefore, there are three options to meet these requirements: installing GIL pipes in a subsea tunnel, which is the most expensive option; coating GIL pipes with a thick layer of polyethylene; or installing the GIL pipes in another steel pipe, which is called pipe in pipe laying technology.

6.5.1 GIL Tunnel Laying Option

6.5.1.1 Tunnel Constructed with a Tunnel Boring Machine

The exact method of tunnel construction, that is, with a tunnel-boring machine (TBM) or a drilled tunnel, depends on the geological and hydrogeological conditions along the selected route. The basic concept of building a tunnel is that the ground is dismantled gradually under the protection of a shield. The tunnel tubes are lined with waterproof concrete shell elements. The required equipment and material are brought into the tunnel through the tunnel portal using a transport system. Excavated material is taken out using the same route. Intermediate constructions, such as shafts, are not necessary using this construction technique. The main purpose of a drilled tunnel is to bridge a certain distance from land into the sea, which will then be connected to a subsea immersed tunnel; a shaft is required at this point [126].

Finishing the tunnel is the most difficult stage of construction of a PTP system. Subsequently, the GIL pipes are fitted inside the tunnel. The tunnel features include energy supply, ventilation, monitoring and communications systems as well as a transport system. The transport system is necessary to overcome the

long tunnel distances during the construction period and later for servicing purposes. Tunnels are constructed usually with four three-phase systems both for economic reasons and for operational and personnel safety reasons. Two tunnel construction methods are available: a closed construction tunnel using a TBM, such as those used worldwide for the construction of traffic tunnels, and the immersed tunnel method, which forms a part of current offshore building techniques [126].

6.5.1.2 Immersed Tunnel

The immersed tunnel is a kind of underwater tunnel composed of concrete segments, constructed in another place, and floated to the tunnel site to be sunk into place after they have been connected together. Immersed tunnels are usually used in combination with other forms of tunnel at both ends, such as a drilled tunnel or bored tunnel, as this is usually necessary to continue the tunnel from near the water's edge to the entrance at the land surface. Figure 6-3 shows a cross section of prefabricated immersed tunnel segments [126].

The tunnel is fabricated in separate segments, with each segment prefabricated in a manageable length. The ends of each segment are blocked with bulkheads so they can be floated. At the same time, the corresponding parts of the tunnel path are prepared, with a submarine trench in the selected route being dredged and graded to fine tolerances to support the elements. The next stage is to place the segments into place; each is towed to the final location and in most cases, assistance is required to keep the segments buoyant. Once the segments have been placed in the required position, additional weight is used to sink the elements into the final location; this is the most critical stage as it is essential to

ensure that each piece is aligned correctly. Once this stage is finished, the joint between the new element and the tunnel is dewatered and then made watertight; this process is continued sequentially along the tunnel [126].

The trench is then backfilled and any necessary protection, such as rock armour, added over the top. The ground beside each end tunnel element will often be reinforced, to permit a TBM to drill the final links to the portals on land. Once these stages have been finished, the tunnel is complete and the internal fit out can be carried out [126].

The segments of the tube may be constructed using one of two methods. The first method is to construct steel or cast iron tubes, which are then lined with concrete. This allows the use of conventional ship building techniques, with the segments being launched after assembly in dry docks. The second method, which is a reinforced concrete box tube construction, has been the standard; the sections are cast in a basin, which then flooded to allow their removal [126].

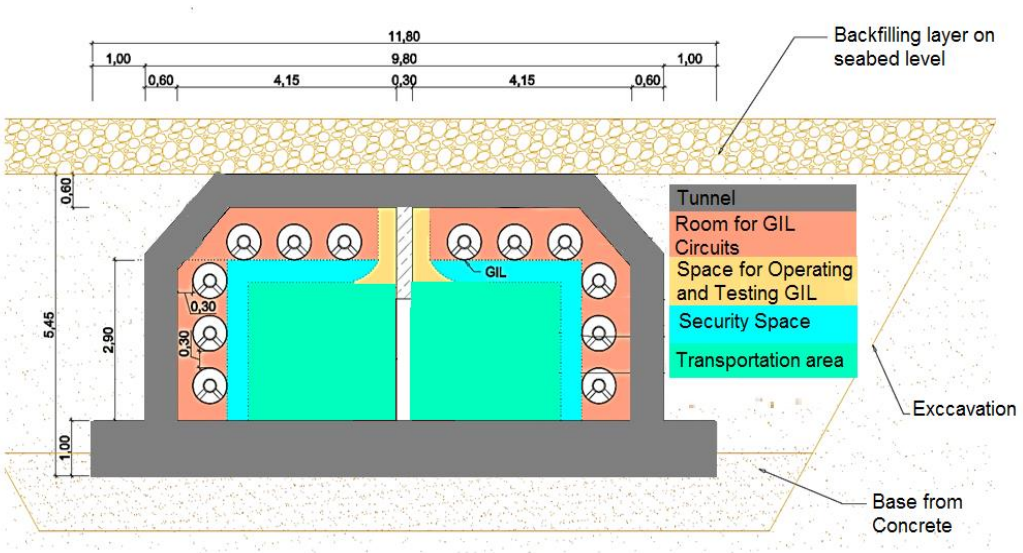

Figure 6-3: Prefabricated Immersed Tunnel Segments [122]

6.5.1.3 Fitting GIL inside the Tunnel

GIL is laid after the completion of the tunnel. Preassembled GIL pipes are delivered to the landing shaft and lowered into the shaft using a crane. In the welding tent, individual elements are completely assembled, welded together, and then pulled into the tunnel. The GIL is kept on rollers or mounts equipped with sliding contact bearings, which allows for thermal expansion of the coat tube. The compensator units, built in at regular intervals, permit the respective thermal expansion in the conductor tubes.

6.5.2 GIL Coated Pipes

Coating the GIL pipes with a thick layer of polyethylene or polypropylene is the cheapest and most trouble free installing method. Adding a thick layer of polyethylene or polypropylene can give the pipe the physical strength required to withstand the external pressure and provide corrosion protection as well [127].

The global pipeline manufacturers have developed a high quality polyethylene and polypropylene coating for aluminium and steel pipes for the transmission of gas, oil, water, and other fluids, making the pipes highly resistant to corrosion from moisture, chemicals, and other harmful substances. The thickness of the coated layer depends on the external pressure that will be applied to the pipe, which is strongly related to the water depth. Figure 6-4 shows the coating process of the aluminium pipe [127].

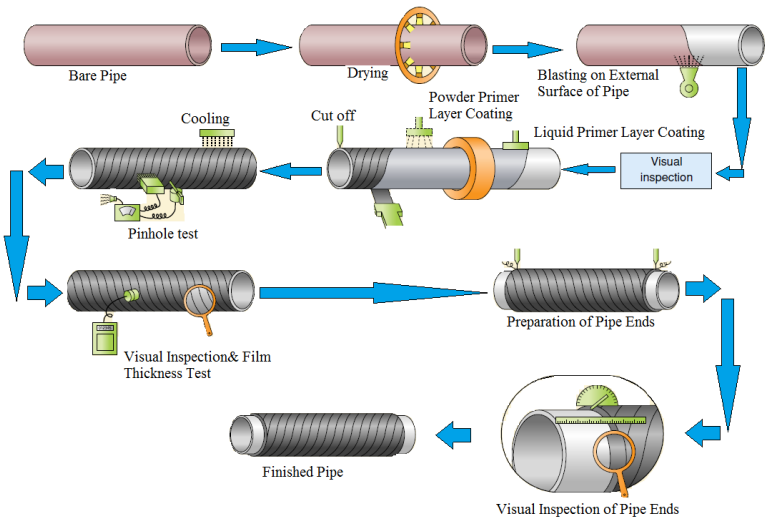

Figure 6-4: Coating Process of Aluminium Pipe [127]

6.5.3 Pipe in Pipe Layout Technology

Due to the high cost of the immersed tunnel and the special protection requirement of the aluminium GIL in a seawater environment, the pipe in pipe technology and the concrete coated pipe are recently being considered. Pipe in pipe technology can offer a cheaper solution and less installation effort than an immersed tunnel. In this case, the protective steel casing pipe and the GIL are laid together as a PTP system. Figure 6-5 shows the pipe in pipe technology[128].

As with offshore pipelines from the oil and gas industry, laying takes place on offshore pipe laying vessels. Here, the entire assembly of the GIL and casing pipes is carried out aboard the ship. During the laying process, the tough requirements of the PTP regarding external conditions during construction are of paramount importance. In addition to procedures for laying, welding, and connecting along the various pipes, material properties must be taken into account

during construction. As the laying, operational, and repair technology of this extremely complex pipe in pipe system will not be available for the foreseeable future, this concept is currently considered a future option[128].

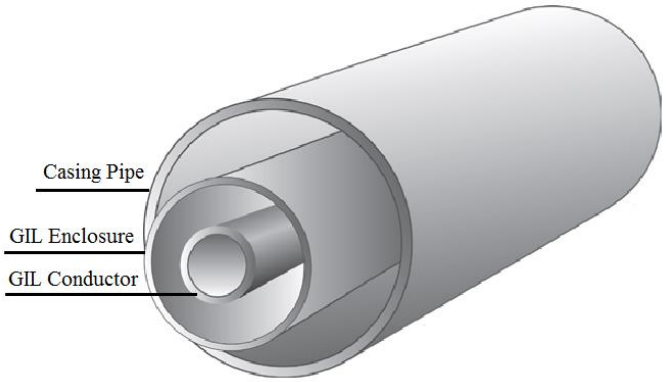

Figure 6-5: Pipe in Pipe Layout Technology [128]

6.6 Offshore Wind Farm Substations and Platforms

The traditional voltage level for connecting offshore wind turbines to the medium-voltage wind farm collection system is 33 kV. However, due to the maximum transmission capacity limit, it is not possible to transmit generated power to the onshore grid at this voltage level. Hence, for many of the projects, offshore substations are required to accumulate the power from the internal wind farm cable arrays and step up the voltage to an appropriate level for transmission over long distances.

The amount of power that can be accumulated at the PTP main offshore substation and the number of offshore wind farm substations required for the project will be decided by the total power carrying capacity of the onward transmission medium. The power carrying capacity of the array cabling and the

number of wind turbines will determine the size of the offshore wind farm substations. The distance from the platform to the furthest wind turbine in the array must also be taken into consideration, as using excessive lengths of 33 kV cable to connect an array can lead to excessive power losses.

An offshore wind farm platform is required to house the substations that gather the wind turbine connection cables. A step up transformer and switchgear are the main components. A bus bar and additional control and measurement equipment are required as well. Export cables then connect the offshore wind farm platforms, generally by HVAC cables, to the PTP main substation for feed-in power to the PTP transmission system to shore.

The PTP main substation is shown in Figure 6-6. It is designed to house the substation that gathers the connection cables of the offshore substation platforms. Platform topsides are supported on jackets made from steel pipes each having three to eight legs piled into the seabed. Monopiles can be used for smaller platforms.

In addition to housing transformers, cooling radiators, fans, switchgears, and the associated control panels, the platform will typically include emergency accommodation and life-saving equipment, a crane for maintenance lifts, a winch to hoist the subsea cables, a backup diesel generator, fuel, a helipad, communication systems, and the means to support the J-tubes that contain the subsea GIL [128].

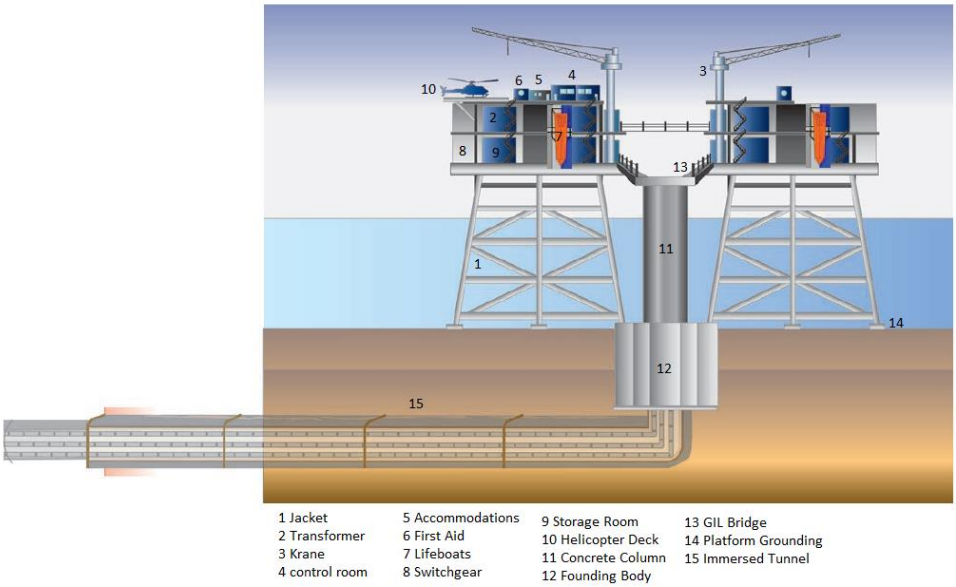

Figure 6-6: The PTP Main Substation [128]

6.7 Shafts

Three types of shafts are required during the construction of a PTP system: working shaft, reception shaft and intermediate shaft. All shafts should be of an appropriate size to permit safe temporary access for construction work and operational access to the completed tunnel; for the insertion and removal of electrical and services equipment, such as preassembled GIL segments; and for the safe installation and removal of the TBM and its equipment. The working shaft and reception shaft can be removed after finishing the construction process. Figure 6-7 shows an intermediate shaft for a PTP system [128].

Figure 6-7: Intermediate Shaft for PTP System [128].

6.8 PTP System Construction Challenges

As explained previously, the PTP project is a field with great challenges and unique design needs. The PTP developer needs to concentrate on the techno-economic assessment of the offshore projects, which are strongly affected by policy trends, regulatory issues, and industry developments [129].

Identifying a concrete path for the PTP project after the spatial analysis for the maritime area will ensure the technical and political feasibility of the project. This will force the developer to accept some regulatory, industry or policy issues. Once the developer has identified an optimal offshore grid design, the next question raised is whether the design can be done within a reasonable time frame. More challenges are discussed below [129].

6.8.1 Operation and Maintenance of an Offshore Grid

Offshore grid faults have to be cleared as soon as possible with quick and large primary control actions, especially in the case of high wind penetration. The

question is whether these primary control actions already exist at all sites. If not, their construction or market integration is a necessary condition for maintenance of an offshore grid. The offshore grid outage can take longer to repair than is the case for an onshore grid, due to difficulties accessing the offshore equipment [6], [129].

In general, the maintenance costs for the offshore grid are much higher than for the onshore grid, mainly due to offshore weather variations during the seasons and a small number of offshore cable production. At the aggregate level (PTP), based on the long experience gained from onshore insulation, the GIL does not require much maintenance. Therefore, maintenance issues are a minor issue for the offshore PTP system itself.

In the case of a fault leading to a failure in the PTP system, a very good monitoring system is required to identify the exact place of the failure. Due to the special design of the GIL, there are disconnecting units placed every 1200 m to 1500 m to separate the insulation gas and to connect high voltage test equipment; this makes it possible to repair the failed section without releasing all the insulation gas.

6.8.2 Operational Responsibilities and Offshore Grid Codes

As mentioned previously, most of the developed projects occur in the North Sea. Therefore, some of the planned projects will be shared between countries. The clear division of operational responsibilities for an international offshore grid is more complicated than for between national transmission operators. In addition, the agreement of which offshore grid codes should be used represents a challenge. The development of European network codes as initiated by the European

Commission, which is expected to be made public very soon, is the first step towards overcoming this challenge. Uniform grid connection requirements need to be determined for connecting wind plants to the transnational offshore grid [6],[7],[129].

6.8.3 Financing the Large Investments

Establishing such offshore grids will be expensive due to the large amount of high cost equipment and the high cost of installing this equipment in an offshore environment. The overall benefits of an international offshore grid from the system perspective cannot directly be returned to the investor. Therefore, an indication of long-term commitment and reliability in national offshore policies is needed to attract investors. Otherwise, investments in onshore and offshore grid infrastructure will not be made in sufficient magnitude. In addition, it may be the case that publicly funded securities are needed to give a breakthrough for pioneering offshore investments. At the aggregate level, raising enough funds for an offshore grid is viewed by the offshore grid consortium as a major challenge [6], [7], [129].

6.9 Summary

The PTP system is an AC transmission system for high and extra high voltage based on GIL. Compared to other transmission technology, a PTP system has high transmission capacity; a low power loss, which means high efficiency; and a high overload capacity. Moreover, it allows the transfer of bulk power over long distances.

The idea of a PTP system is based on clustering wind power projects in one main substation. Sharing the transmission system offers the most advantages. When a high number of wind farm capacities are connected in a small area and when the clusters' capacities are about the standard size of the PTP transmission system, sharing one transmission system can reduce the amount of planning, installation, and maintenance and can even be more economical than individual connections.

In addition, apart from the economic comparison with other transmission technologies, a PTP system can help to mitigate the environmental and social impact of laying multiple cables through sensitive coastal areas and allow for more efficient logistics during installation. These benefits need to be balanced with the risk of bounded investments.

CHAPTER 7: ECONOMIC COMPARISON OF ESTIMATION COST FOR HVAC-PTP AND HVDC-VSC OFFSHORE TRANSMISSION SYSTEMS

7.1. Introduction

The decision to use HVAC or HVDC transmission technology involves an economic analysis of the proposed project where the costs of the transmission line, stations, and power losses have to be considered. As mentioned in previous chapters, the rapid growth in the development of offshore wind farms requires a transmission system with high transmission capacity and low power losses [6].

Moreover, the capability of transmitting power over long distances is an important feature. Therefore, due to their capability of transmitting high power over long distances, an economic comparison has been made between two possible offshore transmission technologies: HVAC-PTP and HVDC-VSC systems. The most difficult part of this study was finding the most recent data concerning the cost of the various components of the transmission technologies that are under investigation. This is because the related industry treats this information and data as confidential, or they just give estimated data.

In this chapter, the total build costs of a new transmission system for both transmission technologies have been estimated; these are subdivided into the fixed build cost and the variable build cost. The variable operation cost has been estimated as well and has been divided into maintenance cost and power losses cost during the lifetime of the equipment. The overall lifetime cost of both

transmission technologies has been estimated as lifetime cost per km. The power transmission cost (PCT) has been calculated as lifetime cost per km for each MVA/MW being delivered to the receiving end of the proposed transmission line length.

7.2. Proposed Transmission Systems

Two basic factors affect the total cost of any electrical transmission system: the amount of power they are expected to transfer and the length of the transmission line. In this study, two different transmission capacities have been considered. The HVAC-PTP low transmission capacity consists of two AC circuits, each of 2000 MVA at 420 kV, whereas the HVAC-PTP high transmission capacity consists of two AC circuits, each of 3180 MVA at 420 kV.

The HVDC-VSC low transmission capacity consists of two DC bi-poles, each of 1500 MW at ± 320 kV while the high transmission capacity consists of four DC bi-poles, each of 1500 MW at ± 320 kV. Two basic route lengths have been chosen to carry out this comparison study. The first is a 75 km line length, as this distance is the maximum economic distance for utilizing XLPE cables as a transmission system, and the second is a 300 km line length, which can fulfil the transmission distances required for an offshore development scenario in the North Sea with the transmission equipment having a lifetime of 25 years.

It should be noted that two layout options for the PTP technology have been considered, the first option is directly buried aluminium pipes coated with a thick layer of PE or PP, and the second option is aluminium pipes laid in a subsea

tunnel. However, the only layout option for HVDC technology under consideration is directly buried cables under the seabed.

These choices have been made based on a consideration of future offshore wind farm requirements with a close evaluation of planned projects in the Dogger Bank Teesside project, Round 3 in the UK, and German planned projects in the North Sea [130], [121].

The main components of the total cost of the HVAC-PTP transmission technology are: the main collection substation, the GIL equipment including the insulation gas, and the layout technology option, that is, whether it is coated with a PE insulation layer or installed inside a subsea-constructed tunnel. The main components of the total cost of HVDC-VSC transmission technology are the converter stations both offshore and onshore, the DC cables, onshore land use, and the offshore substations.

The implementation of such large projects is extremely complicated and involves many factors and variables that affect their total economic cost; however, many of these are not recognized by the public. Such costs include the settlement cost of the seabed the transmission connection runs through; the onshore land cost for the onshore substation; the world metal price, which fluctuates daily, and the cost of labour.

The blue boxes in Figure 7-1 show the boundaries of each transmission system considered in this calculation. The offshore wind farm platform and its electrical equipment, including the XLPE cables connecting the wind farm collection points to the main collection substations, are considered as forming part of the wind-farm generation side rather than the transmission system side [131].

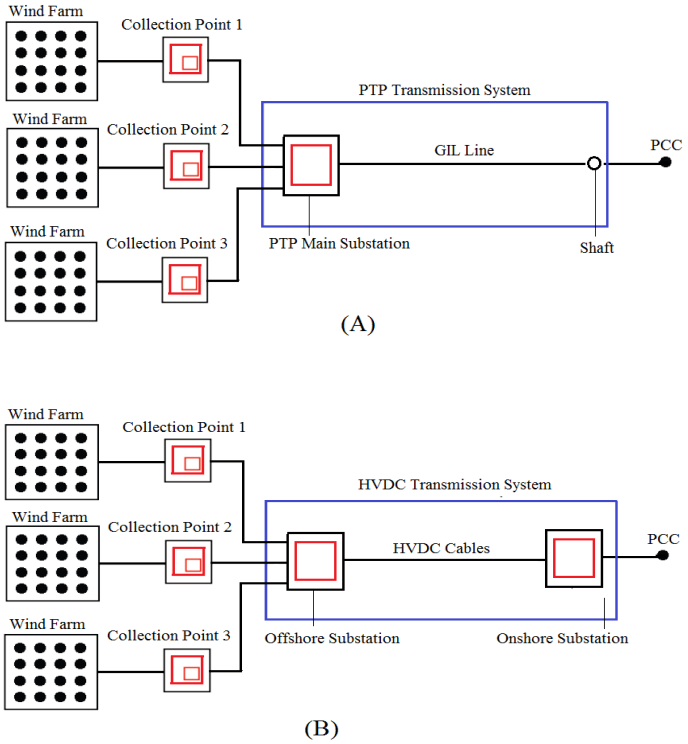

Figure 7-1: Transmission System Boundaries (A) HVAC-PTP System, (B) HVDC-VSC System

7.3. Economic Comparison

7.3.1. Introduction to the Lifetime Cost Method

The following steps indicate the method used to calculate the lifetime cost [132]:

- The total build cost for each new transmission technology has been divided into the fixed build cost and the variable build cost. The fixed build cost is not dependant on the length of the new transmission system being constructed, such as costs for project planning and management and equipment for the termination of the transmission line at both ends, that is, offshore and onshore. The variable build cost varies depending on the transmission system length, such as costs for studying the route and the transmission line layout option requirements.

- Variable operation costs also include costs that depend on the length, such as the cost for the transmission line and whether it is conventional cable or aluminium pipes, including the insulation gas. Moreover, the maintenance of the equipment during its lifetime and the power losses costs are also included. These costs increase over the lifetime of the equipment. The sum of the fixed build cost, the variable build cost, and the variable operation cost combine to make the total lifetime cost.
- By dividing the lifetime cost by the length of the transmission system, the value of the lifetime cost per km can be calculated.
- By dividing the lifetime cost per km by the total transmission capacity, the power transfer cost (PTC) for each MVA/MW delivered to the receiving end can be calculated, which will compensate for the difference in the transmission capacities between the proposed transmission systems.

7.3.2. Initial Investment Cost

The transmission systems component costs data were taken from the most recent electrical transmission costing reports. In 2012, European Network of Transmission System Operators for Electricity (ENTSOE) prepared a report for the EU about different offshore transmission technology options and their costs [133]. Moreover, on 31 January 2012, the Institution of Engineering and Technology and Parsons Brinckerhoff published a report about the costs of a new electricity transmission infrastructure [132].

The price given in [132] was based on the British market and the British currency; this study has been shown by the UK national grid on February 2012 to be a very valuable costing data source [134]. For other price sources, exchange rates of

GBP£/EUR€ = 0.88 and EUR€/US$ = 1.4 [132] have been used to convert the price to pounds sterling.

The previous sources considered in this study are considered the most recent and reliable sources since their authors have listed as their price sources most of the industrial companies that have a relationship with this kind of projects, which has provided them with the most accurate data. However, none of them have costs for an offshore transmission system 300 km from the shore; therefore, adjustments have been made in order to match the specific characteristics of the proposed transmission systems.

7.3.3. HVAC-PTP Investment Cost

7.3.3.1. Total Fixed Build Cost

The overall fixed build cost comprises the costs for project launching and management studies; the PTP main substation; and the equipment needed at both ends, such as GIL termination equipment compatible with air-insulated switchgear. It also includes the cost of the transmission line route selection.

According to [132], the fixed build cost value for 75 km of directly buried GIL aluminium pipes with 2*2000 MVA low transmission capacity is £7.4 M. However, the fixed build cost of 2*3190 MVA high transmission capacity is similar to the fixed build cost of low transmission capacity, due to the high transmission capability of GIL, which can transmit up to double the low transmission capacity with no additional equipment [19].

Moreover, the total fixed build cost value for 75 km GIL aluminium pipes laid inside a subsea tunnel and having low transmission capacity is £278.2 M [132].

The fixed build cost of high transmission capacity is also similar to the fixed build cost for low transmission capacity for the same reason. It can be noted that the big difference in the fixed build cost for both layout options is due to the high cost of the subsea tunnel construction.

The fixed build cost value for 300 km line length and directly buried GIL aluminium pipes is £7.4 M for both low and high transmission capacities. However, the fixed build cost value for 300 km GIL installed inside a subsea tunnel for both low and high transmission capacities increases to £1090.6 M. This cost was calculated based on assumption taken from [132]. The fixed build cost value for 300 km was calculated by multiplying the cost of 75 km cost for the components depend on the transmission line length by four times [132]. The components that make up the total fixed build cost for both layout options and different transmission capacities for both 75 km and 300 km are shown in Table 7-1.

Table 7-1: Estimated Total Fixed Build Cost for both Layout Options and Different Transmission Capacities for 75 km and 300 km HVAC-PTP Transmission Technology [132]**.**

Fixed Build Cost Component	Directly Buried GIL 2*2000 MVA 75 & 300 km	GIL In Tunnel 2*2000 MVA 75 km	GIL In Tunnel 2*2000 MVA 300 km	Directly Buried GIL 2*3180 MVA 75 & 300 km	GIL In Tunnel 2*3180 MVA 75 km	GIL In Tunnel 2*3180MVA 300 km
GIL Termination (AIS) and Testing	£2.3 M [132]	£2.3 M [132]	£2.3 M	£2.3 M [132]	£2.3 M	£2.3 M
GIL Terminal Compound	£5.1 M [132]	£5.1 M [132]	£5.1 M	£5.1 M [132]	£5.1 M	£5.1 M
Tunnel + Shafts Design and Equipment	-	£149.6 M [132]	£598.4 M	-	£149.6 M	£598.4 M
Tunnel Boring Machine Cost	-	£23.6 M [132]	£94.4 M	-	£23.6 M	£94.4 M
Tunnel PM	-	£97.6 M [132]	£390.4 M	-	£97.6 M	£390.4 M
Total Fixed Build Costs	£7.4 M [132]	£278.2 M [132]	£1090 M	£7.4 M [132]	£278.2 M	£1090 M

7.3.3.2. Total Variable Build Cost

The variable build cost makes up the biggest part of the total lifetime cost. The variable build cost of the PTP covers the cost of those items that principally vary by transmission line length. The material and the insulation gas cost for the GIL aluminium pipes required for the proposed line length is included in the variable build cost. The costs associated with construction of the tunnel and shafts are also included.

The volume of the aluminium material required for the GIL pipes is defined by the diameter of the pipe and the wall thickness of the pipe. The diameter of the pipe is defined by the rated voltage for the enclosure and the conductor pipe. Depending on the power to be transmitted per circuit and the voltage level the volume of aluminium required can be calculated.

For 420 kV GIL, 1 km of single phase GIL aluminium pipe requires 47.310 tonnes of aluminium material [78]. To make a three-phase circuit requires 141.93 tonnes per km. For example, 300 km of GIL requires 42579 tonnes of aluminium material. The price of aluminium on the international metal markets in January 2012 was £1867 per tonne [132]. Based on this calculation, the total aluminium material required for 300 km GIL costs £79.495 M. It should be noted that this cost does not include the sampling of GIL pipes and fitting the conductor inside the enclosure with all the equipment required and the outer PE insulation coated layer.

The volume of the insulation gas required for a 1 km single-phase GIL is 5.72 tonnes, which makes 17.16 tonnes per three-phase system [78]. In addition, 5148 tonnes of insulation gas are required for 300 km. CF_3I is the insulating gas

considered for this calculation. However, as noted in the literature review, CF_3I is a new artificial gas, and its production still does not meet the industrial requirement [135].

Recently, at least two manufacturers have invested in producing commercial quantities of CF_3I to create sufficient capacity to fulfil all foreseeable requirements. Active competition is already occurring, and the price of CF_3I has been reduced from over £630 per kg to around £62.86 per kg at present [136]. For this calculation, the price of £62.86 per kg has been used, which makes a total cost of £323.6 M.

It should be notes that, the recovery of aluminium pipe material and the disposal of insulation gas after 25 years lifetime was taken in consecration in [132]. The increase of the aluminium material cost on the international metal markets has reduced the variable build cost by 10% after the accounting of the cost of extracting the aluminium pipes from the sea bed and the disposal of the insulation gas.

According to [132], which has considered all previous factors, the total variable build cost for 75 km of directly buried GIL aluminium pipes for low transmission capacity is £937.4 M. The variable build cost of high transmission capacity is also similar to the variable build cost of low transmission capacity because no additional equipment is required.

The total variable build cost value for 75 km of GIL aluminium pipes inside a subsea tunnel for low transmission capacity is £1606 M, which is similar to the variable build cost of high transmission capacity [132]. The components making

up the total variable build cost for a 75 km line length and both layout options are shown in Table 7-2.

The total variable build cost for 300 km with both layout options was calculated based on the same assumption taken from [132]. The fixed build cost value for 300 km was calculated by multiplying the cost of 75 km for the components depend on the transmission line length by four times [132]. The total variable build cost for 300 km directly buried GIL with low transmission capacity is £3750 M, which is equal to the cost of high transmission capacity. The total variable build cost for 300 km of GIL installed inside a subsea tunnel is equal to £6424 M. This cost is similar to the variable build cost of high transmission capacity. The components making up the total variable build cost for a 300 km line length and both layout options are shown in Table 7-2.

Table 7-2: Estimated Variable Build Cost of Different Layout and Different Transmission Capacities Options for 75 km and 300 km HVAC-PTP Transmission System.

Variable Build Cost Component	Directly Buried GIL 2*2000 MVA 2*3180 MV 75 km	GIL In Tunnel 2*2000 MVA 2*3180 MV 75 km	Directly Buried GIL 2*2000 MVA 2*3180 MV 300 km	GIL In Tunnel 2*2000 MVA 2*3180 MV 300 km
Equipment Costs (GIL Aluminium Tubes + Gas insulation)	£561.2 M [132]	£561.2 M [132]	£2244.8 M	£2244.8 M
Civil Costs Including EP Coating Layer or Special Tunnel Construction	£131.3 M [132]	£211.2 M [132]	£525.2 M	£844.8 M
Project Launching + mgmt.	£140 M [132]	£140 M [132]	£560 M	£560 M
Build Contingency (GIL)	£105 M [132]	£489.4 M [132]	£420 M	£1957.6 M
Tunnel Boring Machine Costs	-	£147.5 M [132]	-	£590 M
Tunnel PM	-	£56.7 M [132]	-	£226.8 M
Total Variable Build Costs	£937.5 M [132]	£1606 M [132]	£3750 M	£6424 M

7.3.3.3. Total Operation Cost

The variable operation cost is a combination of the operating and maintenance costs. The cost related to power losses at the power station and the transmission system as well the cost for reactive power compensation. In general, the real power losses in the GIL are relatively low, as was shown in Chapter 4, comprising less than 2% of the total power losses for a 300 km GIL line length.

Wind farms have a variable output and they will not operate at their full nameplate capacity all the time. Therefore, the GIL will not operate at 100% load condition. As the load condition decreases the voltage drop at the load bus increases which require reactive power compensation to be connected to the load bus to maintain the bus voltage within acceptable limit.

The normal way of controlling the voltage drop is to install reactive power compensation in the form of shunt reactors or shunt capacitors. the capacitor affect in the GIL line is high than the inductive affect, but due to the large inductive load connected to the bus load, the GIL will require capacitive reactive power compensation to be connected at the load bus.

These compensation devises are, however, large and expensive. According to [133] the cost of supplying and installing a 200 Mvar capacitor has been estimated to be £5.786 M. Thus the cost of reactive compensation has been estimated to be £28.9 per Mvar.

According to the reviewed literature, the gas-insulated technology does not require much maintenance during their lifetime. Therefore, the variable operation cost for 75 km of directly buried GIL is £37.3 M for low transmission capacity

whereas the variable operation cost for high transmission capacity is £48.2 M [132].

The total variable operation cost for 75 km of GIL inside a subsea tunnel is £54.85 M for low transmission capacity whereas the variable operation cost for high transmission capacity is £70.9 M [132]. The components making up the total variable operation cost for both layout options are shown Table 7-3.

Table 7-3: Estimated Variable Operation Cost of Different Transmission Capacities and Different Transmission Layout Options for 75 km PTP Transmission System [132]**.**

Variable Operation Cost component	Directly Buried GIL 2*2000 MVA 75 km	GIL In Tunnel 2*2000 MVA 75 km	Directly Buried GIL 2*3180 MVA 75 km	GIL In Tunnel 2*3180 MVA 75 km
Cost of Power Losses (Station)	£10.4 M	£10.4 M	£15.3 M	£15.3 M
Cost of Energy Losses (Fuel)	£18.2 M	£18.2 M	£18.2 M	£18.2 M
Operation and Maintenance	£8.7 M	£19.6 M	£21.35 M	£37.4 M
Total Variable Operation Cost	£37.3 M	£48.2 M	£54.85 M	£70.9 M

The variable operation cost for 300 km of directly buried GIL is £149.2 M for low transmission capacity whereas the variable operation cost for high transmission capacity is £219.4 M.

The total variable operation cost for 300 km of GIL aluminium pipes inside a tunnel is £192.8 M for low transmission capacity whereas the variable operation cost for high transmission capacity is £283.6 M. The components making up the total variable operation cost for both layout options are shown in Table 7-4.

Table 7-4: Estimated Variable Operation Cost of Different Transmission Capacities and Different Transmission Layout Options for 300 km PTP Transmission System

Cost component	Directly Buried GIL 2*2000 MVA 300 km	GIL In Tunnel 2*2000 MVA 300 km	Directly Buried GIL 2*3180 MVA 300 km	GIL In Tunnel 2*3180 MVA 300 km
Cost of Power Losses (Station)	£41.6 M	£41.6 M	£61.2 M	£61.2 M
Cost of Energy Losses (Fuel)	£72.8 M	£72.8 M	£72.8 M	£72.8 M
Operation and Maintenance	£34.8 M	£78.4 M	£85.4 M	£149.6 M
Total Variable Operation Cost	£149.2 M	£192.8 M	£219.4 M	£283.6 M

7.3.3.4. HVAC-PTP Total Lifetime Cost

The lifetime cost for both different HVAC-PTP layout technologies and different transmission lengths are shown in Table 7-5.

Table 7-5: Calculated Lifetime Cost with both Different Layout Technologies and Different Transmission Capacities for 75 and 300 km Line Length

Cost component	Directly Buried GIL 2*2000 MVA	GIL In Tunnel 2*2000 MVA	Directly Buried GIL 2*3180 MVA	GIL In Tunnel 2*3180 MVA
75 km Line length				
Total lifetime cost	£982.2 M	£1932.4 M	£999.75 M	£1955M
Lifetime cost per km	£13.1 M	£25.8 M	£13.33 M	£26.1 M
Power Transfer Cost £/MVA-km	3274 £/MVA-km	6441.3 £/MVA-km	2096 £/MVA-km	4104 £/MVA-km
300 km Line length				
Total lifetime cost	£3906.6 M	£7707.4 M	£3976.8 M	£7798.2 M
Lifetime cost per km	£13.02 M	£25.7 M	£13.256 M	£26 M
Power Transfer Cost £/MVA-km	3255.5 £/MVA-km	6425 £MVA-km	2084.3 £/MVA-km	4088.1 £/MVA-km

7.3.4. HVDC-VSC Investment Cost

Several economic studies have been conducted to determine the final HVDC-VSC transmission system price. For the converter substations, ENTSOE has reported a price of £70-£75 M for 800 MW $\pm$ 320 kV and £86.43-£107 M for 1250 MW $\pm$ 500 kV [133]. This price includes all electrical equipment (valves, reactors, filters, capacitors, etc.).

In [137], a price of £32.14 M for 375 MVA $\pm$ 150 kV was reported. In [13], the author stated a price of £99.75 M for a 600 MW substation. This price included £85.7 M for the converter station; £2.89 M for the power auxiliary transformers; £4.857 M for the HV and LV switchgears; £1.5 M for the standby generator, ancillary services, workshop accommodation and fire protection; and finally £4.75 M for the installation of the electrical equipment.

Regarding the DC cable cost, ABB reported a cross section area of 1400 mm^2 per cable for a M9 converter module with a rated capacity of 1216 MVA at $\pm$ 320 kV [138]. ENTSOE has reported a cost of £0.246-£0.37 M per km/cable with 1200-1500 mm^2 cross-section area at $\pm$ 320 kV.

In [13], a price of £0.153 M per km/cable for 1600 mm^2 was reported. In 2010, [137] £0.43 M per km/cable-pair was recommended. As can be seen, the price differs from source to source possibly because of the commodity price fluctuation for copper and aluminium.

ENTSOE has reported that the cable installation cost is very difficult to estimate as many factors affect that estimation. Therefore, ENTSOE has estimated a value ranging between £0.411-0.75 M per km for a twin cable in a single trench. A

value of £0.5-£0.98 M per km has been estimated for two single cables in different trenches. In 2010, [137] a value of £0.245 M per km/cable-pair was reported. While, in [13], a value of £0.26 M per km/cable-pair plus £3.6 for cable mobilization was reported.

The offshore platform is an additional cost to the previous costs. ENTSOE reports a case study of 800-1000 MW at ± 320 - 500 kV of 8000 tonne, where the topside costs £49.3-£66 M, the jacket £23-£29 M and the installation £22-£26 M; also, it reports a self-installing platform of £100-£120 M.

In [137], the author has reported a cost of £24 M for installation of a 300 MW substation with dimensions of 30*40*20 m. In [13], a £27.6 M offshore platform of 60*40*30 m of 600 MW and 4500 tonne was reported, with a topside of £3.51 M, a jacket of £4.072 M, and pile pins of £2.81 M. Thus, it is clear how difficult it is to find an intermediate value due to the wide cost range.

Therefore, according to [132], which considered all previous factors affecting the final build cost of the HVDC-VSC transmission system, a fixed build cost of £717.9 M was stated for 75 km line length and low transmission capacity whereas the fixed build cost of 1376.3 M for 75 km and high transmission capacity [132].

A fixed build cost of £1169.7 M was calculated for 300 km and low transmission capacity whereas a £2228 M fixed build cost was calculated for 300 km and high transmission capacity due to the double amount of equipment required for the project. Table 7-6 shows the cost of components that make up the total fixed build cost for both transmission capacities.

Table 7-6: Estimated Fixed Build Cost of Different Transmission Capacities for 300 km HVDC-VSC Transmission Technology.

Estimated Cost Component	2*1500MW 75 km	4*1500 MW 75 km	2*1500MW 300 km	4*1500 MW 300 km
Converter Project Launch + mgmt.	£67.8 M	£84.8 M	£102 M	£129.74 M
Converter EPC Contract Cost	£76.3 M	£152.6 M	£113.1 M	£233.5 M
Converter EPC Contract Cost (EUP Costs)	£488.7 M	£977.5 M	£816 M	£1632 M
Converter Build Contingency	£63.3 M	£121.5 M	£96 M	£185.9 M
Cable Studies and Assessments	£0.2 M	£0.8 M	£3.4 M	£7.8 M
Cable landing Costs Materials	£18.3 M	£36.5 M	£18.3 M	£18.3 M
Cable mobilisation	£3.4	£3.4	£20.9	£20.9
Total Fixed Build Cost	£717.9 M	£1376.3 M	£1169.7 M	£2228 M

The total variable build cost, which is strongly affected by the transmission line length and the commodity price fluctuation for copper and aluminium, has been taken as £185.9 M for low transmission capacity and 75 km, whereas the variable build cost of high transmission capacity and 75 km is £367.3 M [132].

The variable build cost of £772.8 M was calculated for low transmission capacity and 300 km and £1469.2 M for high transmission capacity and 300 km. Table 7-7 shows the cost of components that make up the total variable build cost for both different line lengths and different transmission capacities.

Table 7-7: Estimated variable Build Cost of Different Transmission Capacities for 300 km HVDC-VSC Transmission Technology.

Cost Component	2*1500MW 75 km	4*1500 MW 75 km	2*1500 MW 300 km	4*1500 MW 300 km
Cable Contractor PM	£6.8 M	£13 M	£27.2 M	£52 M
Cable Studies and Assessments	£20 M	£38 M	£80 M	£152 M
Cable Material and installation	£95.6 M	£191.3 M	£382.4 M	£765.2 M
Bad Weather Allowance (Cable)	£12.1 M	£24.2 M	£48.4 M	£96.8 M
Marine Insurance (Cable)	£4.6 M	£9.1 M	£20.4 M	£36.4 M
Cable Subsea Service Crossing	£5.1 M	£10.3 M	£48.4 M	£41.2 M
Cable Project Launch + mgmt.	£16.6 M	£32.6 M	£66.4 M	£130.4 M
Cable system build contingency	£24.9 M	£48.9 M	£99.6 M	£195.6 M
Total Variable Build Cost	£185.7 M	£367.3 M	£772.8 M	£1469.2 M

The variable operation cost depends on the route length of the transmission system. It is a combination of the costs related to power losses at the power station, and operation and maintenance over the lifetime of the transmission equipment with a converter refurbishment at the midlife time. System losses are a very important factor for the economic efficiency of an HVDC system.

VSC-HVDC losses are divided into two elements: converter station losses and cable losses. The losses for a VSC-HVDC converter depend on many parameters (switching frequency, IGBT losses, snubber circuits, etc.) and are complicated to

calculate. The power losses in the HVDC cable are lower than the power losses at the converter station [137].

Therefore, the power losses are often specified as a guaranteed value. They should be verified in a suitable manner by the manufacturer. Losses above the specified guaranteed value are subject to monetary penalties. Direct measurement of system losses is not possible due to the lack of precision of available measuring instruments and methods. For this reason, it can be taken as a fixed value.

The variable operation cost for 75 km line length and low transmission capacity is £325.1 M and for high transmission capacity is £643 M [132] whereas a variable operation cost of £1283.3 M has been calculated for 300 km line length and low transmission capacity. A £2537.7 M variable operation cost for high transmission capacity has been calculated due to double the amount of equipment being required. Table 7-8 shows the cost of components that make up the total variable operation cost for the different line lengths and different transmission systems.

Table 7-8: Estimated Variable Operation Cost of Different Transmission Capacities for 300 km HVDC-VSC Transmission Technology.

Cost Component	2*1500MW 75 km	4*1500 MW 75 km	2*1500 MW 300 km	4*1500 MW 300 km
Combined Cost of Power Losses	£51.5 M	£100.4 M	£206 M	£401.6 M
Combined Cost of Energy Losses	£90.6 M	176.6 M	£362.4 M	£706 M
Combined Operation and Maintenance	£177.3 M	£354.7 M	£709.2 M	£1418.8 M
Converter Refurbishment	£5.7 M	£11.3 M	£5.7 M	£11.3 M
Total Variable Operation Cost	£325.1 M	£643 M	£1283.3	£2537.7

7.3.4.1. HVDC-VSC Total Lifetime Cost

The lifetime cost for HVDC-VSC transmission technology has been calculated for different transmission capacities and different transmission line lengths. The calculation results are shown in Table 7-11.

Table 7-9: Calculated Total Lifetime Cost of HVDC-VSC Transmission Technology for Different Transmission Capacities and Different Transmission Line Lengths

Cost component	2*1500 MW 75 km	4*1500 MW 75 km	2*1500 MW 300 km	4*1500 MW 300 km
Total lifetime cost for 300 km	£1228.9 M	£2386.6 M	£3225.8 M	£6234.9 M
Lifetime cost per km	£16.4 M	£31.82 M	£10.75 M	£20.8 M
Power Transfer Cost £/MW-km	5461 £/MW-km	5303.6 £/MW-km	3584.2 £/MW-km	3467 £/MW-km

7.4. Lifetime Cost Comparison

Total lifetime cost analysis has been carried out for different transmission distances from the main collecting offshore substation to the first onshore connection point (PCC) and for different transmission capacities as presented in the next section.

7.4.1. Transmission Distances

Figure 7-2 shows the lifetime cost per km for both HVAC-PTP and HVDC-VSC transmission technologies and 75 km route length. From Figure 7-2 it can observe the following:

- The directly buried GIL appears to be the cheapest transmission option for this line length for both transmission capacities. The 1km lifetime cost for

directly buried GIL and low transmission capacity costs £13.1 M, whereas for the high transmission capacity costs £13.33 M. It can be notes that there is no much deference in the life time cost by increasing the transmission capacity from low to high.

- The lifetime cost for 1km GIL laid in tunnel has been increased by about 98% comparing to the directly buried GIL transmission option, due to the high cost of the variable operation cost, which include the cost of the subsea tunnel. The 1km GIL laid in tunnel costs £25.8 M for low transmission capacity and it costs £26.1 M for high transmission capacity. It can be observed also the lifetime cost deference between low and high transmission capacities is verily low.
- The lifetime cost for 1km HVDC-VSC transmission technology and low transmission capacity is £16.4 M, which is higher than the directly buried GIL transmission technology for both low and high transmission capacity. For high transmission capacity the 1km costs £31.82 M.

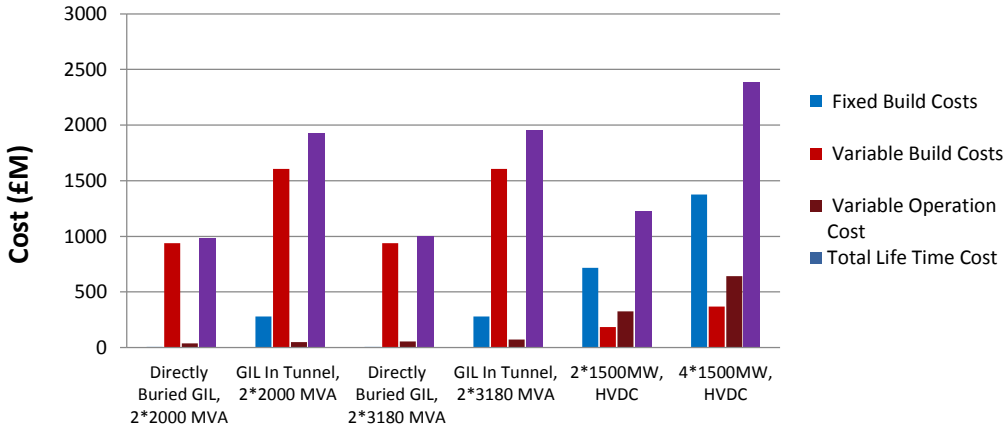

Figure 7-2: Total Lifetime Cost for both HVAC-PTP and HVDC-VSC Transmission Technologies and Length of 75 km.

Figure 7-3 shows the lifetime cost per km for both HVAC-PTP and HVDC-VSC transmission technologies and 300 km route length. From Figure 7-3 it can observe the following:

- The 1km lifetime cost for directly buried GIL and low transmission capacity costs £13.02 M, whereas for the high transmission capacity costs £13.3 M. It can be notes also there is no much deference in the lifetime cost when the transmission capacity increases from low to high.
- The lifetime cost for 1km GIL laid in tunnel has been increased by about 98% comparing to the directly buried option due to the high cost of the subsea tunnel. The 1 km GIL laid in tunnel costs £25.7 M for low transmission capacity and it costs £26 M for high transmission capacity. It can be observed also the life time cost deference between low and high transmission capacities is verily low.
- The life time cost for 1km HVDC-VSC transmission technology and low transmission capacity is £10.75 M, which is cheaper than the directly buried GIL transmission technology for both low and high transmission capacity. For high transmission capacity the 1km costs £20.8 M, Which more expensive than directly buried GIL option and cheaper than the GIL laid in subsea tunnel for this route length.

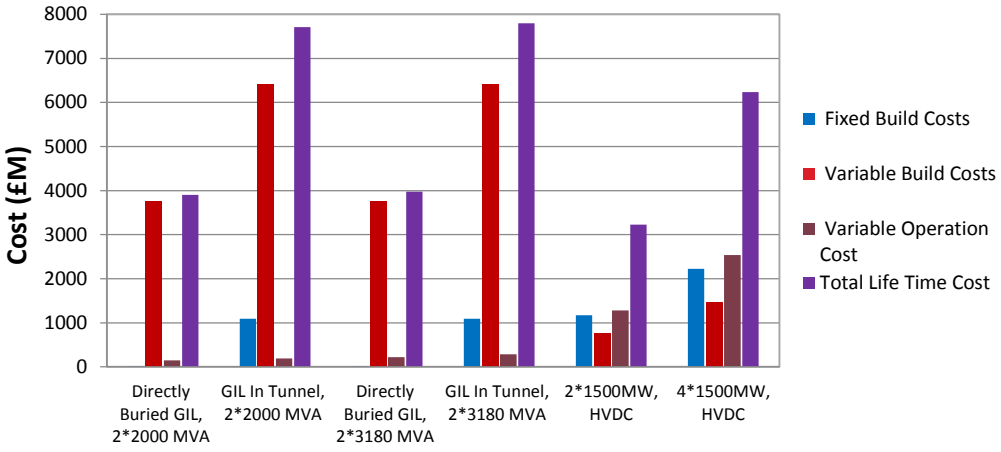

Figure 7-3: Total Lifetime Cost for both HVAC-PTP and HVDC-VSC Transmission Technologies and Length of 300 km.

7.4.2. Transmission Capacity

Figure 7-4 shows the effect of different transmission capacities on the total cost of each MVA/MW delivered to the receiving end of the proposed transmission line lengths:

- For HVAC-PTP and 75 km directly buried transmission system with low transmission capacity, each MVA delivered to the receiving end costs £3274, whereas each MVA delivered by the high transmission capacity costs £2096.
- For HVAC-PTP and 75 km line length using a subsea tunnel, each MVA delivered to the receiving end costs £6441.3 for a low transmission capacity system, while it costs £4104 when the transmission capacity is increased to a high transmission level.
- For HVAC-PTP and 300 km directly buried transmission system with low transmission capacity, the MVA delivered to the receiving end costs

£3157.5, whereas it costs £2013 when the transmission capacity is increased to high transmission capacity.

- For HVAC-PTP and 300 km line length using a tunnel construction under the seawater, each MVA delivered by a low transmission capacity system costs £5964.5, whereas it costs £3559.7 for a high transmission capacity system.
- For HVDC, the high cost of each MW delivered to the receiving end for both transmission capacities and 75 km line length can be seen from figure 7-3. Each MW delivered to the end of a 75 km line length with low transmission capacity costs £5467, whereas it costs £5303.3 for high transmission capacity.
- For 300 km line length, each MW delivered to the receiving end for low transmission capacity costs £3583.3, whereas it costs £3467 for high transmission capacity.

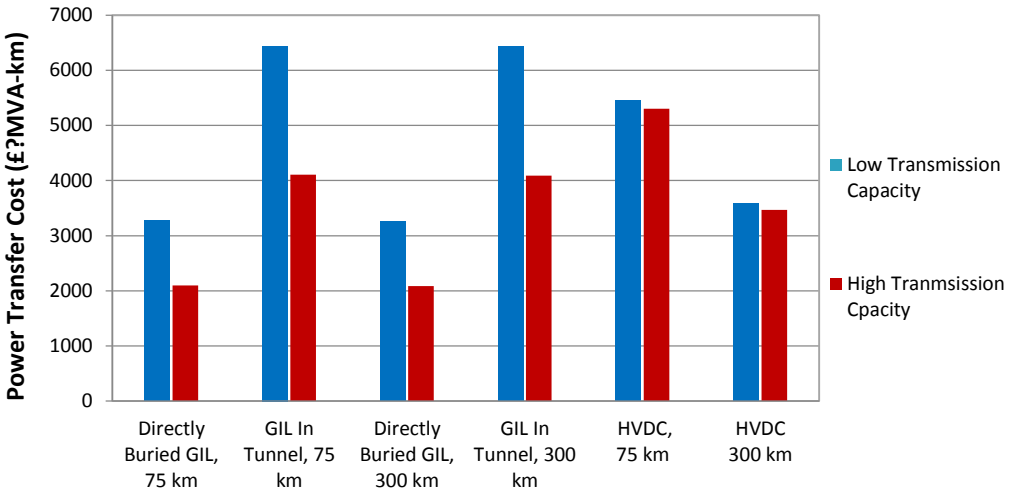

Figure 7-4: Power Transfer Cost for Each MVA/MW Delivered to the Receiving End of Proposed Transmission Line Lengths

7.5. Summary

The lifetime cost per km and the power transfer cost per MVA/MW for both transmission technologies, that is, HVAC-PTP and HVDC-VSC, have been calculated. The different transmission capacities and different layout options, especially for the HVAC-PTP transmission technology, have been considered, whereas the layout technology considered for HVDC-VSC transmission technology is directly buried cables under the seabed due to the strong characteristics of XLPE cables. These cables can be laid under difficult conditions, such as subsea, without the need for a tunnel to protect them. The economic comparison of both transmission technologies, HVAC-PTP and HVDC-VSC, reveals the following.

The increase in the lifetime cost for HVAC-PTP between low and high transmission capacities are verily low, due to the high transmission capacity of the GIL which can transmit about double of the transmission capacity without needs for extra equipment. Therefore, from the economic point of view, increase the power capacity that can be transmitted through the PTP system lead to decrease the cost of each MVA delivered to the reserving end.

The 1km lifetime cost of HVAC-PTP transmission technology with high transmission capacity and directly buried transmission technology appears to be the most economic transmission option for line length of 75 km. For subsea tunnel layout option the lifetime cost has increased by about 98% but it is still cheaper than the HVDC-VSC transmission technology with high transmission capacity for this line length.

The 1km lifetime cost of HVAC-PTP transmission technology with high transmission capacity and directly buried transmission technology is still the most economic transmission option for line length of 300 km. Whereas, the HVDC-VSC transmission option with high transmission capacity is more economic option than the HVAC-PTP with subsea tunnel for this line length due to the high cost of the subsea tunnel.

Furthermore, the power transfer cost has shown that the HVAC-PTP with high transmission capacity and directly buried layout option delivers the cheapest MVA to the receiving end of both proposed transmission line lengths.

The HVAC-PTP with a tunnel construction layout technology appears to be significantly expensive, and the MVA delivered to the receiving end by this layout option is the most expensive compared to the other transmission options, which make this layout option not viable.

The HVDC-VSC transmission technology with both transmission capacity and short line length 75 km delivers the most expensive MW for this route length. Whereas, for 300 km the MW delivered to the receiving by high transmission capacity slightly cheaper than the MVA delivered by HVAC-PTP laid in subsea tunnel.

CHAPTER 8: GENERAL CONCLUSION, DISCUSSION, AND FUTURE RESEARCH

This chapter discusses the main conclusions and recalls the key parts of the work undertaken. Future research and recommendations are also proposed.

Renewable energy sources will enter the electrical power market as large-scale generators or as distributed small-sized power installations. Large-scale electrical power generators are usually located far away from the load centres, which need to be connected through the electric power grid. The limitation in the transmission distances and the transmission capacity of existing transmission systems are pushing for the development of a new transmission system to fulfil these requirements.

Therefore, the aims of this thesis are to investigate and evaluate the technical and economical suitability of using HVAC gas-insulated transmission line (GIL) technology as a transmission system for high power capacity generated offshore over long distances.

GIL provide high transmission capacities and a fewer power losses than other cable technologies. These properties correspond with the offshore-generated power transmission requirements to the mainland. Moreover, GIL has a proven reliability for more than 40 years inside substations for relatively short lengths without any major failure.

8.1. General conclusion

The work in this thesis has been divided into three main parts. The first part is a steady state power flow study. In this part, the maximum transmission capacity of

the GIL was determined based on the line length. Moreover, the maximum transmission capacity of the GIL is compared with other HVAC transmission technologies, which gives a quick indication about the transmission capability of the GIL from both aspects, that is, the amount of transmission capacity that can be transferred and the line length.

To achieve this aim, a model of the GIL was simulated in an EMTP simulation program. Moreover, for comparison purposes, a model of overhead line and XLPE cable was simulated as well. The GIL showed high power transmission capability over long distance with no reactive power compensation. The economic distances, which were defined by 90% of the power transmission capacity being delivered by GIL, was 7 times higher than the economic distances for the XLPE cable which was operating with 50/50% reactive power compensation connected to both ends.

The electrical transmission characteristics of different line lengths, ranging from 200 km to 500 km were studied. The limiting factor of transmission characteristics was the voltage drop at the receiving end of the GIL, which is the load side. Based on the SQSS, the voltage drop limit for the operation and maintenance of the offshore transmission system was +5% and -10%.

Even though, The GIL showed a good capability for transmitting power over the proposed transmission distances with low power losses and low reactive power generated along the GIL, the voltage drop percentage for this load condition falls outside of the voltage drop limit stated by SQSS.

Heavy inductive load was behind this voltage drop. For this load condition, in order to maintain the voltage within the voltage drop limit, shunt capacitive

reactive power compensation has to be connected to the load bus. Previous results lead to investigate the effect of different load condition on the transmission characteristics.

The transmission characteristics of the GIL for different load conditions ranging from open end to 120% load condition with 0.8 typical power factor were investigated for 300 km and 500 km line lengths. The GIL showed good performance in terms of power losses and reactive power gain along proposed line lengths. The voltage drop was within the voltage drop limit but for low load condition, which is nun-economic condition to operate such expensive transmission line. The voltage drop for higher load condition was outside of the voltage drop limit stated by SQSS. Therefore, investigation of the effect of different load power factor on the transmission characteristics was carried out.

The transmission characteristics of the GIL for different load power factors ranging from 0.8 lagging to 0.8 leading power factors for both line lengths of 300 km and 500 km were examined. The results showed that, according to the voltage drop limit for operation and maintenance of the offshore transmission system, which is +5% and -10%. The acceptable operating power factor for 300 km GIL line length is ranging from 0.95 lagging to 0.98 leading power factor. This range of load power factor was calculated for 100% load condition.

In reality, wind farms output is fluctuating due to the weather condition. They will not operate at their full nameplate capacity all the time. For this reason, the GIL transmission lines will not operate at their 100% load condition. Therefore, for lower load condition higher voltage drop will be seen at the load bus which

requires reactive power compensation to be connected to the load bus to maintain the bus voltage within the acceptable voltage drop limit.

For 500 km line length, the acceptable operating power factor range for the same load condition decreases. It is ranging from a 0.98 lagging power factor to a 0.98 leading power factor.

The impact of transients on insulation system is vital when considering switching operation of offshore transmission system. Therefore, studies on the switching transmission behaviour of the power system during energisation of 300 km offshore GIL transmission line connecting offshore wind farm to the first onshore connection point (PCC) was carried out. For this purpose, a model of the proposed GIL was simulated in EMTP. Moreover, models for other electrical network components, such as circuit breakers, XLPE cables, overhead lines, 420/33 kV generator transformers and equivalent wind farms, were simulated.

In the second part of this thesis, the impact of switching transient introduced in a gas insulated transmission GIL has been further analysed, particularly the statistical distribution of peak magnitude overvoltage at different measurement point for different offshore transmission system energistion scenario. This has been motivated by the needs for analysis of the impact of circuit breaker (CB) contact closure which are random in nature. The magnitudes of overvoltages depend strangle on the point-on-wave where the CB closed and the influence of 3-phase CB pole span.

Although the majority of the peak switching transients overvoltage obtained at different measurement point for different offshore energistion scenario are still at the average level compared to typical value indicated by IEC standard. These

values are not high enough to cause a failure in the insulation gas and further studies to limit the transients are not required. The peak switching transients overvoltage recorded at the low voltage terminal of 420/33kV transformer is 5.94pu which is exceeding the SIWV limit 4.4pu by about 35%. This value is high enough to cause a failure to the insulation at the low voltage side of the transformer terminal. This overvoltage could perhaps be reduced using surge arresters.

The transient overvoltage caused by the trapped charge during re-closing on the unloaded GIL results in the worst overvoltages at the remote end of the 300 km GIL. The transient overvoltages was recorded at the receiving end has exceeded the value specified by IEC by about 27%. This overvoltage is at high level which probability will lead to insulation failure. This overvoltage can be avoided by providing a path for the cable to discharge to earth, by connecting a shunt reactor during energisation of the line.

The effect of the line length and the feeding network on the transient overvoltage during energisation unloaded GIL line was studied as well. For line length up to 500 km line length, the overvoltages magnitude were within the average level compared to the values indicated by IEC standard for different feeding network.

The third part of this thesis deals with the practical side of installing PTP transmission technology and estimated economic comparison between the HVAC-PTP and HVDC-VSC transmission technologies. This part was started with clear explanation to the PTP technology and there components. Besides, the special design for the wind farms and the layout of the PTP, which allow better understanding to the economic comparison.

Moreover, economic comparison between the HVAC-PTP and HVDC-VSC transmission technologies was carried for a proposed offshore wind farm clusters for different transmission capacities and different transmission distances from the main collection substation to the first onshore connection point (PCC).

Two layout options were considered for GIL. First, GIL technology laid inside a subsea tunnel which appears to be very expensive for both low and high transmission capacities compared to the HVDC transmission technology due to the high cost of constructing the subsea tunnel.

Second, GIL technology laid directly under the seabed and coated with thick layer of PE, high transmission capacity appears to be more economical option than the HVDC for offshore transmission technology.

The HVDC transmission technology with high transmission capacity is more economic than the GIL installed inside subsea tunnel due to the high cost of the tunnel that increase the lifetime cost of each km by about 98%.

8.2. Future Work

- Further investigations are required into the economic benefits of the GIL transmission technology when the transmission capacity is increased to 4*3180 MVA in a transmission corridor. Moreover, further investigation is required into the economic benefit when the GIL is operated at a higher voltage, such as 550 kV and up to 4*3800 MVA, in a transmission corridor.

- Investigation is needed into the possibility of increasing the voltage up to 800 kV or the rated current by changing the dimensions of the GIL conductor and enclosure pipes.
- Investigation into the environmental impacts caused during the life cycle of the equipment materials used in the transmission systems would be beneficial from a global warming potential and energy demand perspective.

8.3. Recommendation

There are number of factors that influence the connection of wind farms using GIL technology and that need to be considered in the early stages of planned projects, such as the production of the cladding aluminium tubes and the insulation gas. The production capacities for long distances are currently limited and the availability of cladding tubes and the insulation gas will lead to a longer construction time. As demand increases, the existing capacity must be developed in order to prevent delays when the connections are being implemented.

Table 8-1 shows estimated project timeline which was built based on clos evaluation to the Dogger Bank project [121]. It should be noted that this timeline was built just for the main transmission line between the main offshore collecting substation and the first onshore connection point (PCC) without taking the offshore wind farms construction in consideration.

Table 8-1: Project Timeline for Gas Insulated Pipeline Connecting Main Offshore Collecting Substation to the First Onshore Connection Point (PCC)

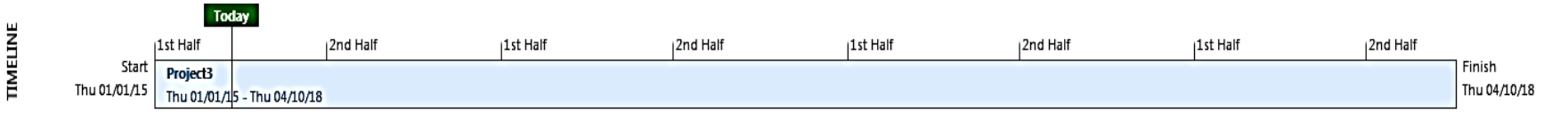

GANTT CHART

	Task Name	Duration	Start	Finish
1	**Phase 1: Project Planning + mgmt**	**981 days**	**Thu 01/01/15**	**Thu 04/10/18**
2	Project Planning + mgmt	180 days	Thu 01/01/15	Wed 09/09/15
3	Route Surveying	180 days	Thu 10/09/15	Wed 18/05/16
4	Project Launching	200 days	Thu 19/05/16	Wed 22/02/17
5	Tunnel + Shafts Design + Offshore Substation	120 days	Thu 23/02/17	Wed 09/08/17
6	**Phase 2: Constructions of infrastructure**	**621 days**	**Thu 19/05/16**	**Thu 04/10/18**
7	Aluminum Pipe Construction	200 days	Thu 19/05/16	Wed 22/02/17
8	Insulation Gas Production	150 days	Thu 19/05/16	Wed 14/12/16
9	Civil Work Including Tunnel and Main Offshore Collecting Substation	150 days	Thu 19/05/16	Wed 14/12/16
10	**Phase 3: Equipment Installation**	**501 days**	**Thu 03/11/16**	**Thu 04/10/18**
11	Laying of the Pipeline	200 days	Thu 03/11/16	Wed 09/08/17
12	Installation of Equipment in the Main Offshore Collection Substation	150 days	Thu 10/08/17	Wed 07/03/18
13	Filling the Insulation Gas in the Pipe	60 days	Thu 08/03/18	Wed 30/05/18
14	Testing the Gas Tightness	60 days	Fri 01/06/18	Thu 23/08/18
15	Energisation the GIL Line	30 days	Fri 24/08/18	Thu 04/10/18
16	**End Off Project**			

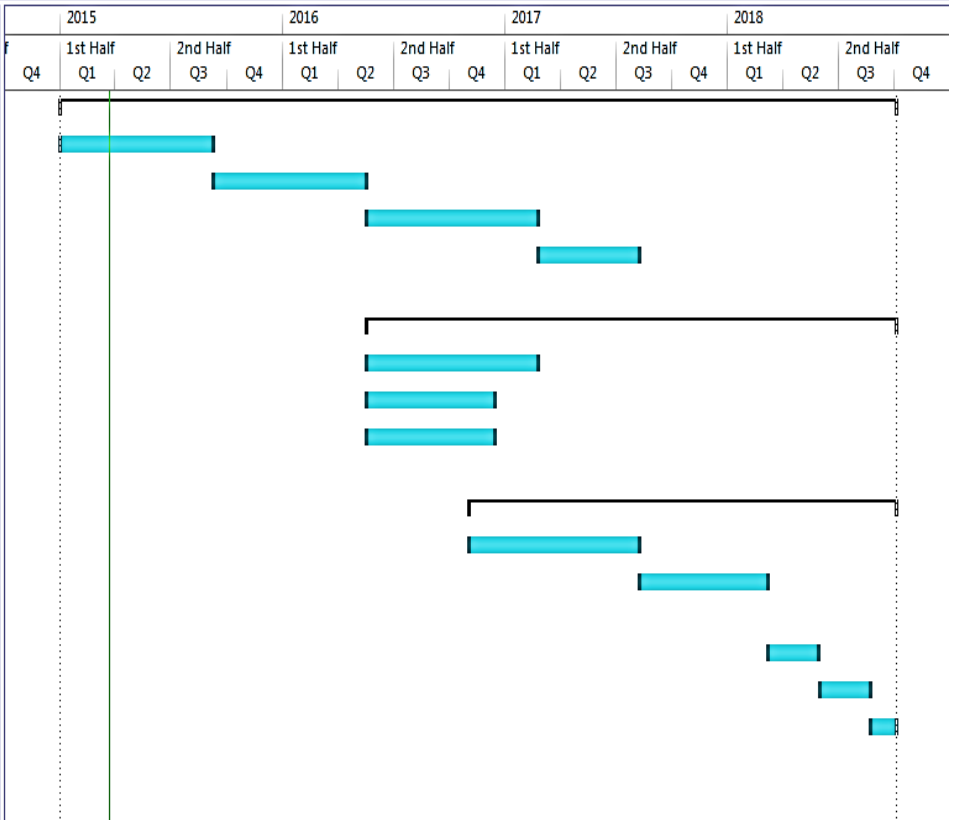

Utilizing GIL as an offshore transmission system requires several wind farms with high capacity to be combined. This means that a total connection power of at least 6-8 GW must be achieved. In order to do this, general legal and regulatory conditions must make it possible not just to connect wind farms individually but also to take into consideration the future development of offshore wind farms in an area. If several wind farms are being connected with a single connection, the connection must be designed in anticipation of future wind farm developments and be installed before the first wind farm is commissioned.

REFERENCES

[1] Roland Berger Strategy Consultants, "Pushing forward: The future of Offshore Wind Energy." [Online]. Available: http://www.rolandberger.co.uk/rbsearch/control/search.html?pid=rbuk_rb_2332035643&lastWasAdvanced=yes&quickSearch=no&initial=true&queryStr=wind&submit.x=16&submit.y=3. [Accessed: 03-Apr-2013].

[2] EWEA, "Wind in power, 2010 european statistics," 2011. [Online]. Available: http://www.ewea.org/fileadmin/files/library/publications/statistics/EWEA_Annual_Statistics_2010.pdf. [Accessed: 05-Apr-2013].

[3] EWEA, "Oceans of opportunity, Harnessing Europe's largest domestic energy resource," 2009. [Online]. Available: http://www.ewea.org/fileadmin/ewea_documents/documents/publications/reports/Offshore_Report_2009.pdf. [Accessed: 07-Jun-2013].

[4] Larsen, Jens HM, Hans Christian Soerensen, Erik Christiansen, Stefan Naef, and Per Vølund. "Experiences from Middelgrunden 40 MW Offshore Wind Farm," *Copenhagen offshore Wind Conf. (pp. 1-8).*, no. October, 2005.

[5] 4C Offshor, "Forecast of Offshore Wind Foundation Demand in North West Europe for the Period 2013 -2023," 2013. [Online]. Available: http://www.4coffshore.com/windfarms/reports/foundationsReport.aspx.

[6] dena, EWEA, ForWind, IEO, NTUA, Senergy, SINTEF, "Offshore Electricity Grid Infrastructure in Europe A Techno-Economic Assessment," 2011. [Online]. Available: http://www.ewea.org/fileadmin/ewea_documents/documents/publications/reports/OffshoreGrid__report.pdf. [Accessed: 28-Feb-2014].

[7] EWEA, "Deep water The next step for offshore wind energy," 2013. [Online]. Available: http://www.ewea.org/fileadmin/files/library/publications/reports/Deep_Water.pdf. [Accessed: 15-Feb-1014].

[8] EWEA, "EU Energy Policy to 2050," 2011. [Online]. Available: http://www.ewea.org/fileadmin/ewea_documents/documents/publications/reports/EWEA_EU_Energy_Policy_to_2050.pdf. [Accessed: 03-Mar-2014].

[9] EWEA, "Wind in our Sails- the coming of european offshore wind energy industry," 2011. [Online]. Available: http://www.ewea.org/fileadmin/ewea_documents/documents/publications/reports/23420_Offshore_report_web.pdf.

[10] Negra, N. Barberis, Jovan Todorovic, and Thomas Ackermann. “Loss evaluation of HVAC and HVDC transmission solutions for large offshore wind farms,” *Electric Power Systems Research, 76*(11), 916-927. 2006.

[11] Behravesh, Vahid, and Nahid Abbaspour. “New Comparison of HVDC and HVAC Transmission system,” *IJEIR* 1, no. 3 (2012): 300-304.

[12] Ackermann, Thomas, Antje Orths, and Krzysztof Rudion." *Transmission Systems for Offshore Wind Power Plants and Operation Planning Strategies for Offshore Power Systems." Wind Power in Power Systems, Second Edition* (2012): 293-327.

[13] (dena) Deutsche Energie-Agentur GmbH., “dena Grid Study II . Integration of Renewable Energy Sources in the German Power Supply System from 2015 – 2020 with an Outlook to 2025 .,” 2011. [Online]. Available: http://www.dena.de/en/publications/energy-system/dena-grid-study-ii.html.

[14] J. Jessus, Rui Castro, J.M. Ferreira,, “HVDC Connection of Offshore Wind Parks : VSC vs LCC with STATCOM,” in *International Conference on Power Systems Transients (IPST2011)., in Delft., the Netherlands.,*.

[15] H. Koch, "*Gas-Insulated Transmission Lines (GIL)"*. Chichester, UK: John Wiley & Sons, Ltd, 2011.

[16] Takuma, Tadasu, Osamu Yamamoto, and Shoji Hamada. *“Gases as a Dielectric,”* In *Gaseous Dielectrics X*, pp. 195-204. Springer US, 2004.

[17] Koch, H., and A. Schuette. “Gas insulated transmission lines for high power transmission over long distances,” *Electric power systems research* 44, no. 1 (1998): 69-74.

[18] Siemens, “Power Engineering Guide, Power Transmission and Distribution Solutions., Edition 7.0,” [Online]. Available: http://www.energy.siemens.com/hq/en/energy-topics/publications/power-engineering-guide/. [Accessed: 19-Feb-2014].

[19] Cigre brochure_218 Joint Working Group 23/21/33.15, “Gas insulated transmission lines (GIL),” no. February, 2003.

[20] Siemens AG, “International Electrotechnical Commission, Rigid High-Voltage, Gas-Insulated Transmission Lines for Rated Voltages of 72.5 kV and above, IEC 61640, IEC,”

[21] Cigre, Working Group B3/B1.09, “Application of Long High Capacity Gas-Insulated Lines in Structures,” no. October, 2008.

[22] Koch, H., and M. Hopkins. “Overview of gas insulated lines (GIL),” In *Power Engineering Society General Meeting, 2005. IEEE*, pp. 940-944. IEEE.

[23] Baer, Gregor P., A. Diessner, and G. F. Luxa. “420 kV SF6-insulated tubular bus for the Wehr pumped-storage plant electric tests,” *Power Apparatus and Systems, IEEE Transactions on* 95, no. 2 (1976): 469-477.

[24] Schichler, U., A. Diessner, and J. Gorablenkow. “Dielectric on-site testing of GIL." In *Properties and Applications of Dielectric Materials, 2003. Proceedings of the 7th International Conference on*, vol. 1, pp. 15-18. IEEE.

[25] International Electrotechnical Commission, Rigid High-Voltage, “ Gas-Insulated Tranmission Lines for Rated Voltages of 72.5 kV and above.", IEC 61640, IEC, 1998.

[26] Environmental News Service, “Potent New Greenhouse Gas Discovered,” 2000. [Online]. Available: http://www.fluoridealert.org/news/potent-new-greenhousegas- discovered/. .

[27] Environment News Service, “California Limits SF6, World’s Most Potent Greenhouse Gas,” 2010. [Online]. Available: http://www.ens-newswire.com/ens/mar2010/2010-03-02-091.html.

[28] Christophorou, Loucas G., and Richard J. Van Brunt. “SF6/N2 mixtures: basic and HV insulation properties,” *Dielectrics and Electrical Insulation, IEEE Transactions on* 2, no. 5 (1995): 952-1003.

[29] Christophorou, Loucas G., James Kenneth Olthoff, and David S. Green. “Gases for Electrical Insulation and Arc Interruption: Possible Present and FutureAlternatives to Pure SF6,” *National Instutute of Standards and Technology (NIST), U.S. Department of Commerce, Washington, USA*, November, 1997.

[30] Marsden, H. I., M. D. Hopkins, and C. R. Eck III. “Lightning Impulse Withstand Performance of a Practical GIC With 5 and 10 Percent SF6/N2 Mixtures,”. In *Electrical Insulation, 1998, Conference Record of the 1998 IEEE International Symposium on*, vol. 2, pp. 710-713. IEEE, 1998.

[31] Boeck, W., W. Taschner, J. Gorablenkow, G. F. Luxa, and L. Menten. “Insulating behaviour of SF6 without solid insulation in case of fast transients,” *CIGRE paper* 15-07 (1986).

[32] Qiu, Y., and Y. P. Feng. “Investigation of SF6-N2, SF6-CO2 and SF6-Air as Substitutes for SF6 Insulation,” In *Electrical Insulation, 1996., Conference Record of the 1996 IEEE International Symposium on*, vol. 2, pp. 766-769. IEEE.

[33] Koch Hermann. “Experience with 2nd Generation Gas-Insulated Transmission Lines GIL,” *In World Energy Transmission System Workshop, Meudon, France.*, 2003.

[34] Koch Hermann, A. Schuette. “Gas insulated transmission lines for high power transmission over long distances,” *Electric Power Systems Research*, 44, no. 1 (1998): 69-74.

[35] Koch Hermann, and Thomas Hillers. “Second generation gas-insulated line,” *Power Engineering Journal* 16, no. 3 (2002): 111-116.

[36] Henningsen, C. G., G. Kaul, H. Koch, A. Schuette, and R. Plath “Electrical and Mechanical Long-Time Behaviour of Gas-Insulated Transmission Lines,” In *CIGRE Session* (Vol. 8, p. 2000), *Paris.*

[37] Koch Hermann. “N2/SF6 gas-insulated line of a new GIL generation in service", CIGRE Session, Paris, 08/2002.”

[38] United Nations, “KYOTO PROTOCOL TO THE UNITED NATIONS FRAMEWORK KYOTO PROTOCOL TO THE UNITED NATIONS FRAMEWORK,” 1998. [Online]. Available: http://unfccc.int/resource/docs/convkp/kpeng.pdf.

[39] Qiu, Y., and E. Kuffel. “‘Comparison of SF6/N2 and SF6/CO2 Gas Mixtures as Alternatives to SF6 Gas,’ *Dielectrics and Electrical Insulation, IEEE Transactions on* 6, no. 6 (1999): 892-895.

[40] MUHAMMAD SAUFI KAMARUDIN, “Experimental Investigation of CF3I-CO2 Gas Mixtures on the Breakdown Characteristics in Uniform and Nonuniform Field Configurations,” School of Engineering Cardiff University, 2013.

[41] Hikita, Masayuki, Shinya Ohtsuka, Shigemitsu Okabe, and Genyo Ueta. “Breakdown Mechanism in C3F8/CO2 Gas Mixture under Non-uniform Field on the Basis of Partial Discharge Properties,” *Dielectrics and Electrical Insulation, IEEE Transactions on* 16, no. 5 (2009): 1413-1419.

[42] Qiu, X. Q., I. D. Chalmers, and P. Coventry. “A study of alternative insulating gases to SF6,” *Journal of Physics D: Applied Physics* 32, no. 22 (1999): 2918.

[43] ISO/DIS 14520-12, “Gaseous media fire extinguishing systems — Physical properties and system design — Part 2: CF3I Extinguishant,” 2013. [Online]. Available: http://www.iso.org/iso/home/store/catalogue_tc/catalogue_detail.htm?csnumber=55348&commid=46628.

[44] Taki, M., D. Maekawa, H. Odaka, H. Mizoguchi, and S. Yanabu. “Interruption capability of CF/sub 3/I Gas as a substitution candidate for SF/sub 6/ gas,” *Dielectrics and Electrical Insulation, IEEE Transactions on* 14, no. 2 (2007): 341-346.

[45] Toyota, Hiroyuki, Shigeyasu Matsuoka, and Kunihiko Hidaka. “Measurement of sparkover voltage and time lag characteristics in CF3I–

N2 and CF3I– air gas mixtures by using steep-front square voltage," *IEEJ Transactions on Fundamentals and Materials* 125 (2005): 409-414.

[46] Mohamad Kamarol bin Mohd Jamil., "Partial Discharge Properties and Gas Decomposition Analysis of Environmental Friendly Gas Insulation Media as a Basis of Diagnostic Technique Development," Department of Electrical and Electronic Engineering Graduate School of Engineering Kyushu Institute of Technology,, 2007.

[47] Katagiri, H., H. Kasuya, H. Mizoguchi, and S. Yanabu. "Investigation of the performance of CF_3I Gas as a Possible Substitute for SF_6," *Dielectrics and Electrical Insulation, IEEE Transactions on* 15, no. 5 (2008): 1424-1429.

[48] IEC 62271-204, "High-voltage switchgear and controlgear – Part 204: Rigid gas-insulated transmission lines for rated voltage above 52 kV, IEC, Geneva, Switzerland," 2011.

[49] Volcker, O., and H. Koch. "Insulation Co-ordination for Gas-Insulated Transmission Lines (GIL)", In *Power Engineering Society Winter Meeting, 2000, IEEE*, vol. 1, pp. 703-711. IEEE.

[50] Chakravorti, S., and H. Steinbigler. "Capacitive-resistive field calculation on HV bushings using the boundaryelement method", *Dielectrics and Electrical Insulation, IEEE Transactions on* 5, no. 2 (1998): 237-244.

[51] Kuffel, John, E. Kuffel, and Walter S. Zaengl. *High Voltage Engineering Fundamentals., Second edition*, Newnes, 2000.

[52] IEC 62271-1 ed1.0, "High-voltage switchgear and controlgear – Part 1: Common specifications, IEC, Geneva, Switzerland, 2007-10." .

[53] EN 50068., "Wrought steel enclosures for gas-filled high-voltage switchgear and controlgear, IEC, Geneva, Switzerland 1991.," no. 1, 1991.

[54] Cigre Working Group 21/23/33-02, "Insulation co-ordination of 420 kV gas insulated lines (GIL)," 1998.

[55] Kuroyanagi, Y., A. Toya, T. Hayashi, and T. Araki. "Construction of 8000A class 275 kV gas insulated transmission line," *Power Delivery, IEEE Transactions on* 5, no. 1 (1990): 14-20.

[56] Babusci B., Colombo E., Speziali. "Assessment of the behaviour of gas-insulated electrical components in the presence of an internal arc," *ENEL Research, CIGRE Session, Paris, France,*, 1998.

[57] Henningsen, C. G., G. Kaul, H. Koch, A. Schuette, and R. Plath. "Electrical and Mechanical Long- Time Behaviour of Gas-Insulated Transmission Lines," In *CIGRE Session*, vol. 8, p. 2000. 2000.

[58] Minaguchi, D., M. Ginno, K. Itaka, H. Furukawa, K. Ninomiya, and T. Hayashi. “Heat Transfer Characteristics of Gas-Insulated Transmission Lines,” *Power Delivery, IEEE Transactions on* 1, no. 1 (1986): 1-9.

[59] Itaka, Koshi, Tomoo Araki, and Takushi Hara. “Heat Transfer Characteristics of Gas Spacer Cables,” *Power Apparatus and Systems, IEEE Transactions on* 5 (1978): 1579-1585.

[60] Chakir, A., and H. Koch. “Turbulent Natural Convection and Thermal Behaviour of Cylindrical Gas-Insulated Transmission Lines (GIL),” In *Power Engineering Society Summer Meeting, 2001*, vol. 1, pp. 162-167. IEEE, 2001.

[61] Chakir, Abdellah, Y. Sofiane, Nicolas Aquelet, and Mhamed Souli. “Long term test of buried gas insulated transmission lines (GIL),” *Applied thermal engineering* 23, no. 13 (2003): 1681-1696.

[62] Koch, H., and A. Chakir. “Thermal calculation for buried Gas-Insulated Transmission Lines (GIL) and XLPE-cable,” In *Power Engineering Society Winter Meeting, 2001. IEEE*, vol. 2, pp. 857-862. IEEE.

[63] McDonald, John D., ed. “ElECTRIC POWER SUBSTATIONS ENGINEERING.” CRC press, 2012.

[64] Henningsen, C. G., G. Kaul, H. Koch, A. Schuette, and R. Plath. “Electrical and mechanical long time behaviour of gas-insulated transmission lines,” In *CIGRE Session*, vol. 8, p. 2000. 2000.

[65] Cigre SESSION B1-103_2004, “New generation of GIL -Characteristics and applications,” 2004.

[66] Poehler, S.; Rudenko, P., “Directly Buried Gas-Insulated Transmission,” *Transmission and Distribution Conference and Exposition (T&D), 2012 IEEE PES* , vol., no., pp.1,5, 7-10 May 2012

[67] Siemens AG, “GIL – high-power transmission technology.” [Online]. Available: http://www.energy.siemens.com/hq/pool/hq/power-transmission/gas-insulated-transmission-lines/GIL_e.pdf. [Accessed: 15-May-2012].

[68] Radiation International and Association Protection., “Human Exposure to Electromagnetic Fields,” 2009. [Online]. Available: http://www.irpa.net/.

[69] Health and Safety Ececutive, “Radiation Home,” *2010*. [Online]. Available: http://www.hse.gov.uk/radiation/ionising/doses/. [Accessed: 03-Sep-2013].

[70] Siemens AG, “Undergrounding Electricity Transmission: Introduction to Gas Insulated Line (GIL) technology,” *National Symposium on Future Electricity Networks, ICE,*. 2011.

[71] Chakir, Abdellah, and Hermann Koch. “Corrosion protection for gas-insulated transmission lines,” In *Power Engineering Society Summer Meeting, 2002 IEEE*, vol. 1, pp. 220-224. IEEE, 2002.

[72] Koch H, “Preferential Subject D1 PS2 Q6: Is there any experience from the application in the field of N2/SF6 mixtures and especially in high voltage Gas-Insulated Lines?,” CIGRE Session 2004, Paris, 08/2004.

[73] Miyazaki, Akinobu, Manabu Yagi, S-I. Kobayashi, C. Min, K. Hirotsu, and H. Nishima. “Development of partial discharge automated locating system for power cable,” In *Electrical Insulation and Dielectric Phenomena, 1998. Annual Report. Conference on*, pp. 424-427. IEEE, 1998.

[74] Okubo, H., M. Yoshida, T. Takahashi, T. Hoshino, M. Hikita, and A. Miyazaki. “Partial Discharge Measurement in a Long Distance SF6 Gas Insulated,” *Power Delivery, IEEE Transactions on* 13, no. 3 (1998): 683-690.

[75] Hoshino, Toshihiro, Hiroshi Koyama, Shiro Maruyama, and Masahiro Hanai. “Comparison of Sensitivity Between UHF Method and IEC 60270 for Onsite Calibration in Various GIS,” *Power Delivery, IEEE Transactions on* 21, no. 4 (2006): 1948-1953.

[76] Orlando P. Hevia., “Alternative Transients Program - Comparison of transmission line models.” [Online]. Available: http://iitree-unlp.org.ar/caue/Archivos/emodlin.pdf.

[77] Dommel. Hermann W, *Electromagnetic Transients Program: Reference Manual:(EMTP theory book)*. Bonneville Power Administration,, 1986.

[78] CGIT Westboro., “Compressed Gas Insulated Transmission Bus Systems Proven Solutions.” [Online]. Available: http://www.azz.com/sites/default/files/documents/CGIT.pdf. [Accessed: 01-Mar-2011].

[79] A. Juan, Martinez-Velasco, Ed., *Power systems transients :parameter determination*, 1st ed. CRC Press Taylor & Francis Group, 2010.

[80] Gustavsen, Bjørn. “Panel Session on Data for Modeling System Transients Insulated Cables,” In *Power Engineering Society Winter Meeting, 2001. IEEE*, vol. 2, pp. 718-723. IEEE, 2001.

[81] Gudmundsdottir, Unnur Stella, Bjørn Gustavsen, Claus Leth Bak, and Wojciech Wiechowski. “Field Test and Simulation of a 400 kV Cross-Bonded Cable System,” *Power Delivery, IEEE Transactions on* 26, no. 3 (2011): 1403-1410.

[82] BS EN, “Conductors of insulated cables,. BS EN 60228:2005.” .

[83] ABB, “XLPE Land Cable Systems User ´ s Guide.” [Online]. Available: http://www.elektroskandia.ee/pub/tooted/keskpinge-korgepinge/XLPE-Land-Cable-Systems-2GM5007GB-rev-5.pdf. [Accessed: 03-Mar-2012].

[84] ABB, “XLPE Submarine Cable Systems Attachment to XLPE Land Cable Systems - User ´ s Guide.” [Online]. Available: http://www04.abb.com/global/seitp/seitp202.nsf/0/badf833d6cb8d46dc1257c0b002b3702/$file/XLPE+Submarine+Cable+Systems+2GM5007+.pdf#page=1&zoom=auto,0,814. [Accessed: 03-Mar-2012].

[85] National Grid, “Electric and Magnetic Fields ‘Geometries for calculating fields from power lines.’”[Online]. Available: http://www.emfs.info/Sources+of+EMFs/Overhead+power+lines/Calculating/geometries/. [Accessed: 05-Apr-2012].

[86] Nasser D. Tleis, *Power Systems Modelling and Fault Analysis Theory and Practice*. Elsevier Ltd., 2008.

[87] CIGRE WG 33.02, “Guidelines for representation of network elements when calculating transients,” *CIGRE Rep. no. 39.,*, 2000.

[88] *Alternative Transient Program (ATP) Rule Book*. .

[89] Schlabbach, Jürgen, and Karl-Heinz Rofalski. *Power System Engineering Planning, Design, and Operation of Power Systems and Equipment*. John Wiley & Sons, 2008.

[90] Institute of Electrical and Electronics Engineers, “IEEE Application Guide for AC High-Voltage Circuit Breakers Rated on a Symmetrical Current Basis,” *IEEE Std C37.010-1999*. p. i, 2000.

[91] Martinez, Jorge, P. C. Kjar, Pedro Rodriguez, and Remus Teodorescu. “Short circuit signatures from different wind turbine generator types,” In *Power Systems Conference and Exposition (PSCE), 2011 IEEE/PES*, pp. 1-7. IEEE, 2011.

[92] Kanellos, F. D., and John Kabouris. “Wind farms modeling for short-circuit level calculations in large power systems,” *Power Delivery, IEEE Transactions on* 24, no. 3 (2009): 1687-1695.

[93] IEC 60909-0, “Short-circuit currents in three-phase a.c. systems - Part 0: Calculation of currents.” 2001.

[94] Samaan, Nader, Robert Zavadil, J. Charles Smith, and Jose Conto. “Modeling of wind power plants for short circuit analysis in the transmission network,” In *Transmission and Distribution Conference and Exposition, 2008. T&D x00026; D. IEEE/PES*, pp. 1-7. IEEE, 2008.

[95] Muljadi, E., C. P. Butterfield, A. Ellis, J. Mechenbier, J. Hochheimer, R. Young, N. Miller, R. Delmerico, R. Zavadil, and J. C. Smith.

"Equivalencing the collector system of a large wind power plant," In *Power Engineering Society General Meeting, 2006. IEEE*, pp. 9-pp. IEEE, 2006.

[96] Martinez, J. A., J. Mahseredjian, and B. Khodabakhchian. "Parameter Determination for Modeling System Transients — Part VI: Circuit Breakers," *Power Delivery, IEEE Transactions on* 20, no. 3 (2005): 2079-2085.

[97] HOTA, BHABANI SANKAR. "LOAD FLOW STUDY IN POWER SYSTEM," Doctoral dissertation, Department of Electrical Engineering National Institute of Technology, 2011.

[98] EPRI, "Increased Power Flow Through Transmission Circuits: Overhead Line Case Studies and Quasi-Dynamic Rating," vol. 3, no. 3, 2006.

[99] CLAIR, HPST. "Practical Concepts in Capability and Performance of Transmission Lines," *Power Apparatus and Systems, Part III. Transactions of the American Institute of Electrical Engineers*, vol. 72, no.2,, pp. 1152–1157, 1953.

[100] Gutman, Richard, P. P. Marchenko, and R. D. Dunlop. "Analytical Development of Loadability Characteristics for EHV and UHV Transmission Lines," *Power Apparatus and Systems, IEEE Transactions on* 2 (1979): 606-617.

[101] National Grid, "National Electricity Transmission System Security and Quality of Supply Standard," 2012.

[102] Colla, L., F. M. Gatta, A. Geri, S. Lauria, and M. Maccioni. "Steady-state operation of very long EHV AC cable lines," In *PowerTech, 2009 IEEE Bucharest*, pp. 1-8. IEEE, 2009.

[103] Gatta, F. M., and S. Lauria. "Very long EHV cables and mixed overhead-cable lines. Steady-state operation," In *Power Tech, 2005 IEEE Russia*, pp. 1-7. IEEE, 2005.

[104] Gatta, F. M., A. Geri, S. Lauria, and M. Maccioni. "Steady-state operating conditions of very long EHVAC cable lines: Two case studies," *Electric Power Systems Research* 83, no. 1 (2012): 160-169.

[105] John J. Grainger, WUliam D. Stevenson, *POWER SYSTEM ANALYSIS*. McGraw-Hill, Inc.,, 1994.

[106] IEC 60071-1, "Insulation Co-ordination Part 1: Definitions. Principles and Rules." 2006.

[107] "IEC 60071-1, 'Insulation Co-ordination Part 2: Application Guide,' 1996.".

[108] A report by the European Wind Energy Association, "Wind in our Sails, The coming of Europe's offshore wind energy industry," 2011. [Online]. Available: http://www.ewea.org/fileadmin/ewea_documents/documents/publications/reports/23420_Offshore_report_web.pdf.

[109] Yu, Cunyi, Nit Petcharaks, and Chairoj Panprommin. "The statistical calculation of energization overvoltages, case of EGAT 500 kV lines," In *Power Engineering Society Winter Meeting, 2000. IEEE*, vol. 4, pp. 2705-2709. IEEE, 2000.

[110] Marzinotto, M., C. Mazzetti, and P. Schiaffino. "Statistical approach to the insulation coordination of medium and high voltage cable lines," In *Power Tech, 2005 IEEE Russia*, pp. 1-8. IEEE, 2005.

[111] Thomas, Mini S., C. S. Indulkar, and P. R. Bijwe. "Sensitivity analysis of peak switching overvoltages in underground cables," *Electric Machines and Power Systems* 16, no. 5 (1989): 331-342.

[112] "IEC 60071-1, "Insulation Co-ordination-part 2: Application guide, IEC STD 60071-2.3. Technical report, IEC, 1996." .

[113] National Grid, "Seven Year Statement 2010 (SYS), Appendix D." [Online]. Available: http://www.nationalgrid.com/uk/Electricity/SYS/current/. [Accessed: 19-Apr-2012].

[114] da Silva, Filipe Miguel Faria. "Analysis and simulation of electromagnetic transients in HVAC cable transmission grids," PhD diss., Videnbasen for Aalborg UniversitetVBN, Aalborg UniversitetAalborg University, Det Teknisk-Naturvidenskabelige FakultetThe Faculty of Engineering and Science, Elektriske anlægElectric Power Systems, 2011.

[115] Ohno, T., A. Ametani, C. L. Bak, W. Wiechowski, and T. K. Sørensen. "Analysis of the Statistical Distribution of Energization Overvoltages of EHV Cables and OHLs," 2013.

[116] King, R., F. Moore, N. Jenkins, A. Haddad, H. Griffiths, and M. Osborne., "Switching Transients in Offshore Wind Farms–Impact on the Offshore and Onshore Networks." IPST, Delft, the Netherlands (2011).

[117] Johansson, Stefan G., J. Hanson, J. Karlström, F. Krogh, and L. Liljestrand "AC Cable solutions for Offshore Wind Energy," *In Copenhagen Offshore Wind Conference.*, pp. 1–10, 2005.

[118] WindTECH International, "PTP Goes Offshore." [Online]. Available: http://www.windtech-international.com/articles/ptp-goes-offshore. [Accessed: 10-Mar-2013].

[119] Kyriakides, Stelios, and Edmundo Corona, “Mechanics of offshore pipelines: volume 1 buckling and collapse. Vol. 1.” Elsevier,, 2007.

[120] Chakrabarti, Subrata, “Handbook of Offshore Engineering (2-volume set). Vol. 1.” Elsevier,, 2005.

[121] Forwind., “Dogger Bank Project One Environmental Impact Assessment Scoping Report,” 2010. [Online]. Available: http://www.forewind.co.uk/uploads/files/project-one-scoping-report.pdf. [Accessed: 20-Nov-2013].

[122] ForWind, E.U. Commission of European Transmission Networks Electricity, “Broshure Grid Connection of Offshore Wind Farms – A Feasibility Study on the Application of Power Transmission Pipelines (PTP®),” 2005. [Online]. Available: http://www.forwind.de/forwind/index.php?article_id=306&clang=1.

[123] ICES, “International Council for the Exploration of the Sea (ICES).” [Online]. Available: https://www.google.co.uk/webhp?tab=ww&ei=zfx2VJyGDMb4UtzKgegJ&ved=0CAYQ1S4#q=+International+Council+for+the+Exploration+of+the+Sea+%28ICES%29. [Accessed: 02-Mar-2014].

[124] “Prysmian Cable and System. High Voltage Cables.” [Online]. Available: www.prysmian.nl/export/sites/prysmian-nlNL/.../Prysmian_HVC_LR.pdf. [Accessed: 02-Aug-2012].

[125] ABB, “XLPE Cable Systems User ´ s guide,” pp. 1–32.

[126] R. Nick, Barton, *TBM tunnelling in jointed and faulted rock*. CRC Press, 2000.

[127] W. Leader, I. N. Large, and D. Pipe, “WORLD LEADER IN LARGE DIAMETER PIPE MANUFACTURING POLYETHYLENE,” no. 510.

[128] ForWind, Siemens, ILF Consultaing Engineers, “Feasibility Study for Large-Scale Grid Connection of Remote Offshore Wind Energy.” [Online]. Available: http://www.forwind.de/forwind/index.php?article_id=61&clang=1.

[129] Carbon Trust, “Offshore wind power: big challenge, big opportunity.” [Online]. Available: http://www.carbontrust.com/resources/reports/technology/offshore-wind-power.

[130] Danielle Lane., “THE CROWN ESTATE Round 3 Offshore Wind Farm Connection Study Version 1.0,” *A report by Senergy Econnect and National Grid for the Crown Estate*. .

[131] Madariaga, A., I. Martínez de Alegría, J. L. Martín, P. Eguía, and S. Ceballos. "Current facts about offshore wind farms," *Renewable and Sustainable Energy Reviews* 16, no. 5 (2012): 3105-3116.

[132] Parsons Brinckerhoff and Institution of Engineering and Technology, "electricity transmission costing study," 2012. [Online]. Available: http://www.theiet.org/factfiles/transmission-report.cfm. [Accessed: 06-Nov-2013].

[133] ENTSOE, "Offshore Transmission Technology," *PREPARED BY THE REGIONAL GROUP NORTH SEA FOR THE NSCOGI (NORTH SEAS COUNTRIES" OFFSHORE GRID INITIATIVE)*, 2011. .

[134] National Grid., "Electricity Transmission Cost Study: How does the independent report compare to National Grid's view?," no. February, pp. 1–3, 2012.

[135] T. A. Moore., S. R. Skaggs., M. R. Corbitt., R. E. Tapscott., D. S. Dierdorf., and C. j. Kibert., "No TitleThe Development of CF3I as a Halon Replacement.," *The University of New Mexico*, 1994. .

[136] Charles J. Kibert., "Fluoroiodocarbons as Halon 1211 / 1301 Replacements : An Overview," *Wright Laboratory, U.S. Air Force*. .

[137] K. S. and R. B. B. Van Eeckhout, D. Van Hetem, M. Reza, "Economic comparison of VSC HVDC and HVAC as transmission system for a 300 MW offshore wind farm," *European Transactions on Electrical Power*, no. June 2009, pp. 661–671, 2010.

[138] ABB., "It's time to connect with offshore wind supplement," 2010. [Online]. Available: http://www05.abb.com/global/scot/scot221.nsf/veritydisplay/1bad1970cd0766eec1257b28005757df/$file/Pow0038 R6 LR.pdf. [Accessed: 09-Dec-2013].

APPENDIX 1: List of Abbreviations

HVAC	High Voltage Alternate Current
HVDC	High Voltage Direct Current
GIL	Gas-Insulate Transmission Line
GIS	Gas Insulated Substation/Switchgear
EMTP	Electromagnetic Transient Program
EU	European Union
EHV	Extra High Voltage
XLPE	Cross-Linked Polyethylene
LCC-CSC	Line-Commutated Current Source Converters
VSC	Voltage Source Converters
PCC	Point of Common Coupling
IGBT	Insulation Gate Bipolar Transistors
pu	Per unit
SF_6	Sulphur Hexafluoride
CF_3I	Trifluoroiodomethane
EDF	Electrical De France
GWP	Global Warming Potential
C	Carbon
F	Fluorine
ODP	Ozone Depleting Potential
SYS	Seven Year Statement
LIWV	Lightning Impulse Withstand Voltage
SIWV	Switching Impulse Withstand Voltage
PFWV	Power Frequency Withstand Voltage
IRPA	International Radiation Protection Association
PE	Polyethylene
PP	Polypropylene
IEC	International Electrotechnical Commission
CIGRE	International Council on Large Electric Systems

Appendix 2: Existing GIL Projects

Examples of Existing GIL Projects [2]

	Examples of existing GIL Projects (1)		
OWNER	Energie Ouest Suisse	RWE Net	Chubu electric power company
DATE OF COMMISSIONING	2001	1975	1998
INSTALLATION PLACE	GENEVA, Switzerland	WEHR, Germany	SHINMEIKATOKAI, Japan
TYPE OF INSTALLATION	TUNNEL	TUNNEL	TUNNEL
LENGTH OF LINK	420 m	670 m	3300 m
NUMBER OF SYSTEMS	2	2	2
NOMINAL VOLTAGE OF NETWORK	220 kV	380 kV	275 kV
HIGHEST VOLTAGE FOR EQUIPMENT	300 kV	420 kV	300 kV
RATED CURRENT PERSYSTEM	2000 A	2500 A	6300 A
INSULATING GAS	7 bar abs	4.9 bar abs	5.4 bar abs
	20% SF_6 / 80% N_2	100% SF_6	100% SF_6
CONDUCTOR			
OUTER DIAMETER (mm)	180	150	170
WALL THICKNESS (mm)	5	5	20
MATERIAL	Al alloy EN AW 6101B E-Al/MgSi0,5 T6 W19	E-ALMgSi0,5	Al alloy
IACS*	61 %	48-54 %	59.5 %
CONDUCTIVITY at 20°C m/Ω.mm^2	35.3857	27.84-31.32	34.518
RESISTIVITY at 20°C m/Ω.mm^2	0.02826	0.032-0.036	0.02897
ENCLOSURE			
INNER DIAMETER	500	520	460
WALL THICKNESS	6	5	10

*IACS = International Annealed Copper Standard (IACS=100 % ⇒ Copper Standard Conductivity = 58,108 m/**Ω**·mm2)

	Examples of existing GIL Projects (2)		
OWNER	National Grid UK	Entergy	BC Hydro
DATE OF COMMISSIONING	2004	2001	1981
INSTALLATION PLACE	Hams Hall, United Kingdom	Baxter Wilson Power Plant USA	Revel stoke Hydro Power Plant Canada
TYPE OF INSTALLATION	Above Ground / Trench	Above Ground	TUNNEL
LENGTH OF LINK	545 m	1250 m	400 m
NUMBER OF SYSTEMS	1	1	2
NOMINAL VOLTAGE OF NETWORK	400 kV	500 kV	500 kV
HIGHEST VOLTAGE FOR EQUIPMENT	420 kV	550 kV	550 kV
RATED CURRENT PER SYSTEM	4000 A	4500 A	4000 A
INSULATING GAS	10.3 bar abs	3.79 bar abs	3.45 bar abs
	20% SF_6 / 80% N_2	100% SF_6	100% SF_6
CONDUCTOR			
OUTER DIAMETER (mm)	512-520	178	178
WALL THICKNESS (mm)	12.7	12.7	12.7
MATERIAL	Al alloy	Al alloy 6061-T6	Al alloy 6061-T6
IACS*	-	59.5 %	59.5 %
CONDUCTIVITY at 20°C m/Ω.mm^2	-	34.57 %	34.57 %
RESISTIVITY at 20°C m/Ω.mm^2	-	0.0289	0.0289
ENCLOSURE			
INNER DIAMETER	500	508	508
WALL THICKNESS	6-10	6.35	6.35

*IACS = International Annealed Copper Standard (IACS=100 % ⇒ Copper Standard Conductivity = 58,108 m/**Ω**·mm2)

Appendix 3: Physical Properties of CF_3I Gas

Physical Properties of CF3I [3]

Physical or Chemistry Property	Value or Description
Molecular weight	195.1
Physical state at 20°C	Gas
Melting point	– 110°C (– 166°F)
Boiling point at 1 atm	– 22.5°C (– 8.5°F)
Liquid density at – 32.5°C	2.36 g/mL
Odour threshold	Odourless
Solubility in water	Slight
Vapour pressure at 25°C	78.4 psia
Pressure-temperature curve	log psia = 5.7411-1146.82/T/K
Critical pressure	586 psia (estimated)
Critical temperature	122°C (estimated)
Critical volume	225 cm^3/mole (estimated)
Electron affinity 150 ± 20 kJ/mole	150 ± 20 kJ/mole
Vapour heat capacity	16.9 cal/mole-K
C-I bond dissociation energy	54 kcal/mole
Vapour density (air = 1)	6.9

Appendix 4: GIL Electrical Parameters

- GIL Inductance *"l"*

The inductance per unit length can be calculated by considering the typical coaxial structure of a GIL as shown in Figure 1 where R_1, R_2 are the phase inner and outer radius and R_3, R_4 the enclosure inner and outer radius respectively [2], [4].

Where $\mu_0 \rightarrow$ Magnetic permeability of free space = $2\pi * 10^{-7}$ H/m

$$l = \frac{\mu_0}{2\pi} \ln \frac{R_3}{R_2} \quad [\mathrm{H/m}]$$

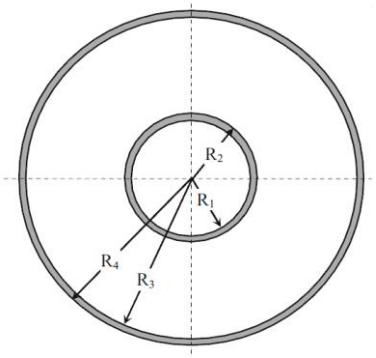

Figure 1: coaxial structure of a GIL

- GIL Capacitance "*C"*

The capacitance per unit length can be computed considering the cylindrical symmetry and the permittivity of the gas mixture $\varepsilon_0 = 8.854 * 10^{-12}$ F/m. Since the nitrogen is 80% of the gas mixture, so then the permittivity considered (as for the free space). R_3 and R_2 are shown in figure 2 [2],[4].

$$C = \frac{2\pi\varepsilon_0}{\ln \frac{R_3}{R_2}} \quad [\mathrm{F/m}]$$

- GIL Resistance “r”

The resistance r per unit length depends on the conductor and enclosure dimensions and electrical resistivity, where the skin and proximity effects of the conductor and enclosure are negligible [2], [4].

$$r = r_{ph} + r_{en} \quad [\Omega/km]$$

$$r_{ph} = \frac{\rho_{ph}}{S_{ph}} \quad [\Omega/km]$$

Where ρ_{ph} is expressed in $[\Omega\,mm^2/km]$ and it must be evaluated at the operation temperature and S_{ph} is the cross section area. R_1,R_2, R_3 and R_4 are shown in fig 1.

$$S_{ph} = \pi * (R_2^2 - R_1^2)\ [mm^2]$$

For the enclosure

$$r_{en} = \frac{\rho_{en}}{S_{en}} \quad [\Omega/km]$$

$$S_{en} = \pi * (R_4^2 - R_3^2)\ [mm^2]$$

- GIL Surge Impedance

$$Z_0 = \frac{1}{2\pi} \ln \frac{R_3}{R_2} \sqrt{\frac{\mu_o}{\varepsilon_o}}$$

Appendix 5: MTLAP Equations for Long Transmission Line

```
R=8.616e-3;
l=2.05e-4;
c=54.2e-9;
f=50;
l=j*2*pi*f*l;
z = R + l
y=j*2*pi*f*c
Zc = sqrt (z/y);
ga =  sqrt(z * y);
L1= [0:50:500];
L2= [0:50:400];
L3=  [0:50:300];
L4=  [0:50:200];
B1= Zc.* sinh(L1.* ga);
B2= Zc.* sinh(L2.* ga);
B3= Zc.* sinh(L3.* ga);
B4= Zc.* sinh(L4.* ga);
A1= cosh(L1.* ga);
A2= cosh(L2.* ga);
A3= cosh(L3.* ga);
A4= cosh(L4.* ga);
C1= (sinh(L1.* ga))./Zc;
C2= (sinh(L2.* ga))./Zc;
C3= (sinh(L3.* ga))./Zc;
C4= (sinh(L4.* ga))./Zc;
Vs=complex (342928.6,0);
Is1=complex (2938.838,-1120.535);
Is2=complex (3048.19,-1415.391);
Is3=complex (3181.1768,-1708.13578);
Is4=complex (3327.33369,-1999.885);
Vr1= (A1.*Vs)-(B1.*Is1);
Vr2= (A2.*Vs)-(B2.*Is2);
Vr3= (A3.*Vs)-(B3.*Is3);
Vr4= (A4.*Vs)-(B4.*Is4);
V1=abs (Vr1);
V2=abs (Vr2);
V3=abs (Vr3);
V4=abs (Vr4);
Plot (L1, V1,'b', L2, V2,'g', L3, V3,'r', L4, V4)
Ir1= (A1.*Is1)-(C1.*Vs);
Ir2= (A2.*Is2)-(C2.*Vs);
Ir3= (A3.*Is3)-(C3.*Vs);
Ir4= (A4.*Is4)-(C4.*Vs);
I1=abs (Ir1);
I2=abs (Ir2);
I3=abs (Ir3);
```

```
I4=abs (Ir4);
Plot (L1, I1,'b', L2, I2,'g', L3, I3,'r', L4, I4)
thV1=angle (Vr1);
thV2=angle (Vr2);
thV3=angle (Vr3);
thV4=angle (Vr4);
thI1=angle (Ir1);
thI2=angle (Ir2);
thI3=angle (Ir3);
thI4=angle (Ir4);
V1=V1. /sqrt (2);
V2=V2. /sqrt (2);
V3=V3. /sqrt (2);
V4=V4. /sqrt (2);
I1/I1. / sqrt (2);
I2/I2. / sqrt (2);
I3/I3. / sqrt (2);
I4/I4. / sqrt (2);
P1= (V1.*I1).*cos (thV1-thI1);
P2= (V2.*I2).*cos (thV2-thI2);
P3= (V3.*I3).*cos (thV3-thI3);
P4= (V4.*I4).*cos (thV4-thI4);
Plot (L1, P1,'b', L2, P2,'g', L3, P3,'r', L4, P4)
Q1= (V1.*I1).*sin (thV1-thI1);
Q2= (V2.*I2).*sin (thV2-thI2);
Q3= (V3.*I3).*sin (thV3-thI3);
Q4= (V4.*I4).*sin (thV4-thI4);
Plot (L1, Q1,'b', L2, Q2,'g', L3, Q3,'r', L4, Q4)
```

REFERENCES for APPENDIXES:

1. EWEA., "Wind in our Sails- the coming of european offshore wind energy industry," 2011. [Online]. Available:http://www.ewea.org/fileadmin/ewea_documents/documents/publications/reports/23420_Offshore_report_web.pdf

2. Cigre, Working Group B3/B1.09, "Application of Long High Capacity Gas-Insulated Lines in Structures," no. October, 2008.

3. Subcommittee on Iodotrifluoromethane, Committee on Toxicology, Board on Environmental Studies and Toxicology, and Division on Earth and Life Studies, "Iodotrifluoromethane: Toxicity Review," *Washington, D.C. Natl. Acad. Press. Press.*, 2004.

4. Cigre brochure_218 Joint Working Group 23/21/33.15, "Gas insulated transmission lines (GIL)," no. February, 2003.